

Laboratory experiments with tidal Helmholtz resonators

Willem Jan van de Berg

3rd September 2003

Abstract

With the experiments that are discussed in this report, the tidal Helmholtz resonator was investigated in a chamber-sized laboratory set-up. A Helmholtz resonator consists of a basin that is connected with the sea by a narrow channel. Examples in nature are the separate tidal basins within the Wadden Sea. The Helmholtz resonator is forced by the incoming tide at the entrance of the channel. In the basin, the tidal response is nearly uniform and strong tidal currents occur only in the channel. If the tidal frequency is close to the resonance frequency of the Helmholtz resonator, i.e. the Helmholtz frequency, the tide is amplified in the basin. In the laboratory set-up, the channel was represented by a pipe. With the intention of decreasing dissipative effects, pipes with smoothly curved pipe ends have been used as well as straight pipes.

The general objective of our experiments was to test predictions that were obtained from mathematical analysis of theoretical models. These comprise three basic elements, which all have not been verified before with laboratory experiments. The first was the linearization of the bottom shear, which quadratically depends on the current velocity in the channel, with a method formulated by Lorentz (1922). The second was the linear behaviour of the Helmholtz resonator that is expected for basins without hypsometric effects (i.e. a basin with vertical sidewalls). The third element concerns the bending of the response curve (i.e. the amplitude of the tide in the basin versus the forcing frequency) due to hypsometric effects (i.e. variation of the wetted surface with elevation of the sea level), such that for a range of forcing frequencies the system has multiple nontransient solutions.

The results of the experiments show that the description of dissipation through the Lorentz' linearized principle performs very well. Furthermore, the results of experiments with straight pipes are well described with the linear behaviour that is predicted theoretically. Experiments with smooth pipe ends however show nonlinear behaviour: bending of the response curve and multiple nontransient solutions for fixed forcing conditions. The experiments indicate that the channel shape is another origin for non-linear behaviour. The physical explanation of this non-linear behaviour is not satisfactorily established yet. Therefore, an indication of the strength of this nonlinear effect for tidal Helmholtz resonators in nature can not be given. Finally, experiments with non-uniform hypsometry did not lead to useful results. Small-scale effects causing tidal delays above the slope, due to the shallowness of the water layer, spoiled the experiments.

Contents

1	Introduction	1
2	Theory	6
2.1	General theory of tides	6
2.1.1	Generation of tides	6
2.1.2	The Helmholtz resonator	10
2.2	Derivation of the free Helmholtz reponse	11
2.2.1	First assumptions	12
2.2.2	The response of a half-open channel	13
2.2.3	Response of channels with 2 widths	15
2.2.4	The Helmholtz mode	16
2.2.5	Derivation of the Helmholtz response equations	17
2.2.6	Possible extentions	18
2.3	Lorentz-linearization	19
2.3.1	Transformation of the bottom friction	19
2.3.2	Solutions of the Lorentz-linearized equation	20
2.3.3	Response functions	21
2.4	Bent resonance	22
2.4.1	Qualitative introduction	22
2.4.2	Mathematical analysis	23
2.4.3	Figures of response shapes	25
3	Experimental set-up and measurement analysis	27
3.1	Arguments for the chosen set-up	27
3.2	Experimental set-up	28
3.2.1	Tidal signal generation	28
3.2.2	Control of the forcing tank	30
3.2.3	Control of the sea level	31
3.2.4	Basin and inlay	32
3.2.5	Pipes	34
3.3	Measurement tools	36
3.3.1	Distance sensors	36
3.3.2	Current measurements	38
3.3.3	Operation program	38
3.4	Data analysis	39
3.4.1	Step wise description of data analysis procedure	40
3.4.2	Effect of the measurement resolution	41
3.5	Data and theory comparison	42
3.5.1	Comparison with the Lorentz-linearized Helmholtz solution	43
3.5.2	Comparison of laboratory data with the non-linear solution	44

3.6	Computer modeling	45
4	Experimental results	47
4.1	Results for large basin area	47
4.1.1	Experimental conditions	47
4.1.2	Results of <i>Pipe one</i>	48
4.1.3	Currents	50
4.1.4	Comparison of the results of all pipes	50
4.1.5	Response curves for trumpet-shaped pipes	52
4.1.6	Summary	54
4.2	Reduced basin area with uniform hypsometry	54
4.2.1	Discussion of the results	54
4.2.2	Comparison with results for a straight pipe	58
4.2.3	Summary	59
4.3	Multiple equilibria for uniform hypsometry	59
4.3.1	Results	60
4.3.2	Persistence under changes in set-up conditions	60
4.3.3	Summary	64
4.4	Experiments with non-uniform hypsometry	64
4.4.1	Fixed inlay	65
4.4.2	Planar inlays	65
5	Discussion and conclusions	71
A	The Newton minimization procedure	74
B	The forcing of the sea	77
B.1	Results	77
B.2	Conclusions	79
C	Additional figures	80
C.1	The reponse of <i>Pipe two</i>	80
C.2	Multiple equilibria	81

Chapter 1

Introduction

The sea has often been an enemy in Dutch history. The Dutch history reveals of many floods bringing dead and misery, although the normal behaviour of the sea was already controllable for centuries. Many Dutch people have the last flood of February 1th 1953 close to mind. Furthermore, it urged the Dutch government to improve the flood barriers and to close deep inland sea arms.

Two processes combined to yield a flood as devastating as in 1953. Firstly, a storm surge excited by a storm depression occurred. Strong north to northwestern winds drove water southwards to the southern North Sea, and eastwards into the long sea arms of the southwest part of the Netherlands. This caused the water level to rise several meters in these arms. Secondly, the water level elevation was enlarged because the storm surge coincided with spring tide. In these sea arms, the tide can reach a tidal range up to 4 meters. The combined effects of both process resulted in strong water level elevation, which enabled wind waves to break over the dikes. The water flowing off the dike at the landside weakened the dikes, causing many dike breakthroughs.

A thorough knowledge of the tides helps to prevent that storm surges like these of 1953 cause floods. Flood prevention is one reason for investigating the tides. Tides cause strong water level elevations in many coastal and inland seas, for example the sea arms of the southwest part of the Netherlands, the North Sea (figure 1.1) or the Bristol Channel (see Defant (1961)). In contrast to storm surges, tides have a regular behaviour, the dominant tidal period is often $12^{\text{h}}25^{\text{m}}$. Tides are important for navigation, not only for sailors. Harbours like Antwerp or Rotterdam can not be entered at low tide by deep ships. Deep ships have to wait until high tide before they enter the harbour. Tides go together with tidal currents. Due to these currents, tides are important for the transport and mixing of nutrients, suspended matter and sand. The transport of suspended matter and sand by tidal currents plays an important role in the stability of sandy coasts.

Basically, tides are excited by the gravitational attracting forces of the moon and the sun. These forces are such small however, that only wide oceans show a significant response to these direct tidal forces. The resulting tidal amplitudes are not larger than 50 cm, see LeBlond & Mysak (1978). Tides in the North Sea (shown in figure 1.1) or seas, like sea arms, are excited by cooscillation with the tide in the ocean. In many cooscillating adjacent seas, tidal amplitudes increase towards the land. The best example of this amplification due to resonance is the Bay of Fundy, Canada (figure 1.2), in which tidal ranges up to 18 meters are found (see for example Defant (1961)).

The occurrence and strength of tidal amplification depends strongly on the geometry of the basin. The geometry and the frequency of the incoming tidal wave determine the location of the lines of equal tidal phase (co-tidal lines) and equal amplitude. In cooscillating seas like the North Sea, the spatial pattern of co-phase and co-amplitudes lines is rather complex. In

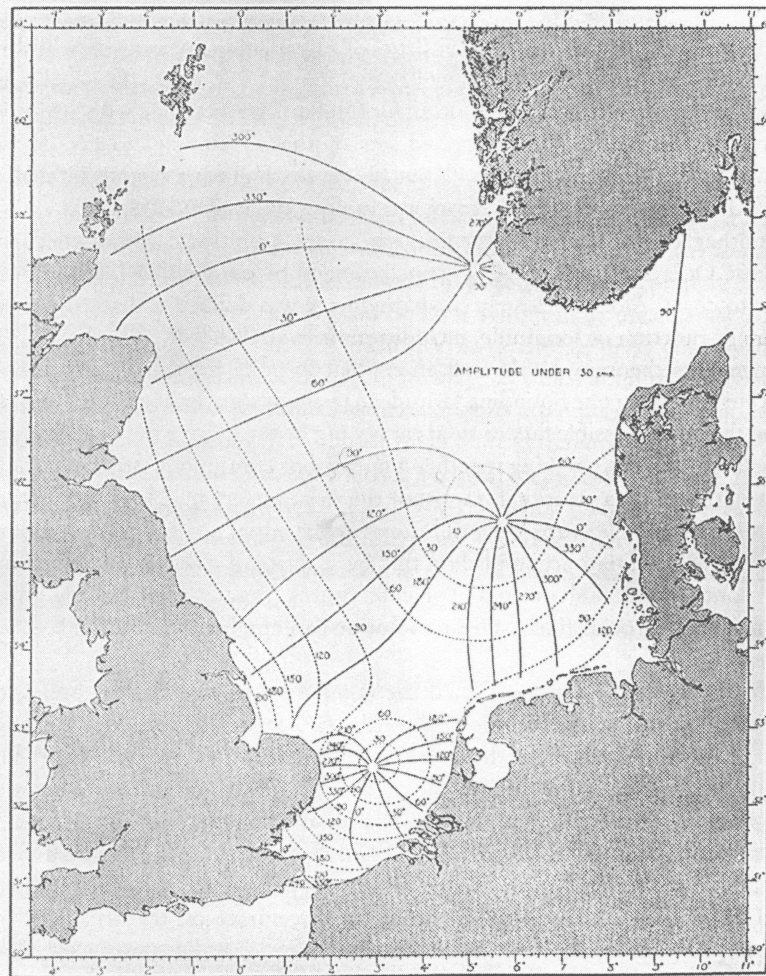


Fig. 17.—Co-tidal lines and co-range lines, denoted by full and dotted lines respectively. The associated numbers give the values of γ in degrees and of H in centimetres.

Figure 1.1: The first definitive map of the semi-diurnal lunar tide in the North Sea, computed by Proudman & Doodson (1924). Full lines are isolines of harmonic phase lag in degrees; dotted lines show harmonic amplitude in centimeters. From Cartwright (1999).

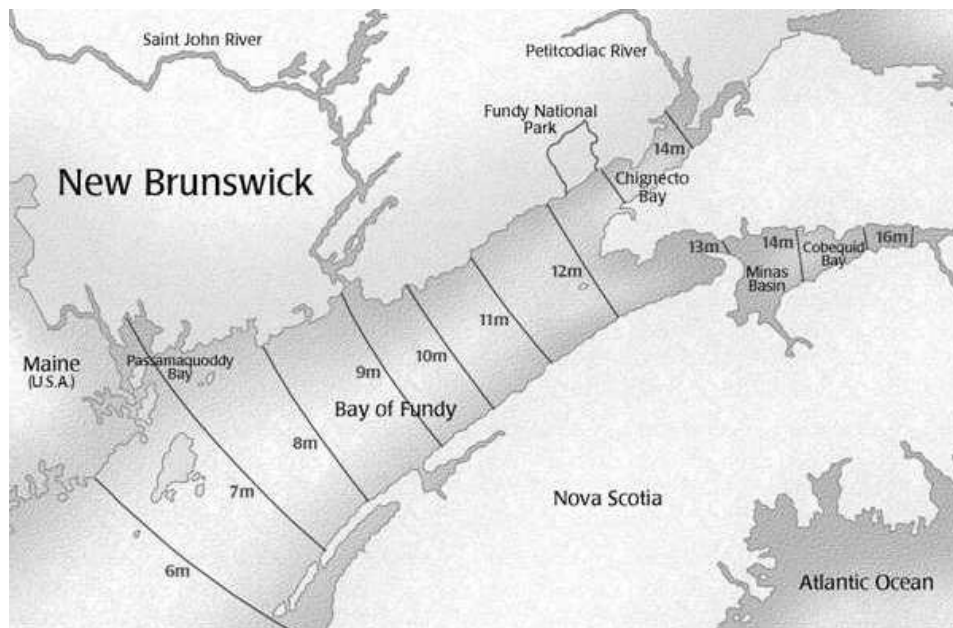


Figure 1.2: Tidal ranges in the Bay of Fundy, Canada. Source *BayofFunday.com*, Parks Canada.

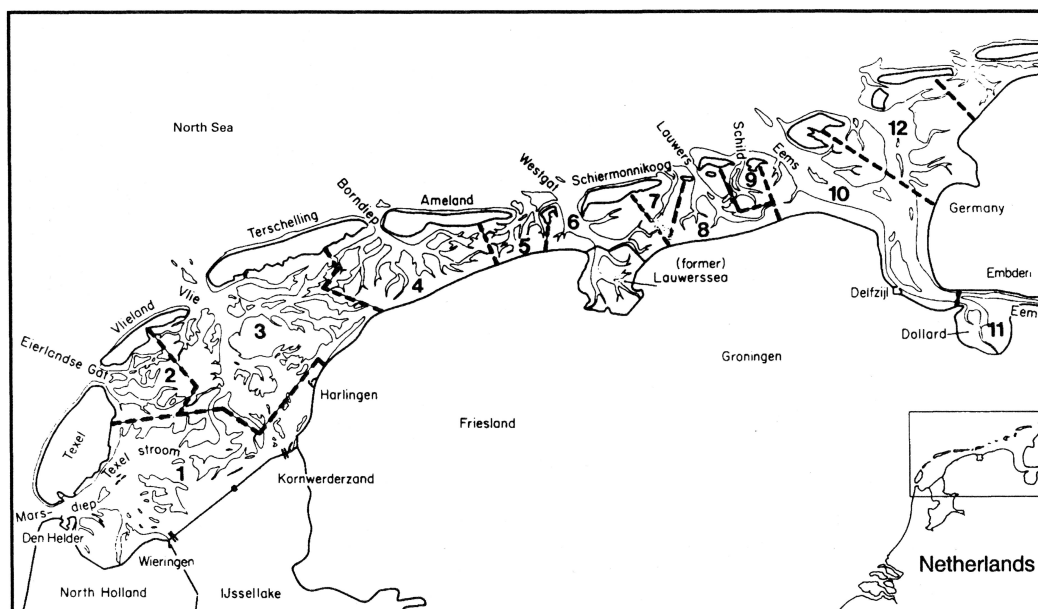


Figure 1.3: The western Wadden Sea. Contours of land and intertidals are drawn. The dashed lines divide the Wadden Sea in different compartments corresponding to one tidal inlet. For example, the tide in area (1) is forced through the Marsdiep. From Maas (1997).

funnel shaped basins, like the Bay of Fundy (figure 1.2), the pattern is more simple: the tide lags a bit towards the end of the channel, but the tidal amplitude increases strongly towards the end of the channel. The Dutch Wadden Sea (figure 1.3) has a different geometry, hence a different tidal pattern. The Wadden Sea can be divided in compartments, each compartment is connected to the North Sea through an inlet. Within the compartment, the tidal phase and amplitude differences are rather small. Within the connecting inlet these differences are much larger.

Helmholtz basins

Almost enclosed basins that are connected with the sea by a narrow channel, are *Helmholtz basins*. Examples are the basins located in the Wadden Sea, harbours with narrow entrances and fjords. The dynamics of Helmholtz basins are the subject of the present study. Helmholtz basins are characterized by their geometry: a wide basin, which is connected to the sea with a relatively narrow channel. The tide within the basin is an almost uniform sea level elevation. The tide in the basin lags the tide at sea, and the tidal amplitude in the basin can be amplified or choked. As a consequence the tidal phase and amplitude differ in the channel.

In absence of friction, the tidal amplitude in the basin grows to infinity for one certain frequency in linear approximation. This frequency is the eigenfrequency of the Helmholtz basin. The eigenfrequencies of the basins in Wadden Sea are calculated between approximately 3 hours (personal comm. Dr. H.E. de Swart) and 14 hours by Maas (1997). Because the eigenfrequencies are of similar magnitude as the tidal frequency (12 hours and 25 min.), resonance could occur in the Wadden Sea.

It appears to be possible to find a simple elegant description for the Helmholtz response, as shown in Defant (1961); LeBlond & Mysak (1978). Mei (1989) considered fjords and harbours, focussing on the response on low frequent gravity waves. But Helmholtz resonators have not been found in hydrodynamic context only. Helmholtz resonators were initially defined in acoustics. The tone excited by blowing on a bottle, is a Helmholtz response in this original context.

Geophysical Helmholtz basins are found in nature and have been investigated. But less comparable laboratory experiments were found. Lee (1971) did experiments with Helmholtz resonators, but only linear behaviour and linear friction are investigated. In Mei (1989), some experiments with harbour response on incident waves were discussed. Amplification was found close to the eigenfrequency.

Experiments with non-hydrographical Helmholtz resonators have been performed as well. For example, Wack (1985) describes an experimental set-up for acoustic Helmholtz resonators.

Recent theoretical work

Two different aspects of Helmholtz basins have been investigated in recent years. The first aspect is a further analysis of damping.

The response of Helmholtz basins can be influenced by two types of damping. Radiation damping by the emission of waves is the first damping mechanism. Zimmerman (1992) derived the response of Helmholtz basin that is damped by radiation damping. In most Helmholtz basins, however, radiation damping is much weaker than damping due to bottom friction. Damping due to bottom friction depends quadratically on the current velocity, therefore it introduces nonlinearity in the system. Because of this, the tide interacts with overtones, which has been observed as well. This nonlinearity makes the response of a Helmholtz basin no longer analytically tractable. A method to deal with this problem was developed by Lorentz (1922), who introduced a linearization method. This method were applied on the Helmholtz resonator by Zimmerman (1992).

Secondly, the effect of intertidal area (i.e. areas that fall dry during low water) on the response has been investigated. The presence of intertidal areas cause the hypsometry to be non-uniform, i.e. the wetted area of the basin is not constant during the tidal period. Green (1992) showed that non-uniform hypsometry introduce overtides and adjustment of the effective eigenfrequency. Maas (1997) compared these results with tidal responses in the Wadden Sea. Furthermore, he investigated the nonlinear behaviour of tidal motion in Helmholtz basins and showed the existence of multiple equilibria — several response regimes under the same forcing conditions — and chaotic behaviour with numerical models. The different chaotic behaviours of a nonlinear Helmholtz resonator was studied by Doelman *et al.* (2002). Finally, Terra *et al.* (2003) extends these results to all coastal basins cooscillating with a sea, of which the Helmholtz basin is a special case.

Objectives of this study

With the recent development of new theory, described above, the need emerged for experiments to verify the predictions from this theory. The present study is meant to fill this lack of experimental data. From this general purpose, the following goals are specified.

- Verification of the existence of a Helmholtz resonator in an experimental environment. In particular, amplification of the tide in a Helmholtz system is expected.
- Verification of the Lorentz-linearization principle for bottom friction. The theory of a Helmholtz system in which bottom friction is linearized, predicts increasing damping of the response for increasing tidal amplitude. This prediction is tested by experiments.
- Investigation of the effect of non-uniform hypsometry on the response of a Helmholtz basin to tidal forcing. Different nonlinear phenomena are expected. Firstly, the weakly nonlinear effect of non-uniform hypsometry on the effective eigenfrequency and the introduction of overtides are considered. Secondly, the presence of multiple equilibria for stronger modification of the effective eigenfrequency is investigated. Finally, the possible occurrence of chaotic behaviour of the nonlinear Helmholtz resonator is investigated.

Overview of subsequent chapters

In chapter 2, the theoretical response of a Helmholtz resonator is discussed. The chapter starts with a description of the excitation of tides by moon and sun, followed by the propagation of the tidal wave into coastal seas like the North Sea. Subsequently, equations of motion for the frictionless Helmholtz resonator are derived as a special case of a half open channel. The equations for frictionless Helmholtz resonator are extended with bottom friction and the Lorentz-linearization principle is elucidated. Finally, the nonlinear effects of a non-uniform hypsometry are discussed briefly.

In chapter 3, the experimental set-up, measurement technique and data analysis are discussed. Furthermore, the procedure used to compare theoretical predictions with measurements is discussed. This chapter ends with a description of numerical models that have been used.

Chapter 4 deals with the comparison of the experimental results with theoretical predictions. Experiments under different experimental conditions have been performed, in large and small basins, with uniform and non-uniform hypsometry. A discussion of the results and recommendations for future research end the paper. Some lengthy technical material can be found in three appendices.

Chapter 2

Theory

The theory describing the response of a (nonlinearly) damped Helmholtz resonator, is described in this chapter. Before narrowing the subject down to Helmholtz resonators, the theory of tide generation in the oceans and tidal wave propagation into adjacent seas, like the North Sea, is briefly discussed in the next section. Furthermore, a qualitative introduction of the Helmholtz resonator and some related phenomena that have been observed, is given in section 2.1.2.

The introduction of the theory concerning the Helmholtz resonator consist of three steps. The first step of the analysis, dealt within section 2.2, is a derivation of the free response of a channel that is open to the sea at one side. Firstly, the response of a channel with constant width is derived, secondly, the response of a channel that consist of two parts with different widths, is derived. Next, the response of a Helmholtz basin is shown as a special case of that latter channel. In the second step, see section 2.3, the linearization procedure of bottom friction by Lorentz (1922), is considered. The linearized damping term is added to the equations of motion describing the free response . The resulting system is analyzed and the response curves within the basin will be shown. In the response curves, the tidal amplification and phase lag of the tide in the Helmholtz resonator is shown as a function of the tidal frequency. Section 2.4 deals with the third step, is a brief discussion of the nonlinear effects introduced by intertidals. Intertidals cause the basin area to depend on the water level elevation, which leads to a nonlinear response on the addition of water. The weakly nonlinear response equations are given and possible response phenomena will be discussed.

2.1 General theory of tides

2.1.1 Generation of tides

It is commonly known that the moon and the sun are the primary causes of tidal motion in the sea. However, the exact physical mechanism is less straightforward as is often assumed. The forcing mechanism of the tide and the function of long waves are discussed *briefly* in this section, only the main ideas are mentioned. In Defant (1961); LeBlond & Mysak (1978) a.o., a complete description is given.

Tidal forces

The earth and the moon, or the earth and the sun, rotate around their common centre of mass. The centrifugal force accelerates the earth away from the moon (or sun); the attractive gravitational force pulls the earth to the moon or sun. At the centre of the earth, the attractive force and the centrifugal force balance, as shown in figure 2.1. The centrifugal

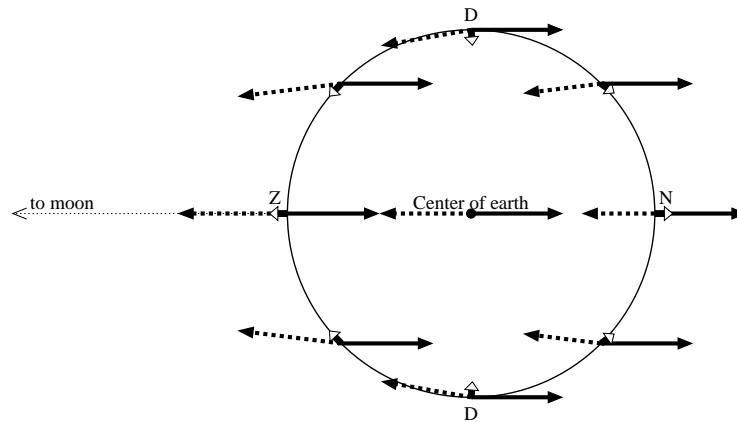


Figure 2.1: Sketch of tide-generating force. The centrifugal force (solid arrow) is equal for each location on earth. The attraction to the moon (or sun, dashed arrow) depends on the location. The tide-generating force (arrow with open hat) is the residual of both.

force is equal for each point on the earth, but the attractive force differs at each point on the earth. The direction and strength of the attractive force depend on the position with respect to the moon. The attractive force is slightly stronger at the zenith (Z) and little weaker at the nadir (N). Moreover, the direction of the attractive force is not exactly opposite to the centrifugal force everywhere; the largest deviation is at point D in the figure. As a consequence, the centrifugal and attractive force do not balance at the surface of the earth, hence a residual force remains.

This residual force is directed vertically (with respect to the surface of the earth) at Z, N and D. This leads to a correction to the local gravity. This correction is negligible, due to the small magnitude of the residual force in comparison to gravity. Between Z and D (and between N and D too), the tide-generating force has a horizontal component as well. This horizontal component is small, but of similar magnitude as other forces acting in the horizontal direction. This horizontal force drives the tide.

The horizontal component drives ocean water to the zenith and the nadir. The equilibrium is the equilibrium tide, in which the pressure gradient, due to water elevation differences, and the tide-generating force balance. The equilibrium tide however is never reached. The positions of the zenith and nadir move over the earth's surface, due to the rotation of the earth. The equilibrium tide hence must move as a wave along the equator to stay in equilibrium. However, this wave cannot exist, the continents block the propagation of this wave. Moreover, the requested wave speed exceeds the maximum wave speed that can occur in the ocean; the ocean is not deep enough¹.

Tidal forces are still exposed on the oceans. The tidal potential — the level of uniform total gravity — is a useful quantity for the calculation of the magnitude and direction of these forces. Furthermore, a complex harmonic analysis of the tidal potential elucidates the effects of the declination and ellipticity of the orbit of the moon and the earth. This declination and ellipticity cause weaker tidal components with deviating periods.

Free waves

Before investigating the tidal pattern in a basin or ocean, the free waves in such basin or ocean will be considered here. Free waves are those waves that exist if no forcing is applied

¹The wave of the equilibrium tide needs a wave speed of 0,45 km/sec to remain in equilibrium. A ocean depth of app. 21 km is requested to allow that wave speed.

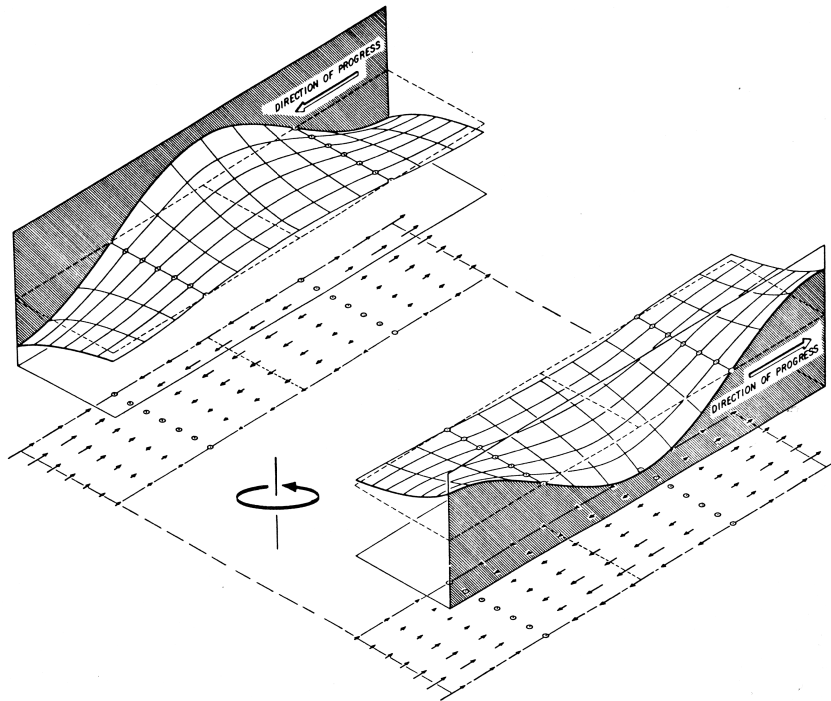


Figure 2.2: Sketch of a Kelvin wave in a wide channel for the Northern Hemisphere. The surface elevation decreases exponentially away from the coast for wide channels, consistent with a geostrophic balance. This implies that Kelvin waves propagate with the coast on their right in the northern hemisphere. From Gill (1982).

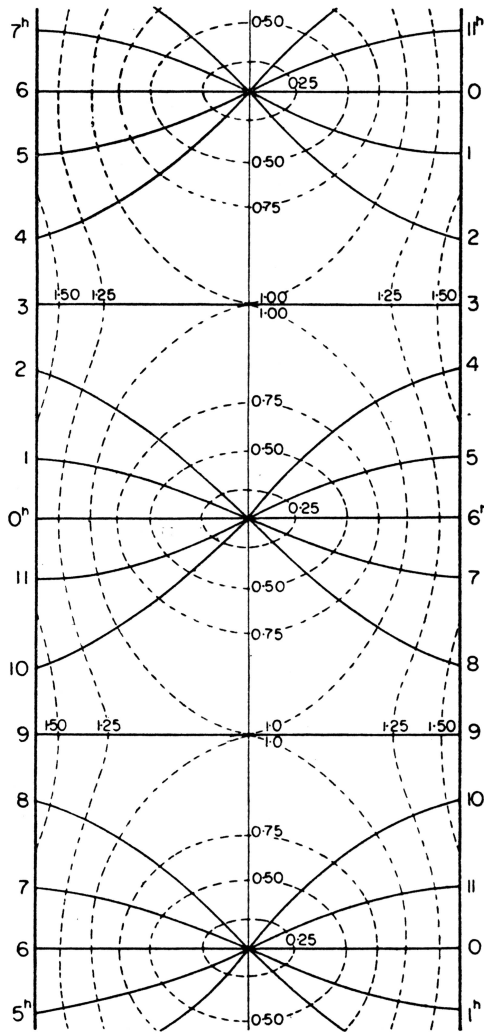
and friction is neglected. If a free wave with a frequency close to a harmonic tidal component exists, the amplitude of that tidal component is strong, but if this frequency difference is large, the tidal response is weak. However, in case of complex geometries, computation of the free waves is not evident.

As shown in LeBlond & Mysak (1978) a.o., free tidal waves in the ocean can be basically described as superpositions of Kelvin and Poincaré waves.

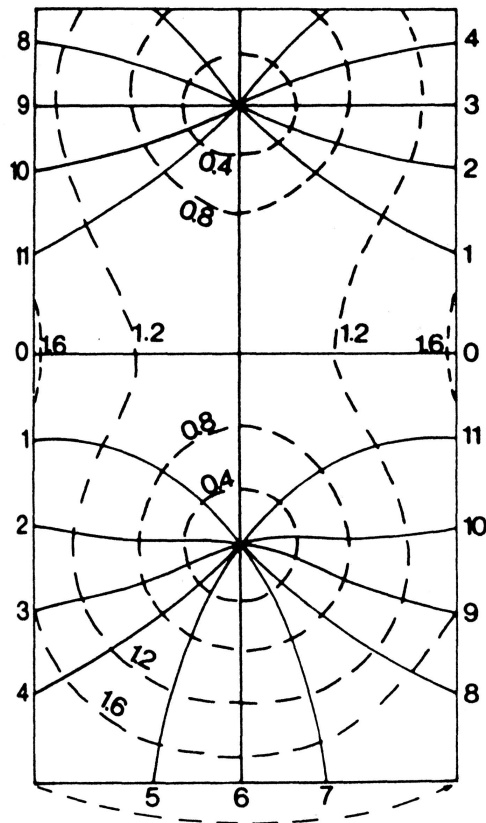
Kelvin waves are determined by a balance between the water surface inclination and the water parcel velocity. This means, Kelvin waves are in geostrophic balance. Figure 2.2 shows two free Kelvin waves travelling through a wide² and infinite long channel with constant depth. In this figure, the exponential decay of the Kelvin wave amplitude away from the coast is visible. Kelvin waves are barotropic waves, which means the water velocity is equal for the whole water column. Within the Kelvin wave, there is no cross-channel motion. If the infinite channel becomes narrower (figure 2.3(a)), amphidromic points are found between the two Kelvin waves. At these amphidromic points the tidal amplitude is zero, while the phase rotates counterclockwise around this point for the northern hemisphere.

If the channel is closed at one side, Poincaré waves are excited to reflect the Kelvin waves. An example of the wave pattern at the channel end for a certain frequency is given in figure 2.3(b). Poincaré waves are defined as waves that are determined by the inertia of the wave motion and the wave frequency. They exist as barotropic and baroclinic waves, which means that the waves have a non-uniform vertical structure. Poincaré waves are generated near

²Wide means that the channel width is much larger than the length by which Kelvin waves decay exponentially



(a) Superposition of two Kelvin waves travelling in opposite directions in a channel with uniform rectangular section. From Defant (1961)



(b) The amphidromic pattern near the closed end of a channel for a reflected Kelvin wave. From LeBlond & Mysak (1978)

Figure 2.3: Tidal waves in a open and halfclosed channel. Period 12 h. Solid lines are co-phase lines, dashed lines are co-amplitude lines.

the coast, the amplitude decays exponentially with increasing distance to the coast.

As shown by the previous examples, wave patterns can be derived analytically for simple geometries. Wave patterns for an ocean with a complex coast line and varying depth are not analytically tractable. These wave patterns can be derived only by numerical models. Although these wave patterns are more complex than for simple geometries, characteristics of Kelvin or Poincaré waves can be recognized in this wave pattern. Because basically this complex wave pattern is a superposition of many Kelvin and Poincaré waves.

Cooscillation

Tides in the ocean are close to free wave response on tidal forces excited by moon and sun. Seas like the North Sea, however, are too small to excite a significant tidal wave directly from the tidal forces. The tide in the North Sea, figure 1.1, is a result of cooscillation with the tide in the ocean. The tidal waves in adjacent seas like the North Sea consist of Kelvin and Poincaré waves as well, but they are driven by the incoming tidal wave from the ocean.

The relatively large tidal amplitude in the North Sea is caused by resonance of the tidal wave in the southern North Sea. The tidal wave, travelling southward as a Kelvin wave along the English coast, can rotate around an amphidromic point in the southern North Sea in the prescribed period. If the tidal wave does not resonate, the tidal amplitude in the North Sea would be much smaller.

This resonance can be compared with a swing. The wave rotating around the amphidromic point is the swing and the Kelvin wave from the North is the rhythmic push that starts the swing oscillating. If the rhythm of pushing is equal to the period the swing needs to make one oscillation, the amplitude of the swing grows. If the push rhythm and swing period are not equal, the swing does not get a large amplitude.

2.1.2 The Helmholtz resonator

In the previous section, the tidal response of adjacent seas like the North Sea was discussed. Resonance of the tidal frequency is an important component for the tidal amplitude occurring in these seas. The geometry of the sea determines strongly if the tide can be amplified.

The Helmholtz resonator, which is investigated in the experiments that are discussed in this report, is a coastal structure. In coastal structures, resonance to the tidal frequency could cause strong tides, where in contrast, the lack of resonance leads to only a weak tide. Examples of coastal structures are estuaries, fjords and harbours. Usually, the extents of these coastal structures are much smaller than the tidal wavelength of the outer sea. Therefore, there will be mainly a local response near the coastal structures and not a significant response of the whole sea. As already mentioned, the local effects can be strong, depending on the dominant tidal frequency and on the local geometry.

The Helmholtz resonator is characterized by its spatial shape. It consists of a basin that is connected with the sea by a narrow channel. An example is the Western Wadden Sea (figure 1.3), figure 2.4 is a general sketch. In the basin, the tide can be amplified, the basin can resonate on the tide of the sea.

The tidal response of a Helmholtz resonator has a characteristic spatial shape as well. The tide is nearly uniform in the basin, so the tidal amplitude and the tidal phase are nearly equal for the whole basin. Furthermore, the currents in the channel are much stronger than the currents in the basin. These currents in the channel are rather uniform in space too.

As a result of this characteristic response, a simple mathematical description of the response can be formulated. The two dimensional shallow water equations were transformed to response equations that depends only on the tidal amplitude in the basin and the sea and the phase difference between both (LeBlond & Mysak 1978). In these equations, the

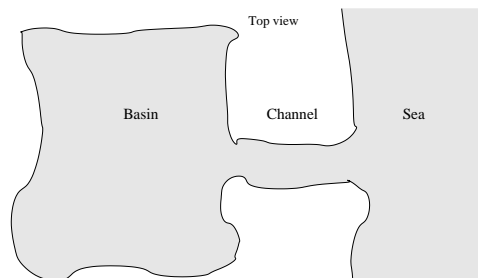


Figure 2.4: Example of a Helmholtz basin

response of a Helmholtz resonator is determined firstly by the pressure gradient between basin and sea, secondly by the inertia of the water in the channel.

Zimmerman (1992) investigated the different ways in which energy could dissipate, by radiation damping and bottom friction. In case of radiation damping, waves are emitted into the sea at the sea side of the channel. Due to this wave emission, energy is extracted from the Helmholtz resonator. The energy lost by radiation damping grows linearly with the current velocity amplitude in the channel. Dissipation due to bottom friction grows quadratically with this velocity amplitude.

If a Helmholtz basin with uniform hypsometry, i.e. a constant basin area, is considered, the tidal response is practically linear. The Wadden Sea however does not have a uniform hypsometry, intertidals cause the basin area to depend on the water level. Maas (1997) proved that this varying basin area could lead to nonlinear behaviour. This means that the tidal response could be not regular but chaotic. The influence of a non-uniform hypsometry is clarified further in section 2.4.

The nearly uniform tide in the basin and nearly uniform currents in the channel give strong arguments for the above described simplified formulation of the response of a Helmholtz resonator. Nevertheless, some observed physical phenomena remains underexposed in this simplification. The most important of them are smaller scale phenomena that occur at both pipe entrances.

The main phenomenon is the observed asymmetry between in- and outflow as shown in fig 2.5, due to advection of momentum in the channel. In the simplified mathematical description, in- and outflow phenomena are both assumed negligible. Observations in nature and in the laboratory set-up shows that the inflow is calm and spread-out but the outstream is jet-like. Firstly this causes a longer effective channel length. Secondly vortices arise at the output side of the channel. The related turbulent friction behaves quadratic to the velocity, and therefore increases the value of the bottom friction damping term. For further discussion see Maas (1997).

Summarizing the theoretical knowledge of Helmholtz basins, the tidal response of Helmholtz basins with (non-)uniform hypsometry could be predicted precisely. The value of these response predictions however must be tested by experiments.

2.2 Derivation of the free Helmholtz reponse

The mathematical analysis of the Helmholtz system contains several steps. At first, the free response of a half-open channel with constant width is derived. Secondly, this system is extended to a half-open channel with two widths. This system is, under conditions which

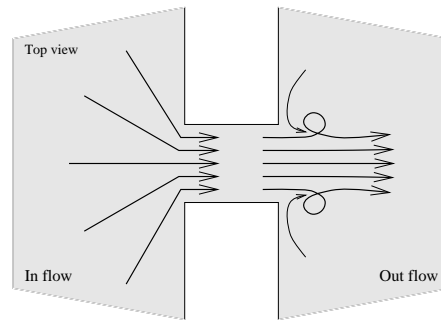


Figure 2.5: In and outstream differences of a Helmholtz basin

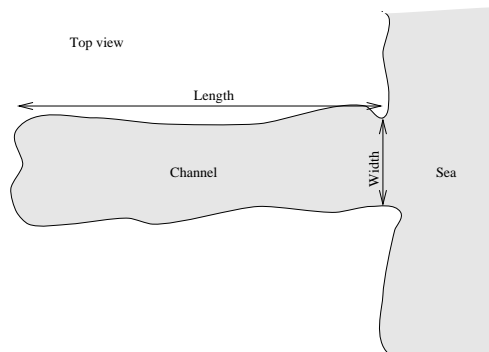


Figure 2.6: Example of a coastal channel

are mentioned there, a Helmholtz resonator. The typical response shape of a Helmholtz resonator is found as limit behaviour. This knowledge is used to derive the Helmholtz response directly from the one-dimensional, linearized frictionless shallow water equations. This section ends with a discussion of adjustments which can be made for including friction or a water level depending basin area.

2.2.1 First assumptions

Tidal motion in channels or bays is caused by their co-oscillation with the outer sea. First co-oscillation in a channel, closed at one side, will be investigated. Next the response of a channel with two different widths will be defined. The Helmholtz resonator will be subsequently obtained as limit behaviour of this two widths system. Derivations of the Helmholtz equations and the typical responses can be found in for example LeBlond & Mysak (1978); Mei (1989) or Zimmerman (1992).

The channel, (see figure 2.6), has a length L and width B , and assume that the channel depth H is small with respect to its length and width. In that case the shallow water approximation may be used. Furthermore Coriolis terms are neglected, since the scales of the channel are assumed to be smaller than the Rossby deformation scale \sqrt{gH}/f , in which g denotes the gravitational acceleration and f the Coriolis parameter. Further the channel width B is small in comparison to its length L , thus all derivatives in width direction may be neglected and all currents in perpendicular direction will vanish. As a result the one dimensional shallow water equations are the starting point for further derivations, in which, for the moment, friction and nonlinear advection effects are also neglected.

2.2.2 The response of a half-open channel

The one-dimensional, linearized frictionless, inviscid shallow water equations are

$$\frac{\partial u}{\partial t} = -g \frac{\partial \zeta}{\partial x} \quad (2.1)$$

$$\frac{\partial \zeta}{\partial t} + H \frac{\partial u}{\partial x} = 0. \quad (2.2)$$

In these equations u denotes the current speed, t time and ζ the water elevation. The left side (where $x = 0$) of the channel is closed, no currents may appear, $u = 0$ at $x = 0$. The right side (where $x = L$) of the channel has contact with the sea, therefore the water elevation is prescribed at $x = L$. The second boundary condition becomes, with using the tidal signal, $\zeta = \tilde{Z} \cos(\omega t)$ at $x = L$.

Elimination of u gives

$$\frac{\partial^2 \zeta}{\partial t^2} - gH \frac{\partial^2 \zeta}{\partial x^2} = 0, \quad (2.3)$$

with boundary conditions at $x = 0$: $\partial \zeta / \partial x = 0$ and at $x = L$: $\zeta = \tilde{Z} \cos(\omega t)$.

The nontransient solution of this equation has the form

$$\zeta = Z(x) \cos(\omega t). \quad (2.4)$$

Using this expression gives (with $k = \omega / \sqrt{gH}$)

$$k^2 Z(x) + \frac{d^2 Z(x)}{dx^2} = 0 \quad (2.5)$$

and boundary conditions $dZ/dx = 0$ at $x = 0$ and $Z = \tilde{Z}$ at $x = L$. This relation³ has the general solution

$$Z(x) = A \sin(kx) + D \cos(kx). \quad (2.6)$$

The boundary conditions fix A and D :

$$\begin{aligned} A &= 0 \\ D &= \frac{\tilde{Z}}{\cos(kL)}. \end{aligned} \quad (2.7)$$

Combining (2.4), (2.5) and (2.7) yields the nontransient solution for ζ :

$$\zeta(x, t) = \frac{\tilde{Z}}{\cos(kL)} \cos(kx) \cos(\omega t). \quad (2.8)$$

Equation (2.8) gives the spatial shape and the time evolution of the response in the channel. If the a forcing is applied, the surface elevation ζ goes for certain frequencies to infinity, when $\cos(kL)$ in the latter equation becomes zero. For these (eigen)frequencies the concerning reponse shape (mode) with a limited amplitude, can exist without forcing as well. An example of a mode is shown in figure 2.7. The mode with only one crest, the quarter wavelength response, has the lowest eigenfrequency, all other possible modes, with a higher number of crests, have a corresponding eigenfrequency which is a multiple of the quarter wavelength corresponding eigenfrequency.

The eigenfrequencies σ can be defined as the corresponding ω which satisfy the relation:

$$\sigma = \frac{\sqrt{gH}}{L} (n + 1/2)\pi \quad \text{for } n = 0, 1, 2, \dots \quad (2.9)$$

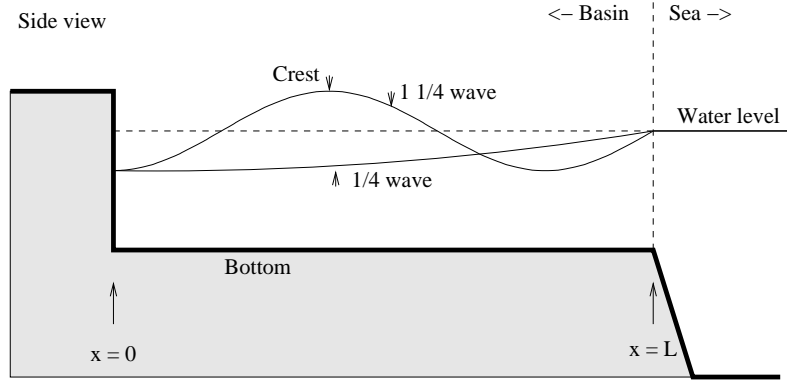


Figure 2.7: Example of wave modes

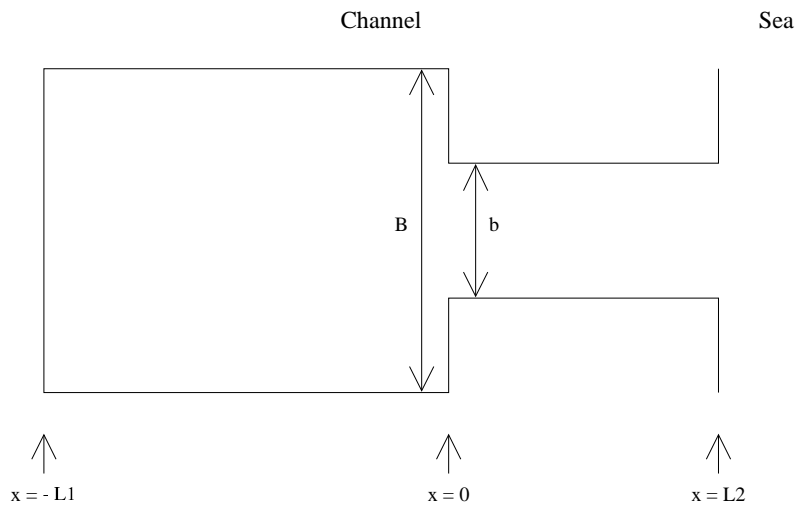


Figure 2.8: Sketch of an embayment that is connected to the sea by a channel.

2.2.3 Response of channels with 2 widths

The system of a half-open channel can be extended easily to a channel with two different widths, as shown in fig 2.8. The assumptions made in section 2.2.1 are assumed to be still valid for the whole channel. The index $_1$ or $_2$ indicates if the property is defined for the landward side, in case of value 1, or 2 for the right sea-side. B is the width of channel part 1, b of channel part 2. For both sides equations (2.1) and (2.2) remain valid. In this situation there are four boundary conditions. They read

$$\begin{aligned} u &= 0, & \text{at } x = -L_1, \text{ the coastal boundary,} \\ \zeta &= \tilde{Z} \cos(\omega t), & \text{at } x = L_2, \text{ matching with the external sea level} \\ \text{and where the two channel parts connect two matching conditions:} & & (2.10) \\ \zeta|_{x \uparrow 0} &= \zeta|_{x \downarrow 0}, & \text{the water elevation is continuous,} \\ H_1 B u|_{x \uparrow 0} &= H_2 b u|_{x \downarrow 0}, & \text{the mass flux is preserved.} \end{aligned}$$

The nontransient solution of shallow water equations (2.1) and (2.2), valid for both channel parts, is (2.4), with (2.5) as the equation for $Z_i(x)$. The general solution of this last equation for each $Z_i(x)$ is $A_i \sin(k_i x) + D_i \cos(k_i x)$.

The boundary conditions (2.10) transform to:

$$\begin{aligned} 0 &= \left. \frac{dZ_1}{dx} \right|_{x=-L_1} = A_1 \cos(k_1 L_1) + D_1 \sin(k_1 L_1) \\ \tilde{Z} &= Z_2|_{x=L_2} = A_2 \sin(k_2 L_2) + D_2 \cos(k_2 L_2) \\ 0 &= Z_1|_{x=0} - Z_2|_{x=0} = D_1 - D_2 \\ 0 &= \left. \frac{H_1 B}{H_2 b} \frac{dZ_1}{dx} \right|_{x=0} - \left. \frac{dZ_2}{dx} \right|_{x=0} = A_1 - \frac{A_2}{J}, \end{aligned} \quad (2.11)$$

in which

$$J = \frac{H_1 B k_1}{H_2 b k_2} = \frac{H_1^{1/2} B}{H_2^{1/2} b}. \quad (2.12)$$

Combining these boundary conditions the value of all integration constants are obtained, such as

$$D_2 = \frac{\tilde{Z} \cos(k_1 L_1)}{\cos(k_1 L_1) \cos(k_2 L_2) - J \sin(k_1 L_1) \sin(k_2 L_2)}. \quad (2.13)$$

When the denominator of (2.13) becomes 0, all amplitudes A_1 , A_2 , D_1 and D_2 , hence the surface elevations ζ , grow to infinity. At these forcing frequencies the channel resonates. The resonance condition can be written as

$$\tan(k_1 L_1) \tan(k_2 L_2) = \frac{1}{J}. \quad (2.14)$$

Dependence of the eigenfrequency on the b/B ratio

In order to illustrate the dependence on the width ratio b/B , assume $H_1 = H_2$ and $L_1 = L_2$. In that case the analytical solution reads

$$\sigma \frac{L}{\sqrt{gH}} = \arctan \left(\pm \sqrt{\frac{b}{B}} \right) + n\pi \quad \text{for } n = 0, 1, 2, \dots \quad (2.15)$$

³When the spatial dimensions are increased, equation (2.5) becomes the Helmholtz equation $(k^2 + \nabla)\phi = 0$, in which ϕ the spatial shape of the wave is.

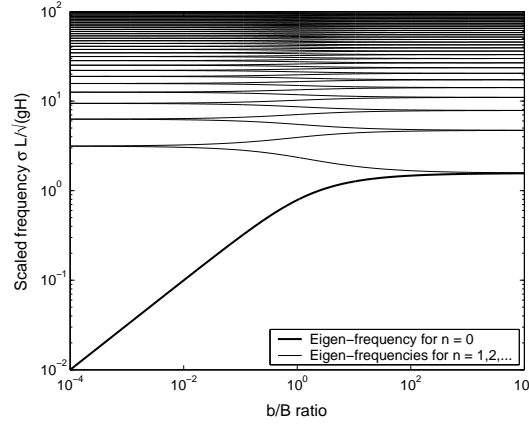


Figure 2.9: Eigenfrequencies for different $\frac{b}{B}$ ratios.

Figure 2.9 shows the behaviour of the dimensionless eigenfrequencies as function of the ratio b and B . For $\frac{b}{B} \gg 1$ the eigenfrequencies coincide with these for a half-open channel with length L_2 and depth H_2 , the effect of the narrow landside channel part is negligible. For $b = B$ the eigenfrequencies are equal to the eigenfrequencies belonging to a channel with length $2L_1$, width B and depth H . For $\frac{b}{B} \ll 1$ the higher order eigenfrequencies approach those for a closed basin with length L_1 and H_1 . The lowest eigenfrequency decreases to zero and separates from higher frequencies. This low frequency mode is the pumping mode of the Helmholtz system.

2.2.4 The Helmholtz mode

For analysing the behaviour of the Helmholtz mode, consider in equation (2.14) the situation that $b \ll B$, $k_1 L_1$ and $k_2 L_2 \ll 1$. The seaward channel part has thus a small width in comparison to the landward part, which is therefore denoted as basin. Besides, the tidal wavelength is set long in comparison to the length of the channel and the basin. First the eigenfrequency is determined.

With the consideration that $k_i L_i \ll 1$, the function $\tan(k_i L_i)$ in equation (2.14) becomes approximately $k_i L_i$, which leads to

$$k_1 L_1 = \frac{1}{J k_2 L_2}. \quad (2.16)$$

This can be reformulated, with $k_i = \omega / \sqrt{g H_i}$ and J as defined in equation (2.12), as

$$\omega = \sqrt{\frac{g H_2 b}{L_1 B L_2}} = \sqrt{\frac{g O}{L_2 A}} = \sigma_H \quad (2.17)$$

The eigenfrequency σ_H of the Helmholtz mode is hence defined. The relevant quantities for the eigenfrequency are reformulated, with $O = H_2 b$, the cross section of the connecting channel and $A = L_1 B$, the basin area.

Next, the response functions Z_i , and hence ζ and u (2.4), are derived. Since $k_1 L_1$ and $k_2 L_2 \ll 1$, Z_i (2.6) and the corresponding boundary conditions (2.11) can be simplified by using Taylor expansion (to first order):

$$\begin{aligned} Z_i(x) &= A_i \sin(k_i x) + D_i \cos(k_i x) \approx A_i k_i x + D_i \\ \frac{dZ_i(x)}{dx} &= k_i A_i \cos(k_i x) - k_i D_i \sin(k_i x) \approx k_i A_i - k_i^2 D_i x \end{aligned} \quad (2.18)$$

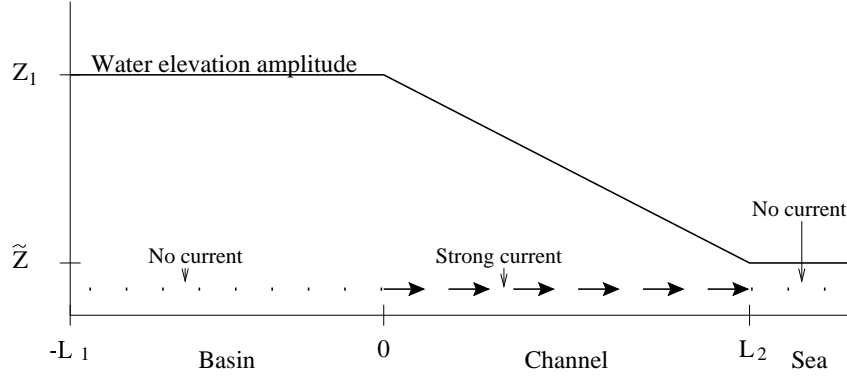


Figure 2.10: A sketch of the amplitude of the free surface and the behaviour of the current in the Helmholtz mode.

$$\begin{aligned}
 0 &= A_1 \cos(k_1 L_1) + D_1 \sin(k_1 L_1) \approx A_1 + D_1(k_1 L_1) \\
 \tilde{Z} &= A_2 \sin(k_2 L_2) + D_2 \cos(k_2 L_2) \approx A_2(k_2 L_2) + D_2 \\
 0 &= A_1 - \frac{A_2}{J} \\
 0 &= D_1 - D_2.
 \end{aligned} \tag{2.19}$$

This leads to

$$\begin{aligned}
 Z_1 &= \frac{\tilde{Z}}{1 - \frac{\omega^2}{\sigma_H^2}} \\
 Z_2 &= \tilde{Z} \frac{x}{L_2} + Z_1 \left(1 - \frac{x}{L_2}\right) \\
 \frac{dZ_1}{dx} &= 0 \\
 \frac{dZ_2}{dx} &= \frac{\tilde{Z} - Z_1}{L_2}.
 \end{aligned} \tag{2.20}$$

Figure 2.10 shows the behaviour of the amplitude of ζ and u . The velocity field u is related to ζ by (2.1). Note that due to the infinite width of the basin, the velocity field in the basin is zero in the first-order solution. The second-order component of the velocity field, which is not derived here, contains a linear increase towards the channel. The total mass transport through the entire width of the basin increases linearly as well and becomes equal to the total mass transport through the channel where the channel connects to the basin.

Important to note for the derivation of the response of Helmholtz basins is that the surface elevation is spatially uniform in the basin. Similarly, the current is spatial uniform in the channel.

2.2.5 Derivation of the Helmholtz response equations

In the preceding sections, the Helmholtz mode was shown to exist for basins connected to the sea by a channel. The necessary conditions are that the channel width is small compared to the width of the basin, and the tidal wavelength $2\pi\sqrt{gH}/\omega$ is longer than the lengths of channel and basin. Furthermore it was shown that for the Helmholtz mode the surface elevation ζ in the basin and the velocity u in the channel are nearly uniform.

Under these conditions the one-dimensional shallow water equations (2.1) and (2.2) can be simplified to capture the Helmholtz mode: integration of equation (2.1) over the channel,

where u is constant, leads to

$$0 = \int_0^{L_2} \left(\frac{\partial u}{\partial t} + g \frac{\partial \zeta}{\partial x} \right) dx = L_2 \frac{\partial u_c}{\partial t} + g [\zeta]_0^{L_2} = \frac{\partial u_c}{\partial t} + \frac{g}{L_2} (\zeta_s - \zeta_b), \quad (2.21)$$

in which $\zeta_b = Z_1 \cos(\omega t)$, the water elevation in the basin.

Integration of equation (2.2) over the basin, where ζ is constant, leads to

$$0 = B \int_{-L_1}^0 \left(\frac{\partial \zeta}{\partial t} + H \frac{\partial u}{\partial x} \right) dx = A \frac{\partial \zeta_b}{\partial t} + [BH u]_{-L_1}^0 = \frac{\partial \zeta_b}{\partial t} + \frac{O u_c}{A}. \quad (2.22)$$

The two derived equations describe the response of a Helmholtz system. Now, a few indices will be removed: $L_2, H_2, u_c \rightarrow L, H, u$.

Note that $\zeta \ll H$ has been neglected in the latter equation (2.22), otherwise O could not be considered to be constant. This amounts to representing the channel by a pipe with constant cross section O .

2.2.6 Possible extentions

Without changing the validity of the general derivation of the Helmholtz equations they can be extended with various physical phenomena. The most important of these extensions is the incorporation of quadratic bottom friction. This friction, caused by turbulent effects, commonly Maas (1997); Zimmerman (1992) parameterized as a deceleration term

$$\frac{c_d}{H} |u|u \quad (2.23)$$

in the momentum equation. Here, c_d denotes the dimensionless drag coefficient of about $2.5 \cdot 10^{-3}$. Since u appears to be constant in the channel, this friction term may simply be added to equation (2.21). This bottom friction term can be found by dimension analysis.

An important consequence of adding a nonlinear friction term is the appearance of non-linearity in the Helmholtz equations. In the next section Lorentz' linearization will be used for making the Helmholtz equations with quadratic friction analytically tractable. In Mei (1989), Lorentz' linearization method is found under the name of equivalent linearization.

Another, commonly mentioned effect, is radiation damping, see Garrett (1975); Mei (1989); Zimmerman (1992) for a derivation. A Helmholtz resonator endures radiation damping if energy is emitted in the sea by waves. Radiation damping results in an additional linear damping term ru in equation (2.21). For a non-varying forcing amplitude the response function of a linearly damped oscillator looks rather similar to the nonlinear damped one. Therefore in some studies (Doelman *et al.* (2002)) linear friction is used.

It is also possible to consider basins with a nonuniform hypsometry. This implies that the surface area of the basin depends on the actual water level. The basin area A transforms to $A(\zeta_b)$ in which $A(\zeta_b)$ denotes the area of the basin at given surface elevation ζ_b . Green (1992) considered this first. This non-uniform hypsometry causes nonlinear behaviour of the Helmholtz equations, see Maas (1997); Doelman *et al.* (2002) for a description of this nonlinear effect. In section 2.4 the effect on the response will be discussed briefly.

In the case that quadratic bottom damping and a non-uniform hypsometry are included, the equations that describe the response of a Helmholtz basin, read

$$\frac{\partial u}{\partial t} + \frac{g}{L} (\zeta_s - \zeta_b) + \frac{c_d}{H} |u|u = 0 \quad (2.24)$$

and

$$\frac{\partial \zeta_b}{\partial t} + \frac{O u}{A(\zeta_b)} = 0. \quad (2.25)$$

They involve two nonlinear terms, the bottom friction term and the hypsometry term, which make the Helmholtz equations difficult to analyse mathematically and create the possibility for multiple non-transient solutions and chaotic behaviour.

2.3 Lorentz-linearization

In the previous section, the equations (2.24) and (2.25), with a damping term and non-uniform hypsometry, have been derived. For constant $A(\zeta_b)$ the damping term $|u|u$ is the only nonlinear term. This nonlinearity makes it difficult to obtain an analytical solution of the equations. In this section, the Lorentz-linearization method is discussed. This method linearizes the nonlinear bottom friction term, while the bottom friction remains depending on the forcing frequency and tidal amplitude.

2.3.1 Transformation of the bottom friction

Applying Lorentz-linearization means that the nonlinear bottom friction term is replaced by a suitable linear term. The condition is that the inserted friction term should satisfy the Lorentz' energy principle (Lorentz 1922), which ensures that the behaviour under changes in forcing amplitude is preserved. The Lorentz method is a multi step method, only the first step here will be done. For a more general derivation including overtides see Zimmerman (1992).

Consider the nonlinear term $(c_d/H)|u|u$ in equation (2.24). This term is replaced by a linear term λu , in which λ is a as yet undetermined friction coefficient. Obeying to the Lorentz' principle, the dissipation during one tidal period T due to the linear friction term, must be equal to the dissipation due to the original nonlinear bottom friction term. The friction coefficient λ can be calculated hence with this principle.

For the sake of simplicity, the currents in the basin and sea are assumed to be small in comparison to the currents in the channel. Therefore, the damping due to bottom friction is only considered in the channel. Note for linear friction that the velocity in the channel with amplitude a_u , caused by the sinusoidal forcing $\zeta_s = a_s \cos(\omega t + \varphi)$, is sinusoidal as well. For the nonlinear damped equation, this is only an approximation.

Mathematically, the energy dissipation of one tidal period by bottom friction is

$$\int_0^T \frac{c_d}{H} |u|u \cdot u \, dt = \frac{c_d}{H} a_u^3 \int_0^{\frac{2\pi}{\omega}} |\sin(\omega t)| \sin^2(\omega t) \, dt \quad (2.26)$$

and the energy dissipation caused by a linear term λu is

$$\int_0^T \lambda u \cdot u \, dt = \lambda a_u^2 \int_0^{\frac{2\pi}{\omega}} \sin^2(\omega t) \, dt. \quad (2.27)$$

The linear damping constant λ can be determined by setting (2.26) equal to (2.27), with the result

$$\lambda = \frac{8}{3\pi} \alpha_u \frac{c_d}{H}. \quad (2.28)$$

Substituting this result in equation 2.24 yields

$$\frac{\partial u}{\partial t} + \frac{g}{L} (\zeta_s - \zeta_b) + \frac{8}{3\pi} \frac{c_d}{H} a_u u = 0. \quad (2.29)$$

Elimination of u and a_u , by combining equation (2.29) with equation (2.25), yields

$$\frac{d^2 \zeta_b}{dt^2} + \frac{Og}{AL} (\zeta_b - \zeta_s) + \nu_0 a_b \omega \frac{d\zeta_b}{dt} = 0, \quad (2.30)$$

in which a_u is rewritten into $a_b \omega A/O$, using (2.25). Here, a_b is defined as the amplitude of the basin, so $\zeta_b = a_b \cos(\omega t)$. The (linear) friction coefficient ν_0 in this equation is

$$\nu_0 = \frac{8}{3\pi} \frac{c_d}{H} \frac{A}{O}. \quad (2.31)$$

Finally $\sqrt{Og/AL}$ can be recognized as the eigenfrequency σ_H (2.17).

2.3.2 Solutions of the Lorentz-linearized equation

In this section equation (2.30) will be solved. The results will be used to express the amplification factor of the tidal signal in the basin, relative to the signal at sea, as a function of the forcing frequency. The phase difference between the tide at sea and in the basin is derived as function of the forcing frequency.

Friction causes a phase difference between the sea and the basin, therefore a phase term φ is included in the response of the basin. This response is hence represented by $\zeta_b = a_b \cos(\omega t + \varphi)$. So, a negative phase difference φ stands for a the tide in the basin preceding that at sea. The tidal forcing in the sea remains represented by $\zeta_s = a_s \cos(\omega t)$.

Substitution of these solutions in equation (2.30) leads to⁴

$$-\omega^2 a_b \cos(\omega t + \varphi) + \sigma_H^2 \{a_b \cos(\omega t + \varphi) - a_s \cos(\omega t)\} - \nu_0 \omega^2 a_b^2 \sin(\omega t + \varphi) = 0 \quad (2.33)$$

This equation is valid for all values of t , therefore this equation is rewritten to

$$a_b(\sigma_H^2 - \omega^2) = \sigma_H^2 a_s \cos(\varphi) \quad (2.34)$$

$$-\nu_0 a_b^2 \omega^2 = \sigma_H^2 a_s \sin(\varphi) \quad (2.35)$$

Amplification factor

To obtain the relation between a_s and a_b , φ is eliminated in equations (2.34) and (2.35). The result is

$$\sigma_H^4 a_s^2 = (\sigma_H^2 - \omega^2)^2 a_b^2 + \nu_0^2 \omega^4 a_b^4, \quad (2.36)$$

from which follows

$$\frac{a_b}{a_s} = \frac{\sqrt{-(\sigma_H^2 - \omega^2)^2 + \sqrt{(\sigma_H^2 - \omega^2)^4 + 4\nu_0^2 \omega^4 \sigma_H^4 a_s^2}}}{\sqrt{2}\nu_0 \omega^2 a_s}. \quad (2.37)$$

Before this equation is visualized graphically, the phase difference φ is determined as well.

Phase difference

The phase difference φ of the tidal signal between the sea and the basin can be derived from equations (2.34) and (2.35). The phase difference φ is defined to be between $[-\pi, \pi]$. Equation (2.35) causes φ to be between $[-\pi, 0]$; since $\nu_0 \omega^2 a_b^2$ and $\sigma_H^2 a_s$ are positive. Similarly, equation (2.34) leads for $\omega \leq \sigma_H$ to $\varphi \rightarrow [-\pi/2, 0]$ and for $\omega \geq \sigma_H$ to $\varphi \rightarrow [-\pi, -\pi/2]$.

In order to describe φ with forcing quantities, the response amplitude a_b is eliminated by using equation (2.37). The result is

$$\sin \varphi = \frac{\left(\frac{\sigma_H}{\omega} - \frac{\omega}{\sigma_H}\right)^2 - \sqrt{\left(\frac{\sigma_H}{\omega} - \frac{\omega}{\sigma_H}\right)^4 + 4\nu_0^2 a_s^2}}{2\nu_0 a_s}. \quad (2.38)$$

⁴A ‘dispersion relation’ for ω can be derived if complex functions are substituted in equation (2.30). In that situation, ζ_b is represented by $\alpha e^{i\omega t}$ and ζ_s by $\alpha_s e^{i\omega t}$, in which α and α_s denote complex tidal amplitudes. The complex phase between α and α_s gives the phase difference between the sea and basin. These functions contrast with the fact that ζ is a real quantity, but simplify strongly the mathematical analysis.

The ‘dispersion relation’ reads

$$(\sigma_H^2 - \omega^2 + i\nu_0 \omega^2 |\alpha|) \alpha = \sigma_H^2 \alpha_s. \quad (2.32)$$

The amplification factor (2.37) and phase difference (2.38) can be derived easily from this ‘dispersion relation’. The relation is given as well, because the mathematical analysis of the effect of hypsometry in section 2.4 uses also complex functions.

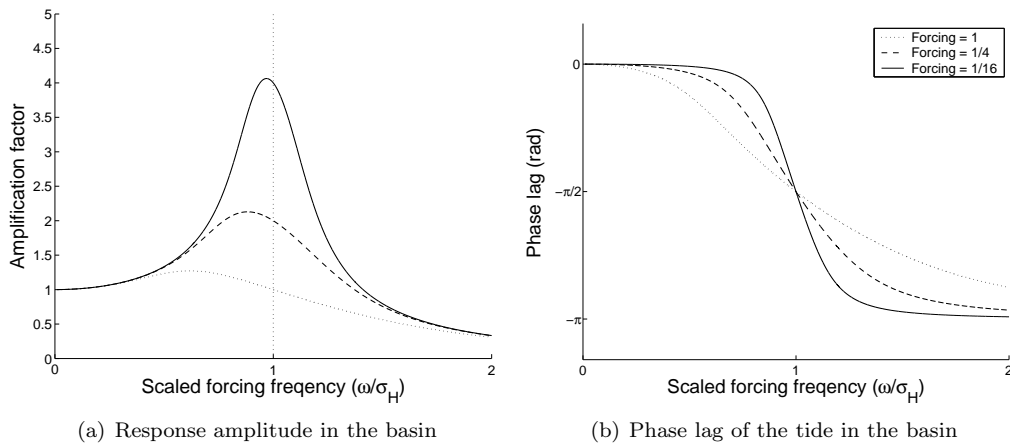


Figure 2.11: Example of theoretical quasi-linear response curves.

2.3.3 Response functions

In the previous subsections, the theoretical response of a Helmholtz basin that is damped by bottom friction, was derived. A relation between the amplification factor and phase difference of the tide in the basin have been formulated. In these equations, there are two parameters defined by the structure of the basin, the eigenfrequency σ_H and the friction coefficient ν_0 (2.31). Two other parameters depend on the applied tidal wave, these are the forcing frequency ω and tidal amplitude a_s . The response function can be analyzed dimensionlessly if the scaled forcing frequency ω/σ_H and the ‘Forcing’ $a_s\nu_0$ are considered. The parameter ‘Forcing’ determines if the response is mainly determined by friction — for ‘Forcing’ is larger than 1 — or mainly by the friction free response of the basin.

The response curves, which are formulated in (2.37) and (2.38) are shown in figure 2.11. In these figures the amplification and phase lag of the tide is drawn as a function of the scaled forcing frequency. They are drawn for different values of the ‘Forcing’ parameter.

A decrease of the ‘Forcing’ parameter causes two changes of the amplification curve and one in the phase lag curve. This decrease of the ‘Forcing’ parameter can have two origins, the friction parameter has decreased, or the amplitude of the tide in the sea has decreased.

The first change is an increase of the amplification of the tide. The amplification increases for all frequencies, but the strongest increase is around the eigenfrequency σ_H .

The second change in the amplification curve is that the frequency for which the maximum response is reached, becomes closer to the eigenfrequency for decreasing ‘Forcing’. This eigenfrequency is the free mode of the Helmholtz basin.

The change in the phase lag curve for decreasing ‘Forcing’ is a smaller phase lag for frequencies below the eigenfrequency. Likewise, the phase lag increases for frequencies higher than the eigenfrequency if ‘Forcing’ decreases. Similarly to the increase of the amplification factor, these differences are strongest around the eigenfrequency.

Note that for all values of ‘Forcing’, the phase difference is $-\frac{1}{2}\pi$ for a tidal forcing on the eigenfrequency.

Differences between quasi-linear and linear response

In figure 2.11, the response curves of a Helmholtz system that is damped by Lorentz-linearized bottom friction are shown. Although these response functions are linear mathematical equations, they are not equivalent to the from response functions that are found for

a Helmholtz system that is damped by a linear damping term.

Due to the differences between quasi-linear and linear response functions, the response curves differ. The differences are small if the tidal forcing amplitude a_s is hold constant. When a_s differs, the quasi-linear response curves differ, as shown in figure 2.11. The response of a linear damped Helmholtz resonator however does not depend on the forcing tidal amplitude. An increase of the tidal amplitude in the sea would not change the amplification factor and phase difference of the tide in the basin. Due to these opposite predictions, the dominant damping mechanism can be recongized out of the measured response curves.

Dependence of the amplification factor on basin and channel characteristics

In figure 2.11, the dependence of the response to the scaled forcing frequency and ‘Forcing’ is shown. Here, the influence of the set-up conditions of the Helmholtz resonator on the amplification factor is discussed. The set-up conditions are the area of the basin (A), the length (L) and the cross sectional area (O) of the channel or pipe. These do not only affect the eigenfrequency, which is defined in (2.17), but the friction coefficient that is defined in (2.31), as well.

For the analysis of such set-up conditions changes, the amplification factor for $\omega = \sigma_H$ is considered. For $\omega = \sigma_H$, the amplification factor did not reach its maximum value, as can be seen in figure 2.11(a), but an increase of the amplification factor for $\omega = \sigma_H$ is always accompanied by an increase of the maximum amplification factor.

The amplification factor (2.37) for $\omega = \sigma_H$ can be simplified to

$$\frac{a_b}{a_s} = \nu_0^{-1/2} a_s^{-1/2} = \left(\frac{3\pi HO}{8 c_d} \right)^{1/2} A^{-1/2} a_s^{-1/2}. \quad (2.39)$$

Equation (2.39) shows that a decrease of the basin area and forcing amplitude leads to an increasing maximum amplification factor. An increase of the cross sectional area of the channel leads to an increase of the maximum amplification factor as well. Due to the quadratic behaviour of the damping, the Harbor paradox is not found. The Harbor paradox is that the amplification increases for decreasing channel width. A narrow channel emits less wave energy than a wide channel, therefore the linear damping term is smaller for a narrow channel. Radiation damping due to wave emission is not included in equation (2.39).

The channel length is not directly represented in this equation, but one may expect an increase of c_d for an increased channel length. This might seem to be an erroneous statement, because c_d is a dimensionless parameter. Note however, that in other hydrographic subjects, a bottom friction term is defined along a spatial axis. In this subject, the bottom friction term is introduced in equation (2.21), which is already integrated over the channel length. This integration introduces a dependence of c_d on the pipe length.

2.4 Bent resonance

In the preceding section the response has been determined for a Helmholtz basin with vertical walls and linearized damping due to bottom friction. In this section the effect of sloping sidewalls on the dynamics of the Helmholtz system will be discussed.

2.4.1 Qualitative introduction

If the sidewalls of a basin are vertical, it has uniform hypsometry. The water surface area is equal for all water levels. The hypsometry is non-uniform if the water surface area depends on the water level. This occurs for example when the basin has sloping sidewalls.

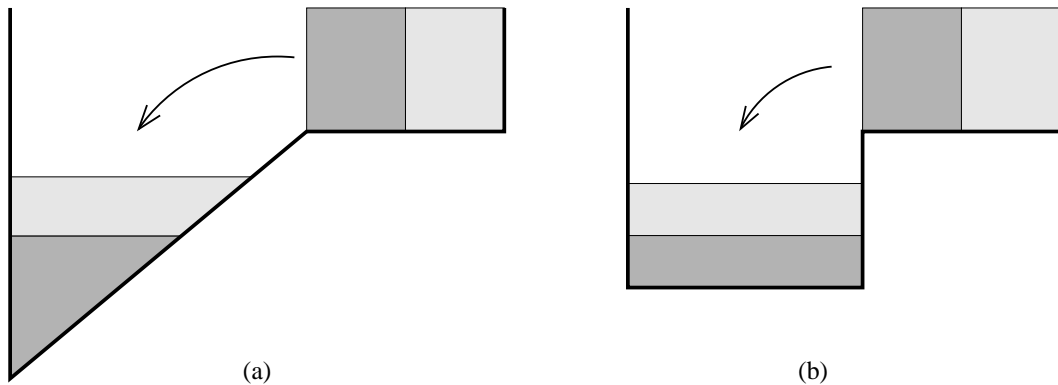


Figure 2.12: Sketch of the different water level elevations when adding equal amounts of water in case of a non-uniform and uniform hypsometry. From Maas (1998)

The effect of hypsometry on the elevation of the water level, when water is added into the basin, is sketched in figure 2.12. In case of uniform hypsometry, equal amounts of water cause equal elevations of the water level. The water level is linearly related to the incoming water flux. In case of a sloping bottom however, a larger amount of water is necessary to yield the same elevation during high water than during low water. So the water level changes more rapidly during low tide than during high tide. Consequently, the duration of the high water period increases relative to the low water period. Figure 4.11 is an example of this. The difference in duration increases with increasing tidal amplitude. Elongation of the high tide duration and shortening of the low tide duration are able to change the eigenfrequency. A more detailed analysis is required to see if the eigenfrequency decreases or increases. The effect on the eigenfrequency is negligible for an infinitesimally small tidal amplitude, but the change will grow with increasing tidal amplitude. Hence the *effective* eigenfrequency depends on the tidal amplitude for non-uniform hypsometry, as will be demonstrated in the next subsection.

2.4.2 Mathematical analysis

The equations for the Helmholtz system that were shown in equations (2.24) and (2.25) are valid still. Hypsometry is introduced in formula (2.25),

$$A(\zeta_b) \frac{d\zeta_b}{dt} = -Ou. \quad (2.40)$$

The quantity $A(\zeta_b)$ is constant in case of uniform hypsometry, in which case the equation is linear. The term $A(\zeta_b) \cdot d\zeta_b/dt$ is nonlinear for non-uniform hypsometry. Hence the equations describing the Helmholtz system are not analytically tractable.

Two different approaches have been used to handle this problem. Firstly, numerical models have been used, for example in Maas (1997). Numerical models have also been applied by us, facilitating the search for interesting experimental set-up conditions. A second approach is by rescaling of the equations (2.24) and (2.25), which has been done in Maas (1997); Doelman *et al.* (2002).

In order to find an analytical description of the dominant nonlinear behaviour, Doelman *et al.* (2002) analysed the equations for the case of weakly nonlinear behaviour close to resonance. They considered systems with very weak friction and a very weak tidal forcing, therefore the resonance is strong in these systems. Since the nonlinearity is only weak, the nonlinear terms are small in comparison to the linear terms. Applying these assumptions,

the nonlinear equations can be dealt by approximation. In that survey, the dissipation has been represented by a linear damping term. Stationary solutions and response curves are shown in that paper. These solutions and curves describe the response close to the eigenfrequency.

In order to make these analytical results usable for comparison with the experimental results of this report, their analysis must be changed at two points.

Firstly, the linear damping term was replaced by the Lorentz-linearized bottom friction term. Quadratic bottom friction is the dominant damping mechanism for the experimental set-up, therefore the analytical solutions must be derived with considering bottom friction. The adjustment was done in the start equations (equations comparable with (2.24) and (2.25)) of the analysis by Doelman *et al.* (2002). To obtain solutions and response curves for these adjusted start equations, the line of analysis by Doelman *et al.* (2002) was followed. The response equation becomes

$$\left(\sigma_H - \omega + \sigma_H \Gamma |\alpha|^2 + \frac{i}{2} \nu_0 \omega |\alpha| \right) \alpha = \frac{\sigma_H}{2} \alpha_s \quad (2.41)$$

(personal comm. G. Terra). The complex response amplitude in the basin α is equal to α in equation (2.32). It is defined as $\zeta_b = \alpha e^{i\omega t}$. The tidal amplitude in the sea α_s is defined similarly. The parameter Γ is called the bending parameter, it depends on the hypsometry. In Doelman *et al.* (2002), Γ is a dimensionless parameter; Γ dimensionally reads

$$\Gamma = \frac{1}{16A_0} \left. \frac{d^2 A}{d\zeta^2} \right|_0 - \frac{7}{24A_0} \left(\left. \frac{dA}{d\zeta} \right|_0 \right)^2 \quad (2.42)$$

(personal comm. G. Terra). The slope *and* the curvature of the bottom at the boundary determines the nonlinear parameter Γ . Note that for constant sloping walls $\Gamma < 0$, which means the amplification curve bends to the left, to lower frequencies.

Equation (2.41) equals response equation (2.32)⁵ for $\Gamma = 0$, when equation (2.32) is considered for $\omega \approx \sigma_H$. Once again, it should be realized that equation (2.41) is derived by analysing the response for the frequency domain around the eigenfrequency. The applied scalings lead to an incorrect limit behaviour for $\omega \rightarrow 0$, namely the response vanishes completely in this limit. The correct behaviour would be that the tidal response follows the tidal forcing at sea instantaneously. The correction of this incorrect limit behaviour for $\omega \rightarrow 0$ is the second change to make the results of Doelman *et al.* (2002) comparable with the results of this report.

A useful response equation can be *constructed* by combining the limit behaviour of equation (2.41) around the eigenfrequency and the limit behaviour of (2.32) further away from the eigenfrequency. The most simple equation which obeys both demands is

$$(\sigma_H^2 - \omega^2 + 2\omega^2 \Gamma |\alpha|^2 + i\nu_0 \omega^2 |\alpha|) \alpha = \sigma_H^2 \alpha_s \quad (2.43)$$

(personal comm. G. Terra). This equation will be used later on in this report as a semi-analytical curve that can be compared with the experimental results.

Uniformity weakly nonlinear analysis

Equations (2.24) and (2.25) can be adjusted with more nonlinear phenomena. Examples are varying cross sectional area of the channel due to tidal elevation of the water level or velocity advection out of the channel. If an analysis similar to these for non-uniform hypsometry is applied, an equivalent response equation as equation (2.41) is found (personal comm. G. Terra). Although a principle cannot be proved by examples, it seems that equation (2.41) describes the response of a weakly nonlinear disturbed Helmholtz resonator under quite general circumstances.

⁵Equation (2.32) can be found in the footnote on page 20.

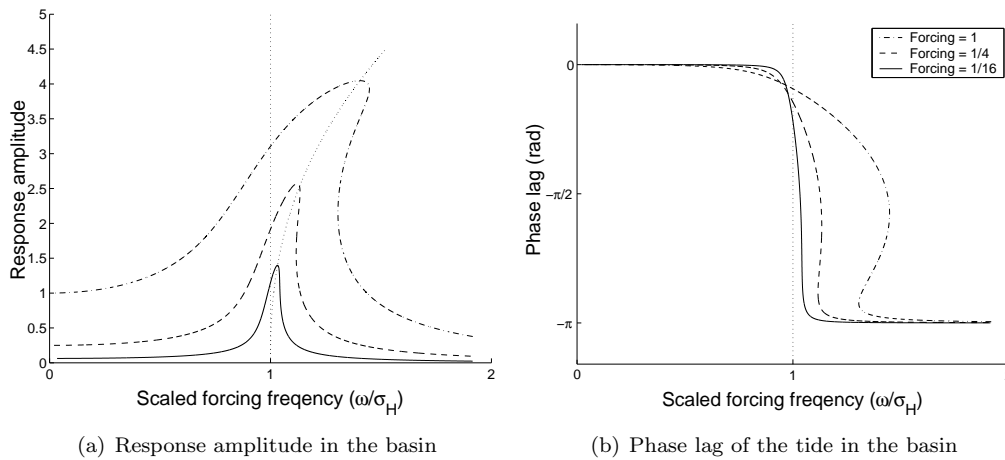


Figure 2.13: Example of theoretical nonlinear response curves as governed by equation 2.43 for positive Γ .

2.4.3 Figures of response shapes

Figure 2.13 shows a typical nonlinear response curve as governed by equation 2.43. A positive Γ is used in this figure. A constant sloping wall causes a negative Γ . Positive Γ leads to bending of the tidal response curve to higher frequencies (figure 2.13(a)), negative Γ bends the curve to the left. If bending is strong enough, a frequency domain in which the curve overlap, develops. As a consequence there are three possible solutions at a single forcing frequency, i.e. there are multiple equilibria.

Linear systems inhibit multiple equilibria. In a weakly nonlinear Helmholtz resonator, which consists of a nonlinear distortion on a linear system, the nonlinearity must grow before multiple equilibria can occur. The most natural simple oscillating systems are almost linear, therefore these systems have one stable equilibrium as well. The initial value is unimportant for these systems. In systems with multiple equilibria however, the initial value determines in which equilibria the system ends up.

Figure 2.13 also shows that bending increases with stronger tidal amplitudes. The strongest bends of the curve occur for the largest forcing amplitudes, although the amplification factor decreases for stronger forcing amplitude, due to the fact that in that case the effective friction increases. For these last, high nonlinear responses, the response equations are probably not valid, because the equations are derived under assumption of weak nonlinear behaviour. Nevertheless, initially the nonlinear behaviour of the response increases with increasing tidal forcing amplitude.

The curve of the phase lag is changed due to the nonlinearity (figure 2.13(b)) as well. In case of quasi-linear response ($\Gamma = 0$), the phase lag is always $-\pi/2$ when the forcing frequency ω is equal to the eigenfrequency σ_H , irrespective of forcing amplitude or friction strength. The phase lag curve is rather symmetric for $\Gamma = 0$. If Γ has a small positive value, the curve steepens in the frequency domain just above the eigenfrequency. The curve starts to overlap when the value of the parameter Γ is further increased. If the amplitude response has an overlap, the phase lag curve also has an overlap, because every point on the amplitude curve corresponds to a unique point on the phase curve.

In the domain with multiple equilibria, three solutions are present. These solutions are not all realized in practice, because one of them is unstable. The upper and lower solutions are stable, the middle solution is unstable. The two stable 'lines' of solutions are

called branches. If forcing frequency or amplitude are slightly changed, the response of the basin tends to remain in the same branch. This is important for experimental purposes. If the forcing frequency is changed repeatedly, while measuring under conditions of multiple equilibria, one will measure the response following one particular branch, until this branch ceases to exist. Then the response of the system will adapt quickly to the other branch. In this way, it is possible to measure the extent of branches and to prove the existence of multiple equilibria. Two series of measurements are necessary, one with increasing forcing frequency and one with decreasing frequency. The two results are equal for the frequency domain in which no multiple equilibria exist. In the frequency domain with multiple equilibria they will differ. The series of measurements with decreasing frequency will remain in the branch which is connected with the solution for high frequencies, until this branch does not exist anymore. Similarly, the series of measurements with increasing frequency will remain in the branch that is connected with the solution for low frequencies.

Chapter 3

Experimental set-up and measurement analysis

After the theoretical background of the Helmholtz resonator in the preceding chapter, in this chapter the experimental set-up and the measurement technique, analysis and comparison will be discussed. In the last section the computer model will be discussed as well, which was applied to search the best set-up conditions for verifying the theory.

3.1 Arguments for the chosen set-up

At the NIOZ, various aspects of the Helmholtz system has been investigated for many years, for example by Prof. Dr. J.T.F. Zimmerman (NIOZ/UU). In 1999 Dr. L.R.M. Maas (NIOZ) proposed to build an experimental set-up, in which on small scale the Helmholtz system could be studied. The work on this experimental set-up forms, together with a theoretical study to nonlinear effects in Helmholtz systems, a PhD subject, which G. Terra carries out. Prof. Dr. A. Doelman (UvA) is concerned for the mathematical part of this PhD subject. FOM subsidized this PhD study and the experimental set-up.

A few arguments determine the size of the experimental set-up. Firstly, it must be as large as possible to make the viscous effects as small as possible. The set-up was placed in a room of the NIOZ, which restricts the length to be at most 4.5 meter. The set-up is at one side placed at a wall. Therefore the width could be at most 1 meter, the maximum distance one can reach easily.

As driving construction was chosen a forcing tank. A piston gives a more direct transmission of the driving signals to a sea water level adjustment, but was too expensive. The motor driving the forcing tank, which can handle the expected forces, could generate a maximum frequency of 0.3 to 0.4 Hz.

- This frequency defines firstly the depth (H) of the sea, since the length of the sea must have the same size as the tidal wave length (\sqrt{gH} , with g the gravitational acceleration).
- Secondly the eigenfrequency of the Helmholtz mode can be at most 0.2 Hz, since also the response for frequencies higher than the eigenfrequency must be possible to be measured. A area of 1 square meter is chosen, which opens possibilities to perform experiments with reduced basin area.

Finally the forcing tank is not directly connected at the sea, but connected by a conduit, to derive a more uniform water elevation in the sea.

The set-up was build to generate tidal amplitudes of around 1 cm. In order to reduce friction, lower amplitudes of around 1 mm were used in the experiments.

3.2 Experimental set-up

The tidal simulator was constructed as shown in fig 3.1. It consist of tree parts:

- The forcing area, in which the forcing tank moves up- and downwards.
- The sea, connected by the forcing area by a conduit below the basin.
- The basin, with a (maximum) area of 0.92 square meter, which can be connected by a pipe or a channel to the sea.

Different pipes were used during the experiments. Therefore, the partition, through which the pipe connects the basin with the sea, was made of replaceable polystyrene. Within the basin, different inlays could be placed that creates intertidals, or partitions could be fixed, reducing the basin area that can be filled by the channel.

The transmission of tidal motion in the set-up procedes in this way: when the forcing tank moves downwards, the water level around the tank in the forcing area rises. This pushes the water through the conduit below the basin to the sea part. Consequently, the water level at sea rises. This causes a water level difference between the sea and the basin, which drives the water to the basin. When the forcing tank moves up, the opposite takes place. The goal of the forcing is to excite a harmonic signal at sea, equal to the sinusoid which was used in the latter theoretical section.

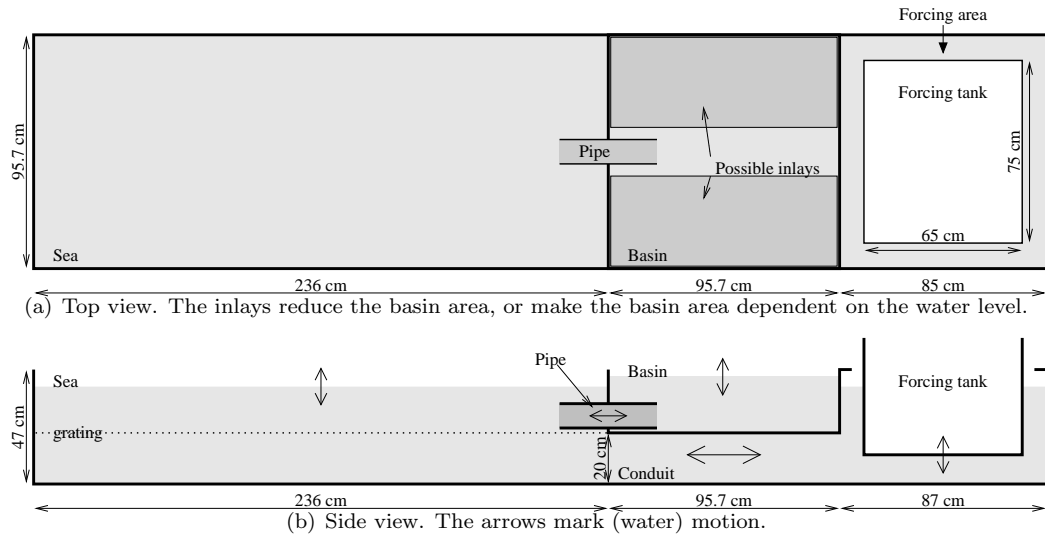
The generation of the harmonic signal will be first described in this section, followed by the control of the driving tank and the sea level, the configurations of the basin and finally the types of pipe that were used.

3.2.1 Tidal signal generation

As already mentioned in the preceding introduction, the water motion in the tidal simulator is driven by a forcing tank. A servo motor pulls this forcing tank up- and downwards. A normal harmonic sinusoid was used as input signal to control the forcing tank position. For the first nine months of the experiments, the input signal was provided by a sine generator. Later on, the input signal was generated by computer, for which the software package LabVIEW™ was used. The main advantages of using the computer for the generation of the control voltage are:

1. A series of experiments could be done without interaction with a human operator. This reduces time one has to spend on doing an experiment and makes it possible to measure during the night. Both aspects increase the efficiency.
2. Smaller frequency and amplitude changes of the harmonic signal can be made. So the precision does not increase, but with LabVIEW™ every frequency and voltage can be made, in comparison to the sin generator which can be varied up to a finite precision, namely with steps of 10^{-3} Hz and 10^{-3} V (with ± 3 V as the maximum input voltage of the servo motor).
3. Not only harmonic signals could be made, but also more complicated signals, such as two interfering frequencies. Such forcing signals are useful when chaos is investigated. Preliminary experiments with such a forcing signal have been performed, but will not be discussed in this report.

The employment of the computer has also two disadvantages, namely:



(c) Picture of the servo motor

Figure 3.1: The experimental set-up: a certain forcing signal is applied to the servo motor, which adjusts the height of the forcing tank according to the applied signal. The motion of the forcing tank alters the water level in the sea. If a water level difference between the sea and the basin exists, the pressure gradient causes a current through the pipe.

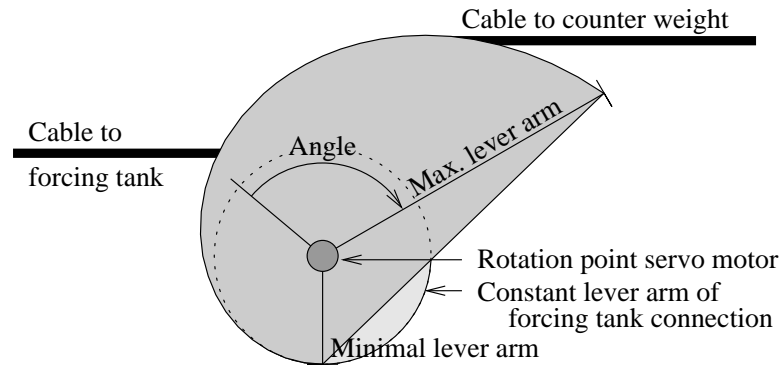


Figure 3.2: Sketch of the fastenings technique of the counterweight on servo motor: when the angle of the motor changes, also the lever arm by which the counterweight is connected, changes. The shortest lever arm is reached at low tide.

1. This automatic experiment control does not involve a direct human check on the measurements. Errors in the experimental control, such as too big amplitudes of the input signal, are not recognized and redressed during the experiment, thus the probability that afterwards experiments appear to be useless, increases.
2. The output voltage of the computer, which was used as input voltage for the servo motor, has to be updated regularly. During the experiments a refreshment rate of 50 times per second was used. If other (LabVIEW™) applications ask much computer processing time, the update of the output voltage can be delayed. Repeated delays causes distortion of the sinusoidal signal.

3.2.2 Control of the forcing tank

The construction for driving the forcing tank is shown in figure 3.1(c). The forcing tank is connected to a servo motor, together with a counter weight. The buoyancy force by the water decreases when the forcing tank rises out of the water. Therefore the lever arm (figure 3.2), by which the counter weight is connected, depends on the angle of the motor, in such a way that the net torque on the motor is equal during the whole tidal period.

The servo system that controls, operate as follows: when a certain voltage is applied, the servo system adjust the position of the motor, which is measured by an angular potentiometer, to the angle that corresponds with the specified voltage. Two motor processes influences the response:

- The time delay caused by the adjustment time of the servo system causes a significant phase shift (between input voltage phase and forcing tank position phase) and amplitude loss for frequencies over about 0.13 Hz. This requires the voltage amplitude to be increased when the forcing frequency increases above 0.13 Hz in order to maintain the same water level amplitude at sea. But besides this, there are other responses in the set-up which necessitates an adjustment of the input voltage, these will be discussed in section 3.2.3.
- For frequencies below about 0.06 Hz the servo system also excites weak multiples of the forcing frequency, caused by slow response of the motor at the turning points.

Both processes are useful to know, but did not affect the domain of frequencies which can be used during experiments.

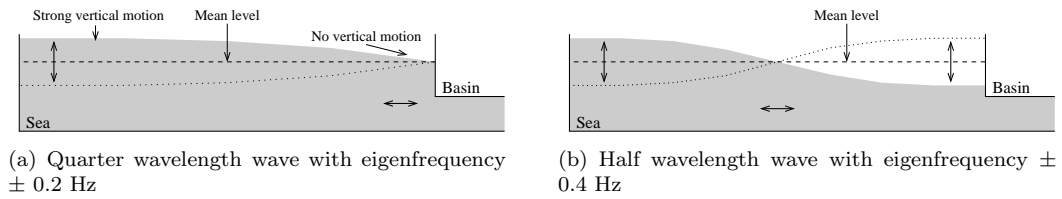


Figure 3.3: Side view snap shot of standing waves in the sea. Arrows mark water motion, the dotted line the water level for the opposite phase. The mean water level is the water level under forcing free circumstances.

3.2.3 Control of the sea level

As discussed in the previous subsection, the forcing tank can apply a sinusoidal signal, which force the sea. But a few issues could hinder the generation of a sinusoidal tidal signal at sea.

1. First of all, the indirect pushing of the water through the connecting conduit generates an unknown delay effect or possibly overtides. The forcing is indirect because the tank does not work like a piston, but in this way: a descending forcing tank first pushes the water in the forcing area up (see figure 3.1). The generated pressure gradient between the water around the forcing tank and the sea, causes the flow through the connecting conduit below the basin.
2. Since the water enters the sea at one side through the conduit, the water elevation in the sea is not automatically uniform. The mode types occurring most are a standing quarter and half wavelength wave in the sea, see figure 3.3. The eigenfrequencies are given by $f = \sqrt{gH}/\lambda$, where H is water depth, and λ the length of the standing wave. For exciting a quarter wavelength wave λ is $\frac{1}{4}$ times the length of the sea (236 cm), for a half wavelength wave λ is $\frac{1}{2}$ times this sea length. The eigenfrequencies are around 0.21 Hz for the quarter wavelength wave and 0.42 Hz for the half wavelength wave. The exact value of the eigenfrequencies depends on the mean water level.

The frequency of the half wavelength mode is too high to be generated directly by the forcing tank, which reaches a maximum frequency of 0.3 to 0.4 Hz. This mode does occur when its eigenfrequency is a multiple of the forcing frequency. In section B.1 measurements are shown that demonstrate the excitation of this mode.

The quarter wavelength mode can be excited directly and its influence can be observed relatively far from the eigenfrequency. This influence can be noticed in an enlargement of the response at the far end of the sea, and a reduction of the response at the basin-side (see figure 3.3(a)). Therefore, one must increase the amplitude of the forcing tank for increased frequency to generate the same tidal signal at the basin-side of the sea. But when the eigenfrequency of the quarter wavelength mode is forced, the response at basin-side is always too weak to be used for experiments. Therefore the maximum frequency which can be generated with the experimental set-up is around 0.2 Hz.

3. The sea is not infinitely big in comparison to the basin. The response of the basin to the forcing affect strongly the tidal amplitude in the sea. A descending forcing tank causes a rising of the sea level, a lowering water level in the basin causes a certain rising of the sea level as well. If the descend of the forcing tank goes simultaneously with a increase of the water level in the basin, a stronger rise of the sea level occurs than if these two processes are in antiphase. So, a larger amplitude must be applied to the forcing tank to excite a desired tidal amplitude at sea, if the tide in the basin is in phase with the tide in the sea, than if the tide in the basin is in opposite phase.

4. The combination of sea and forcing tank can also behave as a Helmholtz system. In that situation, the water in the forcing area around the forcing tank is the respond basin, and the conduit below the basin is the channel (see figure 3.1(b)). This response has an eigenfrequency of about 0.30 Hz. This eigenfrequency can be derived by using shallow water equations for two finite basins. Since this eigenfrequency is higher than the maximum excitable frequency, which is limited by the quarter wavelength wave mode, this mode is unimportant for this set-up.

In the sea a grating is hanged, see figure 3.1(b) and 3.1(c). The sea is forced by water entering the sea through the conduit, which cause horizontal velocities. The grating should decrease horizontal velocities above the grating by redirecting the tidal motion upwards. It could not prevent the occurrence of low frequency standing wave response, high frequency response endures more damping due to the grating, and is a bit reduced.

3.2.4 Basin and inlay

The basin is connected to the sea with a pipe. In the experiments pipes of different shapes and external diameters were used. As a result, the partition between sea and basin, through which the pipe perforate, must be adjustable. Therefore this partition is made of polystyrene and not PVC, which is used for the fixed parts of the tidal simulator. Polystyrene sheets can be molded with simple tools to a partition, in comparison to PVC which only can be molded by machine.

As shown in figure 3.1(a) the maximum size of the basin is approximately 0.92 m². The basin area was reduced with vertical sidewalls, and in several ways a non-uniform hypsometry was constructed, in order to verify the theory for Helmholtz oscillators with hypsometry, which predicts nonlinear response. Each one of them will be discussed in this subsection.

Reduced basin area and sloping walls

To create a smaller area polystyrene partitions are fixed in the basin, as sketched in figure 3.4(a). Additional partitions were used to decrease the basin area further. The partition marked with (1) was not only inserted upright, but also at an angle. Angles up to 50 degrees from the vertical were used. A limitation of this method is that only a small area difference between high tide and low tide — an intertidal — can be reached. The advantage of this method is that, because of the rather steep slope, the adhesive effects, which strongly influence the results, remains negligible.

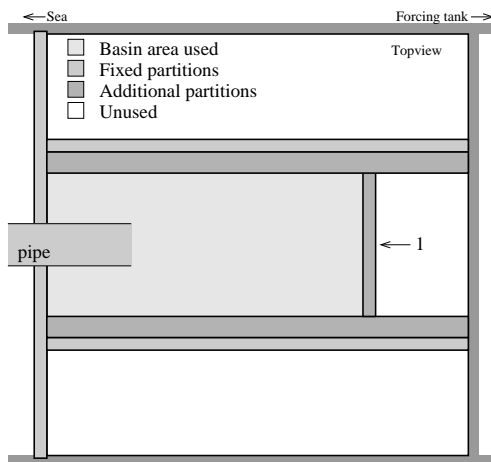
A fixed inlay

The first way a inlay was created, was by inserting a massive polystyrene tidal flat into the basin, see figure 3.4(b). The slope of the tidal flat is decreasing with leaving Γ constant. Γ is a standard which define the nonlinear bending it theoretically would give, see subsection 2.4 for more explanation of Γ .

A disadvantage of this fixed inlay is its inflexibility. The construction of this inlay was a time consuming process and, once placed, no adjustments could be made. If, for example, the response of a slight steeper slope would be investigated, a totally new inlay must be maked and fixed.

Flat plates

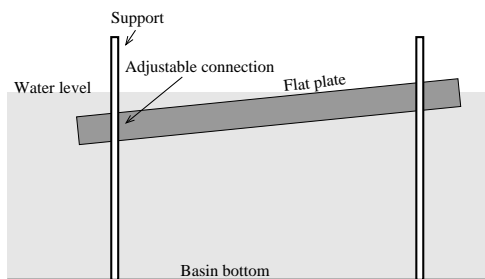
The second type of inlays that were used are flat plates, see figure 3.4(c). The height of the plate is easily adjustable in every corner, but the maximum angle of the plate is ± 6 degrees to the horizontal. Two plates have been used, one for the full basin, another for a narrowed



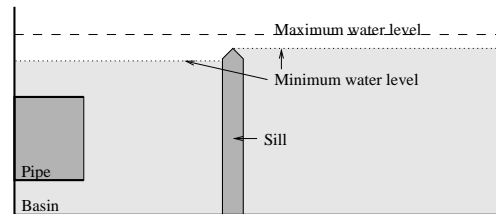
(a) The method to reduce the basin area with partitions.



(b) A picture of the fixed inlay. The inlay has a variable slope and is made of polystyrene sheets.



(c) A sketch of a flat plate. The height on which the flat plate is connected at the support can be varied. Polystyrene (not drawn) fills the space below the flat plate.



(d) A partition used as a sill. Only for high tide the water of the outer basin part can communicate with water in the inner basin part.

Figure 3.4: Some different configurations for the basin.

basin. The first one was made out of 9 mm PVC and has a size of 95 to 65 cm. Because of its relatively small thickness, the stiffness of the plate is too small to prevent bends caused by the tide in the basin. With careful fixing these bends could be reduced to negligible proportions. The second, smaller plate is thicker and stiff. The small one was placed in a reduced basin area as sketched in sub-figure 3.4(a), without the partition marked with (1), the large plate was placed in a further empty basin.

Flat plates do have a disadvantage. The excited water elevations in the basin are in the experimental set-up between 1 and 5 mm. To get a significant area difference between low and high tide, the slope of the inlay must be small, which causes a thin water layer on the lower part of the inlay. In this shallow water layer a water elevation adaption travels slowly. This slow adaption leads to a delay of the tide on the inlay in comparison to the deeper part of the basin. This does not only make the water elevation in the basin no longer uniform, this appears to be a damping process.

Sill

In the previous paragraph the disadvantage of flat plates was discussed, namely a phase lag of the tide on the high side of the inlay. One way to get round this problem, is by introducing a sill. A sill can be compared with a horizontal flat plate. Both generate for low tide a small basin area and for high tide a large basin area. The only difference is that the water layer thickness on the inlay is small, and the water layer thickness behind the sill is large.

The construction (see figure 3.4(d)) divides the basin in two parts, separated by a partition. This partition has such height that there is no connection at low tide and exchange is possible at high tide. The partition thus works as a sill.

A sill also causes delay effects. The water layer above the sill is thin, therefore the flow above the sill appears to behave quickly super-critical, which means that the dynamics of the flow is dominated by pressure differences and advective acceleration. Consequently, a pressure difference, that is a water level difference, between the two basin parts is necessary to generate a flow, thus the sill delays the passage of the tide.

3.2.5 Pipes

In the theory (section 2.2.3) the basin is connected by a narrow channel. In the Helmholtz equations (2.22) and (2.21) however, the important quantities of the channel are only its length and its cross section. Consequently, nothing would change in the Helmholtz equations if the channel is replaced by a pipe.

There are yet two arguments to prefer a pipe above a channel. The free surface of the channel causes a nonlinear effect since the cross section depends on the water elevation. One goal of the experiments is to investigate the nonlinear effects of hypsometry, therefore it is necessary to avoid the occurrence of other nonlinear effects. Secondly, the eigenfrequency of the Helmholtz system is depending on the cross section. A small deviation of the mean water level would change the eigenfrequency if a channel is used. The eigenfrequency is no longer depending on the mean water level if a pipe is used.

Description of all pipe shapes

Two kinds of pipes were used, straight pipes and trumpet-shaped pipes. The characteristics of all pipe configurations are listed in table 3.1. The pipes *Pipe one*, *Pipe two* and *P31* consist of a straight part only. The trumpet (*'T'*) and *'C'*-pipes consist of a trumpet shape begin and end part (see figure 3.5(a)), connected by a straight part of which the length can be varied. A *T42* pipe for example consist of two trumpet shaped end parts, connected by a straight pipe and the total length of the *T42* pipe is 42 cm. The *'C'*-pipes have a partly cut end part at the basin side in comparison to the *'T'*-pipes (see figure 3.5(b)). *C*-pipes were

Name	Length straight part 10^{-3}m	Total length 10^{-3}m	Inner diameter 10^{-3} m	Cross section 10^{-3} m^2
<i>Pipe one</i>	441 ± 1	441 ± 1	76.4 ± 0.3	4.58 ± 0.04
<i>Pipe two</i>	377 ± 1	377 ± 1	94.3 ± 0.3	6.98 ± 0.04
<i>T32</i>	31 ± 1	321 ± 3	92.9 ± 0.3	6.78 ± 0.04
<i>T34 / C34</i>	50 ± 1	341 ± 3	92.9 ± 0.3	6.78 ± 0.04
<i>T42 / C42</i>	129 ± 1	421 ± 3	92.9 ± 0.3	6.78 ± 0.04
<i>T52 / C52</i>	228 ± 1	521 ± 3	92.9 ± 0.3	6.78 ± 0.04
<i>P31</i>	313 ± 1	313 ± 1	92.9 ± 0.3	6.78 ± 0.04

Table 3.1: Pipe characteristics: small *Pipe one*, *Pipe two* and the *P31*-pipe are straight PVC pipes, the ‘*T*’ and ‘*C*’-pipe consist of a widening end part (see figure 3.5) connected by a straight pipe. The whole length in cm forms the index.

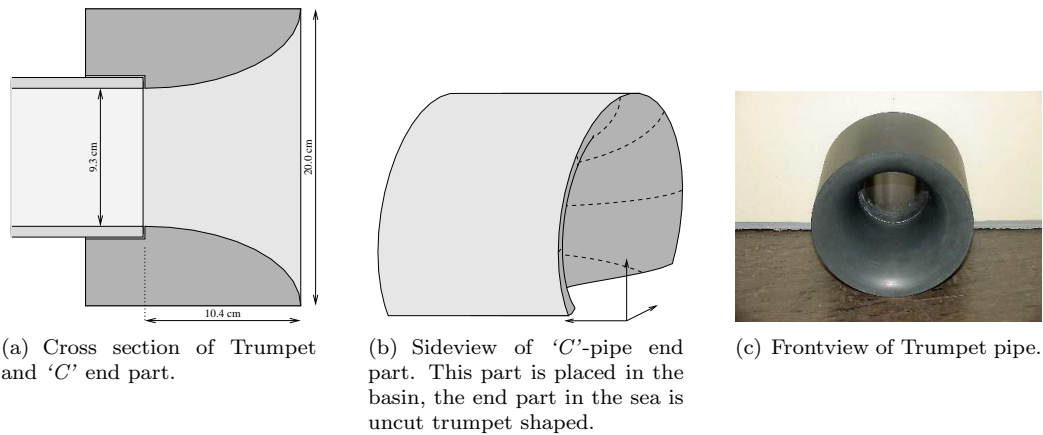


Figure 3.5: Drawing of the trumpet shaped end parts.

used besides T -pipes as well to enlarge the range of possible mean water levels above the pipe, so that could be investigated the possible effect of the mean water level. The height of the uncut trumpet end part is namely 20 cm, where the basin is 26 cm deep. The maximum range over which the mean water level can be differed, is 2 cm for a ' T '-pipe and 6.5 cm for a ' C '-pipe.

The flow in a pipe with smoothly widening end parts experiences less friction, which results in an increase of the tidal response in the basin. The appearance of less friction can be argued: as noticed before, theoretically the out stream of the pipes is expected to be jet like, see figure 2.5. In the first experiments, which are executed with straight pipes, this pattern also appears. At the end of the pipe the jet like outflow meets nearly motionless water, on the interface between the jet and the surrounding motionless water turbulence and vortices appear. This strong transition is sharp when the pipe has a sharp end. Experiments revealed that a smoother transition occurs if the pipe widens at the end.

3.3 Measurement tools

In this section, the measurements procedure is discussed and how the collected data are managed during an experiment are shown.

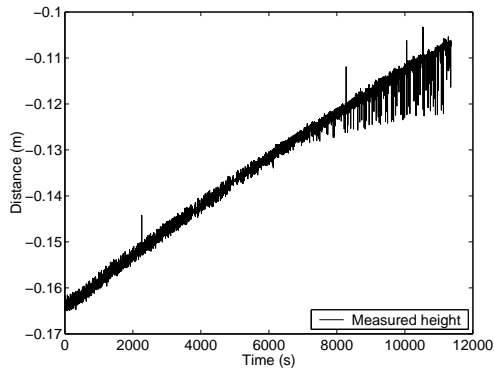
The interesting quantities describing the response of the Helmholtz resonator are the surface elevation at sea and in the basin, and the current through the connecting pipe or channel. Therefore surface elevations were measured with four distance sensors. Currents were not yet measured, because of financial limitations.

3.3.1 Distance sensors

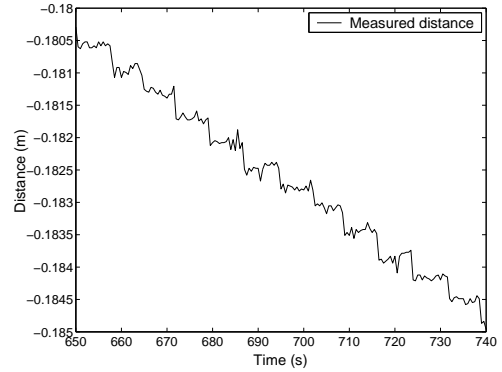
The distance sensors are based on acoustic sounding, like employed by bats. They emit acoustic pulses of 300 kHz, this pulse reflects on the surface right below the sensor, and is detected by the sensor. The time between emission and detection gives the distance, since sound travels with a known constant speed. The sensor converts this delay time, hence distance, linearly to a voltage. This voltage is read by the computer.

A few remarks:

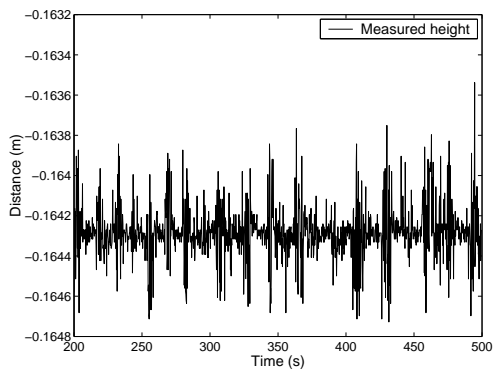
- According to the factory specifications, the sensor can measure distances from 10 to 60 cm. However, for distances below 13 cm, outliers occur frequently, see figure 3.6(a). Once this inaccuracy was discovered, it was made sure that the distance of the sensor to the water surface was always at least 15 cm.
- The sensor measures the distance with steps of approximately 0.35 mm. This is clearly visible in figure 3.6(b), which shows the distance measured by a sensor, while the water level is falling. When the measured tidal signal has an amplitude of the same order as this resolution, it might be impossible or difficult to recover the original amplitude. This problem is discussed further in section 3.4.2.
- The detected signal contains some noise, like shown in figure 3.6(c). The time interval between two 'noisy' parts is not constant, the noise is totally chaotic. Since the noise amplitude is also beneath 1 mm, it is not harmful. This noise is probably generated in the sensor cables by induction effects of the 50Hz background signal.
- The sensors need a smooth water level for a accurate distance measurement. If the water surface is not flat, outliers could occur. An example of this effect is shown in figure 3.6(d). This problem occurs if the sensor is positioned right above the water front on a tidal flat. Due to cohesion effects, the water surface is almost vertical at the



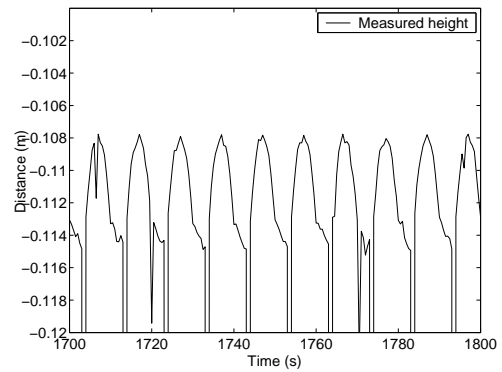
(a) An example of outliers: a steadily increasing water level was measured here. For distances below 13 cm the distance sensor gives frequently erroneous measurements.



(b) Measure interval: A measurement of steady falling water. The steps of 0.35 mm mark the precision of the sensor.



(c) Typical noise: the output of the sensor consists of periods of rather constant signal, alternated by a few seconds of stronger noisy deviates.



(d) Outliers caused by rugged water surface: This measurement was made with a sensor located at the waterline on a tidal flat. At low tide the flat is 'drying', adhesion effects causes a slow removal of the last water, causing a slow linear decrease of the water level. At the start of the flood the convex water front (convex because of cohesion effects), causes an outlier.

Figure 3.6: Occuring distance sensor problems and errors

front when the water move upwards the inlay. As a consequence the acoustic signal is not reflected properly.

- The sensors do have a slow drift, in order of a mm per hour. Therefore it has little effect on the measurements, which have a typical time scale of 10 seconds. If the Helmholtz resonator causes a mean water level difference, it could not be measured.

Measurement locations

In the first months 3, and later 4, distance sensors were available for the measurements. Always one sensor was placed right above the sea-end of the pipe and one was placed at the basin-end of the pipe. Usually another sensor was placed at the far end of the basin. Sometimes a sensor was placed at sea, next to the sensor above the pipe-end, with equal distance to the basin. Sometimes a sensor was placed above the forcing tank or at the far end of the sea.

3.3.2 Current measurements

As remarked before, it would be interesting to measure the current velocity through the channel or pipe. A restriction of current measurements is that the measurement technique does not influence the current. Preferably noninvasive measurements should be used. Accurate, technically applicable and not too expensive methods however were not found. As a consequence, no current measurements have been done.

A few possible methods of current measurement are:

- A propellor: a propellor is an invasive method, but when the propellor is small in comparison with the pipe width, its effect might be negligible. The smallest usable propellor has a propellor diameter of 1 cm. It is very difficult to implement a propellor in a pipe. If the basin was connected at the sea by a channel with a free surface, a propellor could be tried. The arguments for still applying a pipe were discussed in subsection 3.2.5.
- By a heated wire: it is possible to measure the current in an indirect way, by means of a wire across placed perpendicular through the channel. The wire is heated by an electric current and also cooled by the surrounding water. This cooling is stronger for flowing water than for motionless water. The temperature of the wire thus gives an indication of the velocity in the pipe. When the wire is placed along the side-wall of the pipe, its effect on the flow is less, but its accuracy might be lower.

Good sensors based on this technique are available, but their prices were exceeding the available budget. It appears to be too difficult to build such a sensor by ourselves.

- Laser doppler methods: This method uses the reflection of very small particles in the water for the determination of the current speed. Laser doppler sensors are widely applied in oceanographic experiments, but for this purpose, no suitable design was found.

3.3.3 Operation program

The distance sensors, described in the previous section, give output voltages representing distances. This output voltage is read out by the computer. The software package LabVIEW™ is used to collect the data.

Within LabVIEW™, the data collection and storage has been programmed in the following way: LabVIEW™ reads the output voltage of the distance sensors, and converts this to a height. This single measurement is accompanied with the computer time directly after

finishing the voltage read out. With this computer time, the amount of milliseconds passed since the start of the measurement session is calculated. Finally the measured height and time are written to a data file. The frequency of measurement was usually chosen at 2 Hz or 4 Hz. 12 measurements during one tidal period is considered as minimum. For typical periods of 10 seconds, a 2 Hz measurement ratio is enough. Nevertheless, 4 Hz was often chosen to increase the analysis precision.

LabVIEW™ is basically able to analyse the data for all four sensors. In such an analysis, LabVIEW™ calculates the Fourier spectra or the amplitude of the main frequency. Nevertheless, the accuracy is low, caused by unremoved outliers, which occur frequently and have a large impact on the outcome. An outlier removal procedure in a real-time measurement program is rather difficult to implement. Furthermore, a better outlier recognition is reached if this analysis is carried out after completing the measurement series. LabVIEW™ was designed especially for real-time applications, the programming structure is not designed to handle this kind of tasks. Therefore, the ‘preview’ analysis of LabVIEW™ was used only for monitoring the experiments.

Measurement analysis within real-time LabVIEW™ programs encounters another problem as well. LabVIEW™ must deal with large data sets, which uses much computer processing time. It has happened that this need for calculation time is responsible for slowing down the progress of the measurements. Fortunately, this does not harm the value of a single measurement, since the time saved with the measurement is still correct. It does cause the time series not to be equidistant, which affects the outcome of Fourier transformation, which assumes an equidistant time series. The harmonic analysis which will be discussed later on, does not presume an equidistant time series.

LabVIEW™ is also used to control the forcing tank (see section 3.2.1). Simultaneously analysing the measurements and driving the servo motor demands too much CPU, hence the control voltage is not updated regularly, which causes a distortion of the sinusoidal signal. Therefore, LabVIEW™ is not used to analyse the data if LabVIEW™ also supplies the input voltage of the servo motor.

3.4 Data analysis

For the analysis of the measurements, which are collected by LabVIEW™ as described in the previous section, the software package MATLAB® is used.

One experiment contains at least 1000 individual measurements for each of the four sensors. A typical experiment duration of 30 minutes on 4 Hz leads to 7200 measurements for each sensor.

The goal of the data analysis is that these data can be compared with theoretical predictions. Mathematical theoretical analysis presumes a sinusoidal forcing and a sinusoidal response. The experimental set-up is driven by a sinusoid, therefore the tidal response in this set-up should be periodic. The dominant frequencies in the response were determined with Fourier analysis. Furthermore, outliers must be removed, because they can disturb the harmonic analysis. Harmonic analysis however is necessary for an accurate detection of outliers. Therefore, harmonic analysis and outlier removal is an iterative process.

If harmonic analysis is applied, the measured data, denoted as $h(t)$, is represented with a limited number of harmonic components. Each harmonic component has a frequency f_k , an amplitude a_k and a relative phase φ_k . The harmonic reconstruction $\zeta(t)$ is defined as

$$\zeta(t) = a_0 + \sum_k a_k \cos(2\pi f_k t + \varphi_k), \quad (3.1)$$

in which a_0 is the mean water level. The best harmonic reconstruction is found if the quadratic sum of the differences between h_k and ζ_k is minimized. Thus $\sum_t (h_k - \zeta_k)^2$ is

minimized, this is reached by varying all f_k 's, a_k 's, φ_k 's and a_0 . As a consequence, the number of variables for minimization increases if more harmonic components are included. A reconstruction with more harmonic components fits much better if all dominant components are present. So, the recognition of dominant frequencies is important.

Most data series of experiments contain less than five dominant harmonic components. These components are commonly the applied frequency and multiples of this frequency. This knowledge is also used to improve the harmonic analysis. Some series however, contain much more dominant frequencies, due to resonance within the laboratory set-up.

The applied frequency is very often the strongest dominant frequency in the response. This amplitude and relative phase difference between tidal responses at sea and in the basin were used for comparison with theory. This comparison will be discussed in the next section, section 3.5.

3.4.1 Step wise description of data analysis procedure

In this subsection, the data analysis method is described in more detail. Firstly, it is convenient to give some definitions: One distance value of one sensor, accompanied with a time, is called a measurement. A time series is a group of measurements, measured right after each other, for equal set-up circumstances, forcing frequency and amplitude. The four time series of all sensors together form a session. An experiment is a group of sessions for which only the forcing frequency and amplitude changes, the set-up conditions, (basin shape etc.) are equal.

The data analysis performed on each session can be summarized by the following steps:

1. For each time series the measured heights, i.e. the distance between a sensor and the water surface, are transformed to deviations with respect to the motionless water level.
2. The time values, recorded with the height measurements, originally count from zero at the start of a time series. In this situation however, the best fitting frequency and phase of a harmonic component depend on each other. A little error in the frequency induces directly an error phase of this component. This dependency can be removed by centralizing the time values, such that the origin is at the middle of the time series.
3. Individual measurements that deviate more than four times the standard deviation of the whole time series, are removed. Non-chaotic repetitive outliers, like shown in figure 3.6(d) do influence the Fourier spectra. In that situation the outliers could not be flagged any more later on in the analysis, since outliers in the harmonic analysis are defined as too large deviations from the periodic signal.
4. The frequency spectrum is determined by Fourier transformation. The frequencies of the significant peaks will be used for the harmonic analysis. A peak is considered to be significant when it is distinctly above the 'noise'. This 'noise' remains after subtracting the significant peaks from the entire spectrum. As a consequence, this step needs to be repeated about four times, because 'noise' and 'significant peaks' are determined iteratively.
5. The peak frequencies obtained in step 4, are compared with (multiples of) the forced frequency. The experimental set-up was driven with this frequency, so one may expect that the response is periodic with this frequency, thus the expected peak frequencies are equal to (multiples of) the forcing frequency. The forced frequency was known very accurately, but frequencies obtained by Fourier analysis could deviate slightly, because of the finiteness of the time series and reduced equidistantness. Therefore the frequency of a peak with a value near an expected frequency, is replaced by the value of that expected frequency. Frequencies of significant peaks with a frequency away from any expected value are kept unchanged.

6. With the corrected frequencies from step 5, harmonic analysis is performed to obtain the amplitude and phase for all frequencies. The harmonic reconstruction is defined with equation (3.1). In this step a_0 and all a_k and φ_k may be varied, but the dominant frequencies f_k are fixed. Components with an amplitude less than 10^{-6} m are removed.
7. The deviation of each measurement from the harmonic fit is determined. Measurements whose deviation is more than 3.5 times the standard deviation from the fit, are removed.
8. Step 3 to 7 is repeated twice. More iterations does not increase significantly the number of outliers.
9. A least squares fit, with the shape of equation (3.1), of is determined again. In comparison to step 6, time all variables may be varied, thus frequency, amplitude and phase of the different components, and the mean water level. This last harmonic analysis is done, because it can not be taken for granted that the forced frequency is exactly applied and that apparent overtones have exactly the multiple of the forced frequency. Furthermore, a slight error in the frequency of a main component leads to an erroneous large amplitude of overtones of this component.

A minimization procedure has been written for this purpose. minimization procedures implemented in MATLAB[®] needs for time series with more than five components more than a half hour calculation time. The finally applied procedure is the Newton minimisation method. The procedure is discussed further in the appendix, section A.

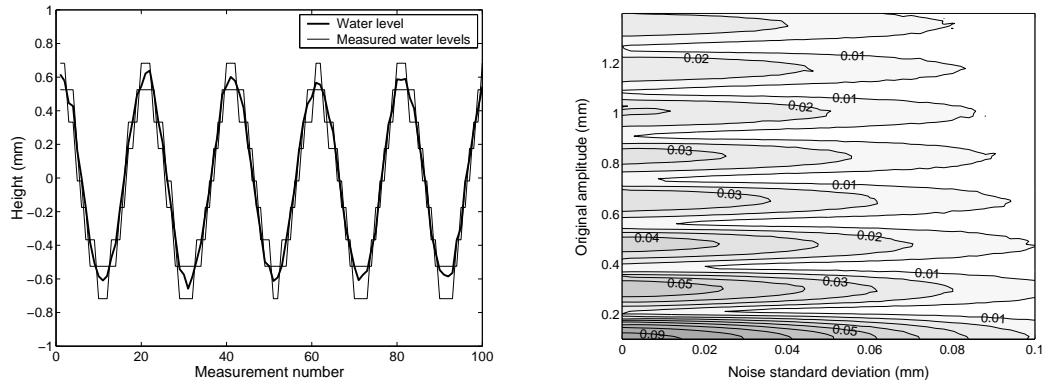
10. For the third time outliers are removed, in the same way as it is done in step 7.
11. The error in the analysis is estimated. For this purpose subsets of the measurement data is made. These subsets contain a fifth of the data, randomly chosen but rather well-balanced on the length of the data as well. The fitting procedure that was described in step 9, is repeated on each subset. The best fit of the subset does vary from the best fit of the whole data series. This is repeated 15 times, which gives 15 best subset fits. The standard deviation of these subset fits to the best fit of the whole data series is taken as error estimation for the harmonic analysis.
12. Finally, at the places where an outlier has been removed, the outlier is replaced by the value of the harmonic reconstruction for that time.

This harmonic analysis gives a harmonic reconstruction of the measured responses. The harmonic component that has been driven during an experiment is the most interesting component of the analysis. The amplitudes and relative phases of this component will be used in the comparison of theory. In chapter 4, the amplitude and relative phase of this component will be called a measurement result.

3.4.2 Effect of the measurement resolution

In section 3.3.1 it was noted that the sensors measure with a resolution of approximately 0.35 mm. The resolution transforms the measured water level to a steppy structure. That causes a significant distortion if the measured tidal signal has a comparable size, see figure 3.7(a) for an example. The shape of the distorted time series depends on the exact location of the mean water level with respect to the ‘resolution grid’ of the sensor. Differences in the mean water level, which, on the scale of the resolution (0.35 mm), can be considered as being random, cause differences in the effect of the distortion.

Numerical experiments were performed to investigate the effect of this distortion. A dataset of a sinusoid with certain amplitude was constructed and noise was added to this.



(a) An example of the distortion: the distortion of a signal is numerically simulated two times. The original sinusoid has an amplitude of 0.6 mm on which noise with a standard deviation of 0.03 mm is added.

(b) Accuracy: For different amplitudes of the sinusoid and pre-measurement noise standard deviation the standard deviation (mm) of the measured amplitude of the distorted sinusoid is calculated numerically.

Figure 3.7: The influence of measurement inaccuracies

The signal is transformed as if it were measured with a sensor with a resolution of 0.35 mm, and a harmonic analysis is applied on the transformed signal. The average amplitude measured for all possible positions of the mean water level appears to be equal to the original amplitude, since enlargement and flattening of the signal caused by the distortion balance each other.

The average deviation of the amplitude of one time series from the original amplitude, is growing with decreasing values of the amplitude, see figure 3.7(b). In this figure results of the latter procedure are shown, for different sinusoid amplitudes and of the standard deviation of the noise. The effect of pre-measurement noise is also analyzed, in spite of the fact that its magnitude is unknown in our experiments. More noise decreases the effect of the measured resolution. Sinusoids with an amplitude that is a multiple of the measurement resolution are affected most, since for this amplitude the grid cuts off or enlarges both the maximum and minimum. This explains the periodic oscillating nature of the deviation. The conclusion is that, with or without noise, measurements of sinusoids with an amplitude of less than 0.5 millimetre can not be measured accurately since the error exceeds 10%.

3.5 Data and theory comparison

In the preceding section, the procedure to determine the harmonic analysis of a time series was described. In this section, the method to compare the experimental data with theoretical results is discussed. For the Helmholtz resonator, two theoretical models have been developed. These are the Lorentz-linearized model without and with bending terms, called respectively the quasi-linear and nonlinear curve. The models define the shape of response curves. The quasi-linear curve depends on the parameters σ_H (the eigenfrequency) and ν_0 (the friction coefficient). The nonlinear curve depends on σ_H , ν_0 and Γ , the bending parameter. The curves prescribe the tidal response for a forcing condition, which was compared with the experimental data. The parameters were fitted to maximize the correspondence between the theoretical curve and the experimental data.

Three or four sensors have been used to collect data during the experiments. One or two sensors have measured the tidal signal at sea close to the pipe. One, two or three sensors

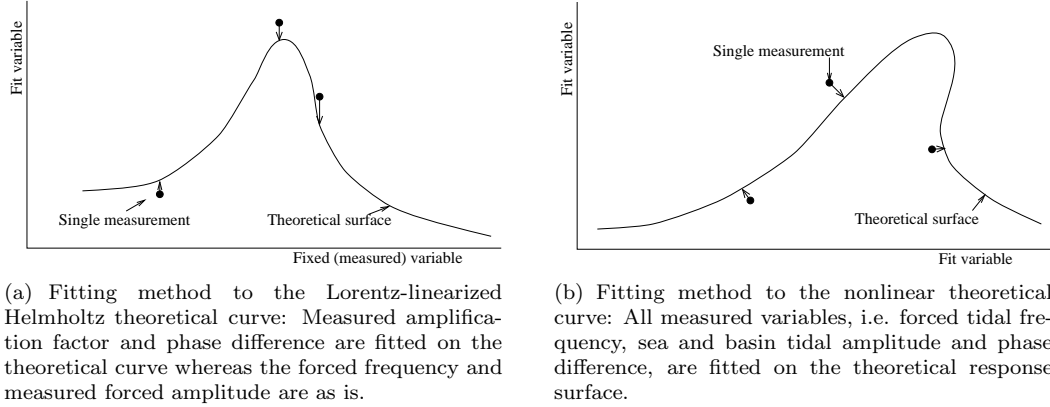


Figure 3.8: Sketches of the fitting methods

have measured the tidal signal in the basin. Each possible pair of a ‘sea’ sensor and a ‘basin’ sensor within one session is considered as one measurement of a tidal amplification and a tidal lag for a tidal frequency and forcing tidal amplitude. These amplitudes and phases were determined with harmonic analysis (section 3.4).

The forcing amplitude α_s is defined as the amplitude of the tidal frequency measured with a sensor monitoring the sea. The response amplitude α_b is defined as the measured tidal amplitude of a sensor monitoring the basin. The amplification factor of the tidal signal is α_b/α_s . Furthermore, the phase difference between sea and basin φ is defined as the difference between the phase determined for the ‘basin’ sensor and the ‘sea’ sensor. Positive φ corresponds with a tidal phase in the basin which precedes the tidal phase in the sea. The angular frequency ω is used as the fourth variable. In this section, predicted values are written with subscript T , measured values without index.

3.5.1 Comparison with the Lorentz-linearized Helmholtz solution

The Lorentz-linearized Helmholtz solution, which will be used to fit on, are the equations (2.37) and (2.38). The fitting parameters in these equations are the eigenfrequency σ_H and the effective friction coefficient ν_0 . The response curve that is defined by these equations, is called the quasi-linear response curve.

With these two fit parameters and ω and α_s , predictions for $(\alpha_b/\alpha_s)_T$ and φ_T is calculated for each session. With these $(\alpha_b/\alpha_s)_T$ and φ_T , a least-square error is constructed as the distance between the measured α_b/α_s and φ and the predicted $(\alpha_b/\alpha_s)_T$ and φ_T . For the calculation of this distance, the response is represented by its complex equivalent. This is done to obtain an equal weight of amplification factor and phase difference. The real part is defined by $\cos(\varphi) \cdot \alpha_b/\alpha_s$, the imaginary part by $\sin(\varphi) \cdot \alpha_b/\alpha_s$. The square error of a single measurement is defined as the square of the distance between the measurement and the theoretical prediction of the response in the complex plane.

The standard MATLAB[®] minimization routine (see appendix A for further information) is used to find the fit parameters σ_H and ν_0 which minimize the square error. In this method for determining single errors, the measured tidal forcing α_s and forced angular frequency are as is (see figure 3.8(a)).

Accuracy of the fit of the parameters

In order to get an estimate of the accuracy of the fit of the parameters, the external and internal error were calculated. The external error is the error margin that is calculated by taking the differences between the measurements and the best fit curve as error margin of each measurement. The internal error is the error margin that is achieved by taking the estimated error of the harmonic analysis (section 3.4) as error margin of each measurement. The external and internal error can not be calculated directly, because of the complex structure of the response curves. Therefore estimation method was used.

The estimation method was that the measurement data were changed with perturbations of the magnitude of the error of the measurement data. The parameters were fitted again on this pertubated data set. If the pertubated data parameters differ strongly from the unpertubed data parameters, the error margin of the fit of the parameters is large. If only small differences were found, the error margin is small.

To find the external error margin on σ_H and ν_0 , the mean difference between the measured and fitted α_b/α_s and φ is calculated, as an estimate of the measurement error of these variables. Each measured α_b/α_s and φ is perturbed. The perturbation is randomly chosen of a normal distribution with a standard deviation equal to this measurement error estimate. A new fit with minimized least-squares error is determined for this perturbed set of measurements. The random perturbation and determination of a fit is done 50 times. The standard deviation of all these fits is used as an estimate for the external error.

The internal error margin is determined in the same way, the difference is that the error obtained in step 11 of the harmonic analysis, described in section 3.4.1, is used as estimate for the measurement error. The relative error in α_b/α_s is determined as rootmean square of the relative errors in α_b and α_s , the error in φ is the rootmean square of the error in the phase of the forcing and response signal. The estimated error margin is different for each measurement, each variable is randomly perturbed with standard deviation equal to the error margin corresponding to that variable.

In the ideal situation, the internal and external error margin are rather equal. An external error which is much smaller than the internal error, indicates an over-estimation of the measurement errors for each variable. An external error which is much larger than the internal error, either indicates an underestimation of the measurement errors or is a consequence of an inaccurate prediction of all measurements by the theory.

3.5.2 Comparison of laboratory data with the non-linear solution

The nonlinear relation for the amplitude response was constructed in section 2.4 and reads

$$(\sigma_H^2 - \omega^2 + 2\omega^2\Gamma|\alpha_b|^2 + i\nu_0\omega^2|\alpha_b|^2) \alpha_b = \sigma_H^2 \alpha_s e^{-i\varphi}, \quad (3.2)$$

in which σ_H , ν_0 and Γ , the bending term, are the fit parameters. This equation defines, for fixed σ_H , ν_0 and Γ , a two-dimensional surface in the four-dimensional space of $(\omega, \alpha_b, \varphi, \alpha_s)$. A measurement is a point in this four-dimensional space. The first step of the fitting process is calculating the smallest distance between each measurement and this surface, as is illustrated for two-dimensions in figure 3.8(b). Calculating this distance, the variables, i.e. α_s , α_b , φ and ω , are scaled with $\langle \alpha_s \rangle$, $\langle \alpha_b \rangle$, 2π and σ_H , that they have equal weight. Scaling is necessary since these variables are measured in different units. In contrast with the comparison procedure described in section 3.5.1, the forcing frequency and the tidal amplitude at sea are now not fixed, they may be varied to find the smallest distance of a measurement to the surface. This different approach is visualized in figure 3.8. For the determination of the minimal distance between each point and the surface, a Newton iteration minimization procedure was used, comparable to the one described in section A.

The quadratic sum of all distances is the error of the fit. The best fitting σ_H , ν_o and Γ is found by minimizing this quadratic distance sum, for which the MATLAB[®] minimization procedure (see section A for further information) was used.

The calculation of the external and internal error is done in the same way as for the Lorentz-linearized Helmholtz solution in section 3.5.1.

3.6 Computer modeling

To get a quick insight in the responses that can be expected, a computer model is useful. The environmental conditions, for example the effective friction ν_o , can easily be altered and different conditions can be investigated quickly. The computer model was used to trace the circumstances under which a phenomenon, that is known to exist under idealized environmental conditions, can be measured with the experimental set-up. This was done specifically to determine inlay shapes which cause enough bending to generate a response with multiple equilibria in the basin.

Computer modeling did not have a big role in the experiments, because the goal of the experiments was to find out if the Helmholtz theory is a good description of the response of Helmholtz basins. The equations that are used for computer modeling, are derived within this theoretical context described in section 2.2.1 and 2.2.5. Therefore, computer modeling cannot show the validity of the theoretical context of Helmholtz modes. Laboratory experiments, however, can do such validation. For more computer modeling with Helmholtz basins see Maas (1997); Doelman *et al.* (2002).

The equations used in the computer model are the Helmholtz equations (2.24) and (2.25), in terms of the excess volume V ($V \equiv \int_0^{\zeta_b} A dh$) and the basin area A . These three equations,

$$\begin{aligned} \frac{du}{dt} + \frac{g}{L} (\zeta_s - \zeta_b) + \frac{c_d}{H} |u| u &= 0 \\ \frac{dV}{dt} + O u &= 0 \\ \zeta_b &= f(V) \end{aligned} \quad (3.3)$$

are discretized using Adams-Bashforth to

$$\begin{aligned} u_{(n+1)} &= \frac{\Delta t g}{L} (\zeta_{s(n+\frac{1}{2})} - \zeta_{b(n+\frac{1}{2})}) - \frac{\Delta t c_d}{H} u_{(n+\frac{1}{2})} |u_{(n+\frac{1}{2})}| + u_{(n)} \\ V_{(n+1)} &= \Delta t O u_{(n+\frac{1}{2})} \\ \zeta_{b(n+1)} &= f(V_{(n+1)}) \end{aligned} \quad (3.4)$$

with $\{u, \zeta_b\}_{(n+\frac{1}{2})} \equiv \frac{3}{2}\{u, \zeta_b\}_{(n)} - \frac{1}{2}\{u, \zeta_b\}_{(n-1)}$, where n is the time step number.

Before the model is run, a parameterisation of ζ_b as a function of V is prescribed: a serie of increasing ζ_b values that enclose the range of water levels in the basin which will occur during the model evaluation, is defined and the corresponding V values are determined. A special hypsometry can be defined here. During the model evaluation these V and ζ_b series will be used to calculate $\zeta_{b(n)}$ as function of $V_{(n)}$.

The timestep Δt is chosen such that during one tidal period around 2000 timesteps are made; moreover the tidal period is taken a multiple of the timestep. This is done to simplify the determination of the convergence to a steady state.

At least 10000 iterations, that is approximately 5 periods, are calculated. After that, the numerical integration is stopped when the differences in u and ζ_b with values that occurred a few tidal periods earlier and for the same phase of the tidal forcing, both are less than the difference to the previous step. The numerical integration is also stopped when the iterations exceed 60000 steps. The last 10000 iterations are used for a simplified version of the harmonic analysis procedure described in section 3.4.1. A stop after 60000 times was

chosen because of memory problems that occurs if more timesteps were made. The memory problems were not solved, because the model is applied to find stable solutions, not to search chaotic behaviour. The stable solution was reached most times in a calculation time of 10 tidal periods.

In order to study multiple equilibria, it is necessary that the model stabilizes “in the same branch” for successive evaluations. If for example a Helmholtz system has a forcing frequency domain where multiple solutions exist, and one would investigate the width of this frequency domain, then the forcing frequency is altered in successive evaluations and the numerical model should stay “in the same branch” until that branch ends. To obtain this, information of the preceding evaluation, namely the final values of u and V are used to initialize the new evaluation.

Chapter 4

Experimental results

Having described the theoretical background in chapter 2 and the experimental set-up in chapter 3, this chapter deals with the results obtained with the tidal simulator. As remarked in the introduction, the subjects were

1. Experimental verification of Helmholtz resonator by generating tidal amplification.
2. Verification Lorentz-linearization principle for bottom friction description.
3. Investigate the nonlinear phenomena like multiple equilibria and chaos, as predicted by models (Maas (1997) a.o.).

In sections 4.1 to 4.3 experiments with uniform hypsometry will be discussed. First all measurements with full basin area (see section 3.2.4) will be considered in section 4.1. Moreover the basin area has been reduced to different sizes in order to reduce the influence of friction. The results of these changes will be discussed subsequently. Finally the existence of multiple equilibria will be shown for these basins with uniform hypsometry in section 4.3.

The second part, section 4.4, is about experiments with non-uniform hypsometry. The specific effects on the response in the basin will be shown for different inlay types. All of these inlays have been discussed in subsection 3.2.4.

4.1 Results for large basin area

The first measurements that will be discussed are those for a full basin area without an inlay or area reduction. This is the obvious starting point for the experiments; this area is present without adaptations on the set-up. Consequently, the experiments can be repeated and the results can be mutually compared easily, because it is easy to reproduce this basin area by removing all inlays. Other basin areas that are constructed with certain inlays are hard to be reproduced identically after removal of the inlay.

4.1.1 Experimental conditions

Measurements that use a full basin area, can be compared well with each other. In order to obtain a set of reference measurements for each pipe, experiments have been done with nearly all pipes. The characteristics of the pipes are listed in table 3.1.

The mean water level has not been changed during one measurement session, but is not equal for all experiments. Mean water levels between 13 and 20 cm has been used, that is 1 to 5 cm above the top of the connecting pipe. The effect of the mean water level has been investigated, but measurements show that it has no influence under these circumstances.

Forcing amplitude and frequency

As an example of the forcing amplitudes and frequencies that have been generated, those for *Pipe one* and *C34* are plotted in figure 4.1. Initially, the experimental set-up has been driven with a constant voltage of the sinusoidal input. This has been done for *Pipe one*, *Pipe two* and *T42*. However, the tidal amplitude generated at sea is not the same for each frequency, if constant input voltage amplitudes are applied. As a consequence, the forcing amplitude at sea varies with different frequencies for these pipes, as visible in figure 4.1(a). In section 3.2.3 the source of this variation was discussed. For this frequency domain, the small size of the sea is the most important effect. Later on the variation is reduced by adjusting the input voltage amplitude, which leads to a nearly constant forcing tidal amplitude, as shown in figure 4.1(b). The forcing amplitudes of the experiments with pipe *T32* and *T52* have some variance, although the input voltage has been adjusted.

For *Pipe one*, *Pipe two* and *T42*, series of measurements with different forcing amplitudes have been carried out, in order to investigate the theoretically predicted dependency of the tidal response on the forcing amplitude. Figure 4.1(a) shows for example the applied forcing amplitudes for *Pipe one*, the different series of measurements are marked with squares, circles and crosses. All these measurements with one pipe are used to obtain one fit on the theoretical predictions. For the other pipes, one measurement series with forcing amplitude of around 1 mm has only been done. The forcing amplitude was minimized, because the tidal amplification increases for decreasing forcing amplitude. The forcing amplitude of 1 mm was chosen, because for this amplitude the detection accuracy is still very good, see section 3.4.2 for a discussion on accuracy. Lower forcing amplitudes have been tried, but the results gave doubts about reliability.

The frequency domain has been investigated from approximately 0.5 to 2 times the theoretical Helmholtz frequency. The pipe modifies the eigenfrequency, therefore the frequency range has been adapted for each pipe. On average 10 different frequencies have been used for *Pipe one*, *Pipe two* and *T42*, which were investigated while manually controlling the set-up. The measurements were automated for the other pipes, for these approximately 20 measurements were done for each of the other pipes.

Finally, a remark has to be made on the solid lines representing the theoretical response curve, i.e the amplification of sea level variation and the phase lag of the tide in the basin. A solid line has been chosen to represent the theoretical response curve, because a solid line is clearer than a ‘point wise’ representation. In a ‘point wise’ representation, each measurement — a point — must be compared with another point, representing the theoretical response for that measurement. The solid line representing the theoretical response, depends on the basin qualities $\sigma_{H(M)}$ (eigenfrequency), ν_0 (friction coefficient) and Γ (bending parameter in nonlinear theory), but also on the forcing amplitude. However, the applied forcing tidal amplitude varies. To obtain an accurate comparison between theoretical predictions — the solid line — and measured results, the ‘forcing amplitudes’ for which the solid line is calculated, should be similar to the applied forcing tidal amplitudes. Therefore, a solid line of ‘forcing amplitudes’ that match the applied forcing tidal amplitudes has to be constructed. An example is given in figures 4.1(a) and 4.1(b).

4.1.2 Results of *Pipe one*

The results with the straight pipe *Pipe one* will be discussed first. These results are compared with the Lorentz-linearized Helmholtz theory; the typical phenomena are indicated. Secondly, the results of all pipes are compared with this quasi-linear theory. Thirdly, the results of trumpet-shaped pipe *C34* are shown, as example of an experimental result that deviates from the quasi-linear theory. The results of this pipe are compared with a generic nonlinear response curve, in order to investigate this apparently nonlinear behaviour. Fi-

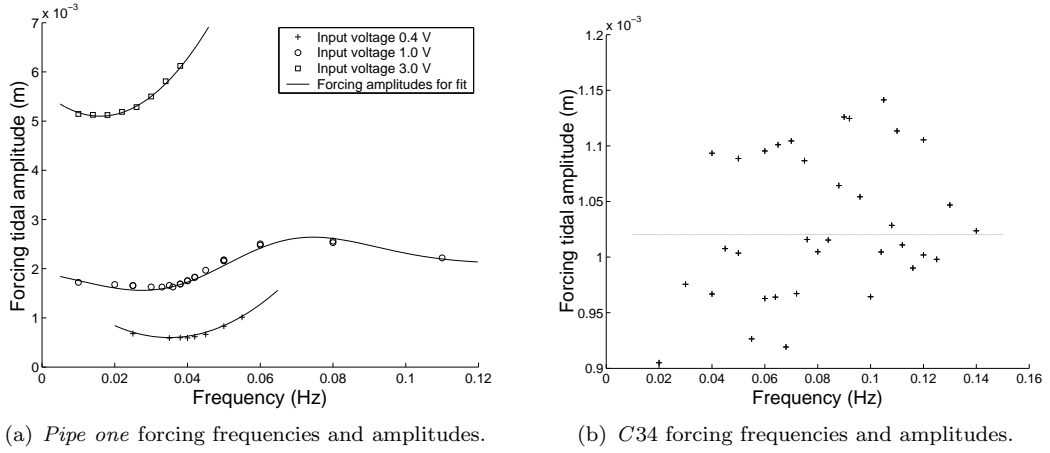


Figure 4.1: All forcing frequencies and amplitudes which have been used for *Pipe one* and *C34*. The solid line shows the forcing amplitudes which have been used for the theoretical curve in figure 4.3.

nally, all results are compared with this generic nonlinear response curve.

The response curve

Figure 4.2 shows the measured responses in case of *Pipe one*. The markers represent the measurements, the solid lines the predicted quasi-linear behaviour, described in section 2.3. The applied forcing tidal amplitudes are shown in figure 4.1(a).

The fitting procedure of the quasi-linear theory on the measurements is described in section 3.5.1. In brief, all measured amplifications and phase lags are matched with the theoretical quasi-linear curve. The differences between both are minimized by varying the eigenfrequency σ_H and the friction coefficient ν_0 , which determine the theoretical curve. So, the measured eigenfrequency $\sigma_{H(M)}$ and friction coefficient is determined by a best fit procedure. The measurements confirms the theory if the measurements can be correlated accurately with a theoretical curve *and* if the determined $\sigma_{H(M)}$ compares well with the theoretical Helmholtz eigenfrequency $\sqrt{gO/AL}$ (equation (2.17)). The gravitational acceleration is denoted by g in this equation; O , A and L denotes respectively the pipe cross sectional area, the basin area and the pipe length.

The figures show that the measured amplification and phase lag corresponds very well with the theoretically predicted behaviour. The amplification factor displays clearly the two aspects of the quasi-linear behaviour of the friction. Firstly, amplification factor decreases with increasing forcing amplitude. Secondly, the frequency for which the largest amplification factor is found decreases with increasing forcing amplitude as well. This quasi-linear behaviour leads to a faster phase lag transition for weaker tidal forcing as well: the phase lag for frequencies lower than the eigenfrequency stays longer close to zero for weaker forcing amplitudes. A linear damped Helmholtz basin does not show these three effects. For such a basin, the response curves — amplification factor and phase lag — are independent of the forcing amplitude.

The results for *Pipe two* are presented in the appendix, in figure C.1. They qualitatively resemble the results for *Pipe one*.

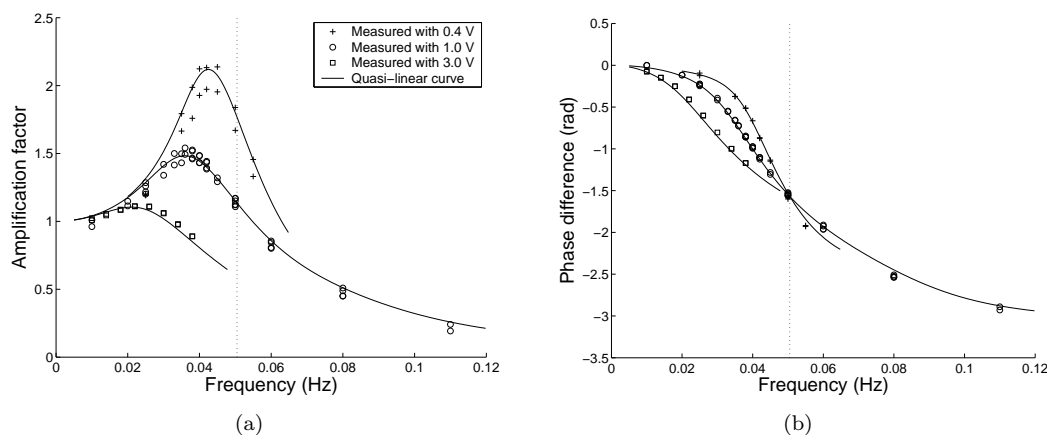


Figure 4.2: Response curves for *Pipe one* with full basin area. The applied tidal forcings were shown in figure 4.1(a). The solid line represent the theoretical quasi-linear response for the applied tidal forcings. The dotted line is the Helmholtz eigenfrequency. The tide in the basin lags behind the tide at sea, if the phase difference is negative.

4.1.3 Currents

The latter analysis that is based on altimetry measurements, is a rather complete description of the main phenomenon of a Helmholtz resonator. Since in the theory however, the current speed in the channel or pipe can be eliminated this statement is not astonishing. Nevertheless an indication of the currents in the pipe is useful for a clear understanding of the experimental set-up. For further analysis they are useless, because they can be determined only indirectly from altimetry measurements.

The current speeds in the pipe are presumed to be rather sinusoidal in time and depends on the tidal amplitude in the basin, the tidal frequency, the cross section of the pipe and finally the basin area. A larger tidal forcing increases the currents through the pipe, because the tidal amplitude in the basin increases as well, although the tidal amplification decreases. Furthermore, an analysis of the effect of a decreasing pipe cross section or an increasing basin area cannot be given, because an alteration would change the eigenfrequency and the friction coefficient. Finally the strongest currents are found when the Helmholtz resonator is driven at its eigenfrequency.

This maximum velocity is approximate 10 cm/s for *Pipe one* when a forcing amplitude of 1 mm is applied. The maximum velocities in the trumpet shaped pipes are around 20 cm/s applying a 1 mm forcing amplitude. The maximum velocities are estimated by using equation (2.25).

4.1.4 Comparison of the results of all pipes

The latter procedure has been applied on the measurements of all pipes for full basin area. The derived results are shown in table 4.1. Here $\sigma_{H(T)}$ denotes the theoretical eigenfrequency, defined by $\sqrt{gO/AL}$ (equation (2.17)), in which g denotes the gravitational acceleration, O the pipe cross sectional area and A the basin area and L the pipe length. The error in the theoretical value is determined by estimated errors in the measurement of the size of the basin, pipe length and cross sectional area. The measured fitted eigenfrequency is denoted by $\sigma_{H(M)}$ and ν_0 is the friction coefficient. These values are the parameters of the fit to the Lorentz-linearized theory, a quasi-linear theory. The description of the procedure

pipe name	$\sigma_{H(T)}$ 10^{-3} Hz	$\sigma_{H(M)}$ 10^{-3} Hz	ν_0 10^2 m $^{-1}$	C_e
<i>Pipe one</i>	53.1 ± 0.5	$50.5 \pm 0.14 / 0.9$	$3.74 \pm 0.007 / 0.09$	1.23 ± 0.10
<i>Pipe two</i>	70.9 ± 0.6	$65.1 \pm 0.2 / 0.8$	$2.39 \pm 0.006 / 0.04$	1.23 ± 0.10
<i>T32</i>	75.8 ± 0.6	$82.4 \pm 0.08 / 2$	$1.52 \pm 0.001 / 0.10$	-1.06 ± 0.09
<i>T42</i>	66.2 ± 0.5	$70.7 \pm 0.10 / 1.4$	$1.23 \pm 0.003 / 0.04$	-1.05 ± 0.08
<i>T52</i>	59.4 ± 0.5	$63.0 \pm 0.06 / 1.4$	$1.17 \pm 0.001 / 0.08$	-1.22 ± 0.10
<i>C34</i>	73.5 ± 0.6	$78.5 \pm 0.10 / 3$	$1.39 \pm 0.002 / 0.2$	-0.89 ± 0.08
<i>C42</i>	66.2 ± 0.5	$70.8 \pm 0.07 / 1.8$	$1.29 \pm 0.002 / 0.12$	-1.14 ± 0.09
<i>C52</i>	59.4 ± 0.5	$62.4 \pm 0.08 / 1.1$	$1.10 \pm 0.002 / 0.09$	-1.03 ± 0.08

Table 4.1: The results for the full basin with different pipes. Here $\sigma_{H(T)}$ is the theoretical eigenfrequency for the Helmholtz equations without hypsometry; $\sigma_{H(M)}$ and ν_0 are the measured eigenfrequency and friction coefficient. They have been determined with Lorentz-linearized linear theory. The first error value of the measurements is the internal error, the second is the external error. Finally C_e is the coefficient that determines the effective length, explaining the difference between $\sigma_{H(T)}$ and $\sigma_{H(M)}$.

to obtain these values and the error estimations has been given in section 3.5.1. The first error in the measured values is the internal error. The second error is the external error.

Note that systematically $\sigma_{H(T)}$ and $\sigma_{H(M)}$ differs. For straight pipes $\sigma_{H(T)}$ is larger than $\sigma_{H(M)}$, while for trumpet shaped pipes $\sigma_{H(T)}$ is smaller than $\sigma_{H(M)}$. This is due to the difference between the physical pipe length L and the effective dynamical length L_e . The coefficient C_e determines the difference between L_e and L . The effective pipe length is defined as that length that gives $\sqrt{gO/AL_e} = \sigma_{H(M)}$. In case of a straight pipe, Morse (1948) showed that L_e depends on the pipe length L and pipe radius R through $L_e = L + C_e \cdot R$, in which the theoretical value for C_e 1.2 to 1.7 is. The measured value is within this range. A theoretical value for the effective length of a pipe with smooth ends has not been found. The differences between the measured effective lengths of the smooth end pipes are rather small, which make the measured value reliable.

The following remarks can be made concerning the friction coefficient:

- Smoother ends of the pipes lead to less friction. The ‘*T*’ and ‘*C*’-pipes, which have smooth ends, yield lower friction coefficients than *Pipe one* and *Pipe two*, which have sharp ends.
- The ‘*T*’ and ‘*C*’ series show that the friction is reduced by an increase of the pipe length. This suggests that frictional effects are dominated by turbulence that is generated at the tube ends.
- Increasing the cross-sectional area decreases the friction coefficient: *Pipe two* is shorter than *Pipe one*, but has a larger cross section in comparison to *Pipe one*. According to the previous remark, a shorter pipe results in more friction. Apparently, the larger cross sectional area of *Pipe two* reduces the friction.
- The friction coefficient ν_0 is determined experimentally. This coefficient is related to the bottom friction coefficient c_D with equation (2.31). Calculation of c_D gives for example a value of 0.67 or 0.45 for respectively *Pipe one* and *C34*. For this purpose however, ν_0 is much clearer than c_D , because c_D depends on variable boundary conditions like the basin area. The friction coefficient ν_0 however corresponds directly to the response curves, which means the shape of a response curves does not change due to altering eigenfrequency — for equal forcing amplitude. So, an equal ν_0 gives

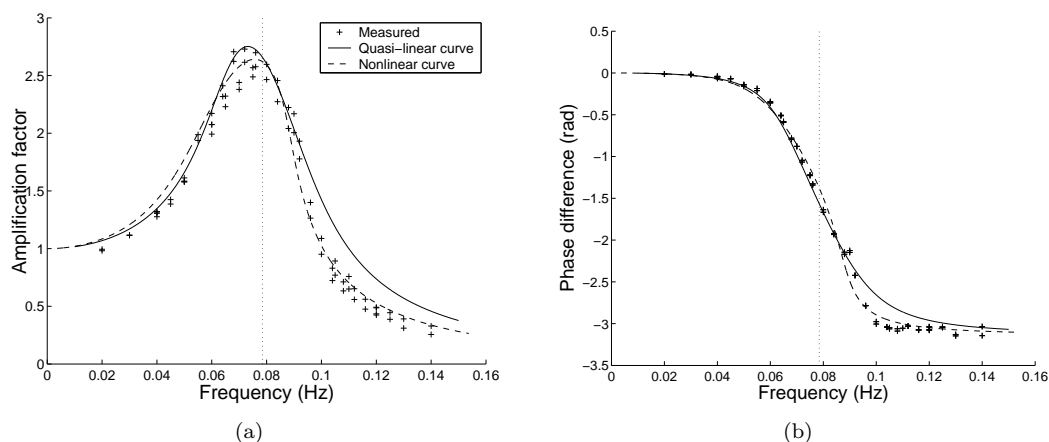


Figure 4.3: Response curves for full basin and for the *C34*-pipe, with a trumpet-shaped pipe end. The solid lines represent the theoretical quasi-linear response curves, the dashed line the generic nonlinear curve. The dotted line is the Helmholtz eigenfrequency determined with quasi-linear theory. The applied forcing amplitudes are shown in figure 4.1. If the tide in the basin lags behind the tide at sea, the phase difference is negative.

always for example the same maximum amplification for a certain forcing amplitude. This quality is an advantage of using ν_0 .

Error estimation discussion

In the latter discussion, the basin quantities eigenfrequency and friction coefficient have been discussed only. As mentioned in the previous section, the quasi-linear Helmholtz theory is proved if firstly the measured eigenfrequency and the theoretical eigenfrequency are comparable. In the latter discussion, this has been shown. The second demand for a proof of the Helmholtz theory is a strong correspondence between the measured response curve and the theoretical curve. This has been shown in the previous section 4.1.2.

Besides the graphical analysis, the error estimations provide a good indication of this correspondence. The calculation procedure of the internal and external error was described in section 3.5.1. The internal error indicates the error of $\sigma_{H(M)}$ and ν_0 which is caused by measurement errors. The external error indicates the total uncertainty of the measured $\sigma_{H(M)}$ and ν_0 , which can be due to a lacking correspondence between measurements and theory as well. In the situation that the external error is much larger than the internal error, the measured response curve may show a different behaviour as predicted by the theory.

The internal error margins for ‘*T*’ and ‘*C*’-pipes, shown in table 4.1, are smaller than those for *Pipe one* and *Pipe two*, because the measurement sessions for the ‘*T*’ and ‘*C*’-pipes were longer. The external error margins for the ‘*T*’ and ‘*C*’ are twice as much as those for *Pipe one* and *Pipe two*. Therefore, the response curves for the measurements with trumpet-shaped pipes are discussed in the next subsection.

4.1.5 Response curves for trumpet-shaped pipes

Figures 4.3(a) and 4.3(b) show the results for one of the trumpet-shaped pipes, the *C34*-pipe. In subsection 3.2.5, a description of the shape of the pipe has been given. The measured amplifications and phases are globally consistent with those obtained from quasi-linear theory. However, in the results of *C34*, two differences appear. The measured amplifications de-

pipe name	Quasi-linear fit		Nonlinear fit		
	$\sigma_{H(M)}$ 10^{-3} Hz	ν_0 10^2 m $^{-1}$	$\sigma_{H(M)}$ 10^{-3} Hz	ν_0 10^2 m $^{-1}$	Γ 10^3 m $^{-2}$
<i>Pipe one</i>	50.5 ± 0.9	3.74 ± 0.09	50.1 ± 1.9	3.39 ± 0.05	0.8 ± 0.8
<i>Pipe two</i>	65.1 ± 0.8	2.39 ± 0.04	66.0 ± 1.0	2.42 ± 0.03	-0.1 ± 0.3
<i>T32</i>	82.4 ± 2	1.52 ± 0.10	73 ± 3	1.15 ± 0.02	20.2 ± 1.0
<i>T42</i>	70.2 ± 1.3	1.31 ± 0.09	65 ± 3	1.13 ± 0.02	10.6 ± 1.1
<i>T52</i>	63.0 ± 1.4	1.17 ± 0.08	58.8 ± 2.2	1.02 ± 0.02	6.7 ± 0.6
<i>C34</i>	79 ± 3	1.39 ± 0.2	70.3 ± 1.9	1.12 ± 0.03	18.0 ± 1.2
<i>C42</i>	70.8 ± 1.8	1.29 ± 0.12	65 ± 4	1.08 ± 0.03	11.3 ± 1.3
<i>C52</i>	62.4 ± 1.1	1.10 ± 0.09	58.4 ± 1.2	0.96 ± 0.01	8.6 ± 0.7

Table 4.2: Comparison of nonlinear and quasi-linear fit parameters for full basin with different pipes. Γ is the bending parameter in the nonlinear response function. The error margin is the estimated external error, which is larger than the estimated internal error.

crease more quickly for frequencies above the eigenfrequency than the theoretical curve does. Similarly the phase lag is steeper. This shows that the basin response reaches the choked mode sooner. This mode is characterized by a strongly suppressed response in opposite phase. Similar changes were found in the response curves for all ‘*T*’ and ‘*C*’-pipes.

As a result of this lack of match between theoretical and measured results, the estimated external error for all ‘*T*’ and ‘*C*’ results is large (see table 4.1). Increasing or decreasing differences between predicted and measured results increase or decrease directly the estimated external error in these data. For the procedure of the derivation of the external error, see subsection 3.5.1.

The clear differences between the response curve generated with quasi-linear theory and the measurements indicate that the response of the laboratory basin is not fully caught by quasi-linear Helmholtz theory. In order to investigate the origin and pattern of this irregular behaviour, the measurements are fitted on a generic weak nonlinear response curve. This generic curve is the dotted line in figures 4.3(a) and 4.3(b). This curve is defined by equation (2.43). The fitting procedure on this curve is described in section 3.5.2. This generic nonlinear curve matched better the measured responses, which means the basin responses are those of a damped Helmholtz resonator that is weakly disturbed by a certain nonlinear mechanism. It is unclear yet, which mechanism is responsible for this nonlinear behaviour. Although the generic nonlinear curve fits better on the measurements, it does not completely match the measurements either. For example, differences are visible for frequencies below the eigenfrequency.

Comparison of quasi-linear and generic nonlinear fit parameters

The fitting parameters for quasi-linear theory and the generic nonlinear curve are listed in table 4.2. The generic nonlinear curve is based on equation (2.43). The nonlinear parameter Γ [m $^{-2}$] determines the bending of the curve in this equation. The quasi-linear and the nonlinear curve coincide if $\Gamma = 0$ (with equal $\sigma_{H(M)}$ and ν_0). A positive Γ implies bending of the amplitude response curve towards higher frequencies. In comparison with *Pipe one* and *Pipe two*, the bending is significant for ‘*T*’ and ‘*C*’-pipes, the external error margin is less than the value of Γ .

In table 4.2, the ‘free’ Helmholtz eigenfrequency $\sigma_{H(M)}$ is listed. This eigenfrequency is the response frequency in a friction and forcing free situation while the tide in the basin has infinitesimal small tidal amplitude. The *effective* eigenfrequency, which is measured, depends on this Helmholtz eigenfrequency, but is affected by the tidal amplitude in the basin and the

bending parameter Γ as well. In order to obtain the Helmholtz eigenfrequency, this deviation that is caused by the nonlinearity, must be removed. So, the determined eigenfrequency $\sigma_{H(M)}$ depends on Γ as well. Consequently, an error in Γ increases the error estimate of the eigenfrequency.

The error margin on the friction coefficient is decreased in comparison to the quasi-linear fit. This decrease indicates that the nonlinear fit is more accurate than the quasi-linear fit.

4.1.6 Summary

The first conclusion is that the Helmholtz theory has been successfully reproduced with an experimental facility, which mimics the Helmholtz configurations with vertical walls. The theoretically predicted and measured eigenfrequency match well. Secondly, the Lorentz-linearized friction coefficient gives a good description of the damping effects. The measured amplitudes and phases agree well for increasing tidal forcing amplitude with those obtained from quasi-linear theory: The amplification of the tide decreases and the frequency for which the maximum response is reached decreases, both for increasing tidal forcing.

Smooth end parts on the pipes reduce friction. However, these pipe ends generate nonlinear bending of the response curves which can not be explained with the Helmholtz theory yet.

4.2 Reduced basin area with uniform hypsometry

Having described the results for full basin area in the preceding section, the results for a number of experiments with reduced basin areas will be discussed in this section. The main reason to reduce the basin area is that the friction will be reduced by an area reduction, as discussed in subsection 2.3.2. Friction obscures nonlinear behaviour. So by reducing friction, it is expected to cause nonlinear behaviour, for example bended resonance, to be more distinct.

The basin area is reduced with partitions, in a way that was described in subsection 3.2.4. The width of the basin was adapted only, the length was not changed. During the experiments of this section, the sidewalls remain vertical. The C34-pipe was used for the experiments. Smooth pipe end have been used, because they cause less friction than straight pipe ends. Indeed, as expected from theoretical considerations, the amplification of the tide tends to increase. Nonlinear behaviour can be noticed earlier in strongly amplified response. Secondly, the unexpected nonlinear bending of the response curve of smooth pipes could now be investigated more.

One phenomenon has to be mentioned before the results can be discussed. In the experiments discussed below, rather high forcing frequencies were applied. The tidal response in the basin requires to have a standing wave character due to this 'high' forcing frequency, which means the amplification is little weaker above the pipe end and increases slightly to the far end of the basin. Nevertheless, this phenomenon is not harmful for the experiments, because no phase difference within the basin was measured.

Figure 4.4 shows the tidal responses for different basin areas, together with nonlinear curves. For the sake of clarity, the results are displayed only for a few basin areas. The fitting parameters of the nonlinear curves are listed in table 4.3. The eigenfrequency and the friction coefficient are plotted as a function of the basin area in figure 4.5.

4.2.1 Discussion of the results

The first thing to be noted from figure 4.4 is that the eigenfrequency (table 4.3) increases with decreasing basin area. Hence, the maximum response and the transition in phase lag is found for higher frequencies. The theoretical relationship between basin area and

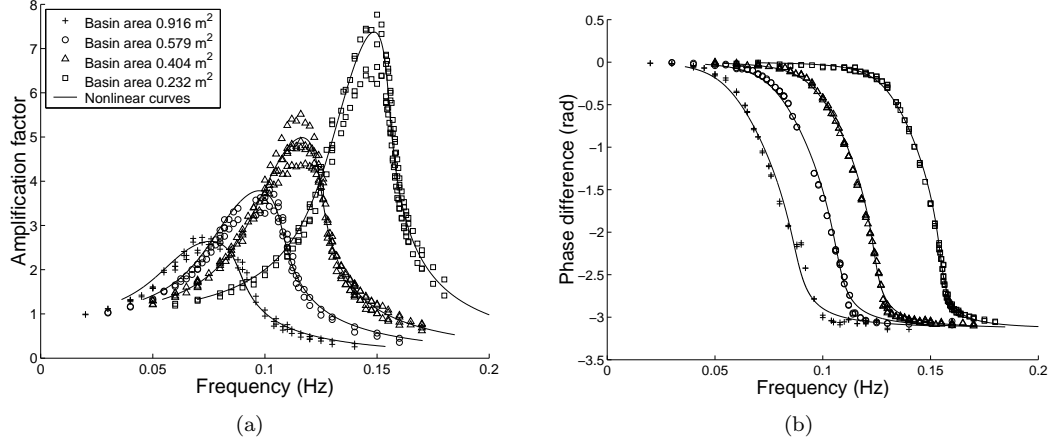
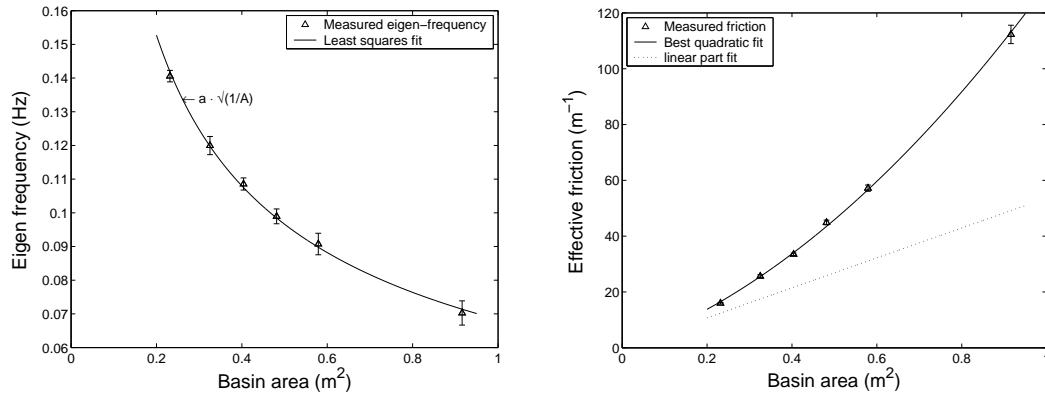


Figure 4.4: Response curves for different basin areas. Markers are measurements, lines are generic weak nonlinear response curves. The tidal amplitude increases slightly towards the far end of the basin. Therefore, two different amplification curves are measured, which belong to different sensor positions.

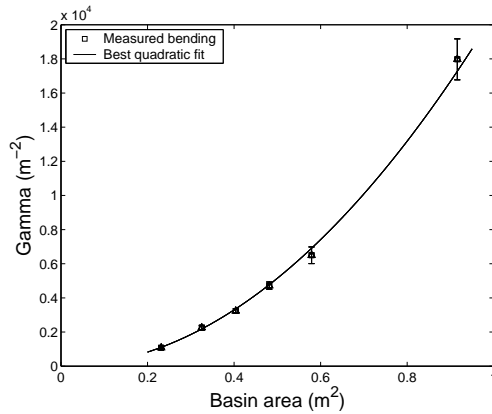
Basin area m^2	$\sigma_{H(T)}$ 10^{-3} Hz	$\sigma_{H(M)}$ 10^{-3} Hz	ν_0 m^{-1}	Γ 10^3 m^{-2}
0.916	73.5 ± 0.6	$70. \pm 4$	$112. \pm 3$	18.0 ± 1.2
0.579	92.5 ± 0.8	$91. \pm 3$	57.2 ± 1.1	6.5 ± 0.5
0.481	101.4 ± 0.9	98.9 ± 2	44.9 ± 0.8	4.71 ± 0.2
0.404	110.8 ± 1.0	108.5 ± 1.9	33.9 ± 0.5	3.12 ± 0.11
0.325	123.4 ± 1.2	$120. \pm 3$	25.6 ± 0.5	2.26 ± 0.13
0.232	146.3 ± 1.7	140.6 ± 1.7	16.0 ± 0.3	1.08 ± 0.05
For comparison, results with a straight pipe:				
0.232	152.4 ± 1.7	132.5 ± 2	61.1 ± 0.7	0.60 ± 0.17

Table 4.3: Fitting parameters of the nonlinear curves. These experiments have been done with a forcing amplitude of ~ 1 mm and with the *C34* pipe. For comparison, a measurement with a straight pipe (*P31*) is shown as well.



(a) The measured eigenfrequency as a function of the basin area. The solid line is the least squares fit for the relation $\sigma_H \sim \sqrt{1/A}$ (equation (2.17)). This relation is confirmed.

(b) The friction coefficient ν_0 as a function of the basin area. The solid line is the best second-order polynomial that cross the origin. The dotted line is the linear part of this polynomial. A linear dependency was expected (equation (2.31)).



(c) The bending coefficient Γ as a function of the basin area A . The solid line is the least squares fit for the relation $\Gamma \sim A^2$.

Figure 4.5: Dependence of the eigenfrequency, friction and bending coefficient on the basin area.

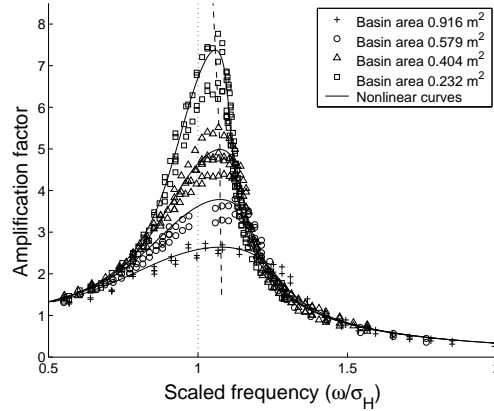


Figure 4.6: Scaled plot of the amplification factors. The right-hand dashed line is drawn through the maximum responses; it shows that the displacement of the maximum response frequency stays rather equal.

eigenfrequency is equation (2.17): $\sigma_H = \sqrt{gO/L_e} \cdot \sqrt{1/A}$. The effective pipe length can be derived again with this relation by fitting on the measured eigenfrequencies. The solid line is the least-squares fit obeying this relation in figure 4.5(a). The differences with the measured pattern are smaller than the error margin on the measurements, so the theoretical relation is confirmed. Finally, the effective pipe length ($L_e = 36.1$ cm) has been calculated with the fitting parameter. In the previous section an effective length of 37.2 cm has been calculated for full basin area, using the generic weak nonlinear curve.

The maximum response in the basin increases when basin area decreases. This is a result of the reduction of friction, which causes a steeper transition of the phase lag as well. When this transition steepens, the frequency range in which the phase lag change from ‘in phase’ to the opposite phase, becomes smaller. The friction coefficient is shown as a function of the basin area in figure 4.5(b). The definition of ν_0 (equation (2.31)) predicts a linear dependency of ν_0 on the basin area (A), so $\nu_0 \sim A$. The figure shows that a parabolic fit corresponds much better with the measured friction.

Apparently, the friction coefficient increases more quickly than predicted. An explanation might be that the friction coefficient does not only consist of the dissipation by bottom friction. The generation of a jet and vortices at the out-flow are phenomena that dissipate energy as well. These phenomena are also enclosed in the friction coefficient.

The theoretical relation between ν_0 and c_d is $\nu_0 = \frac{8}{3\pi} \frac{c_d}{H} A/O$ (equation (2.31)) for a channel. For the derivation of c_d with a pipe, the channel depth H is replaced by the pipe radius R , which leads to

$$\nu_0 = \frac{8}{3\pi^2} \frac{A}{R^3} c_d. \quad (4.1)$$

The value for c_d (the dimensionless drag coefficient, subsection 2.2.6) can be derived as the linear part of the curve in figure 4.5(b). The measured value of c_d becomes $1.6 \cdot 10^{-1}$ when it is determined in this way. This value is two magnitudes larger than the experimental value that is measured in coastal structures ($2.5 \cdot 10^{-3}$).

The final remark concerns the observed nonlinear behaviour of the response. Theoretical analysis does not lead to strong nonlinear behaviour for Helmholtz basins with vertical side-walls. Nevertheless, the tidal amplification curve (figure 4.4(a)) tends to bend to the right, a nonlinear phenomenon. The dependence of the bending parameter Γ as a function of the basin area is shown in figure 4.5(c). In the figure, the relation $\Gamma \sim A^2$ can be seen.

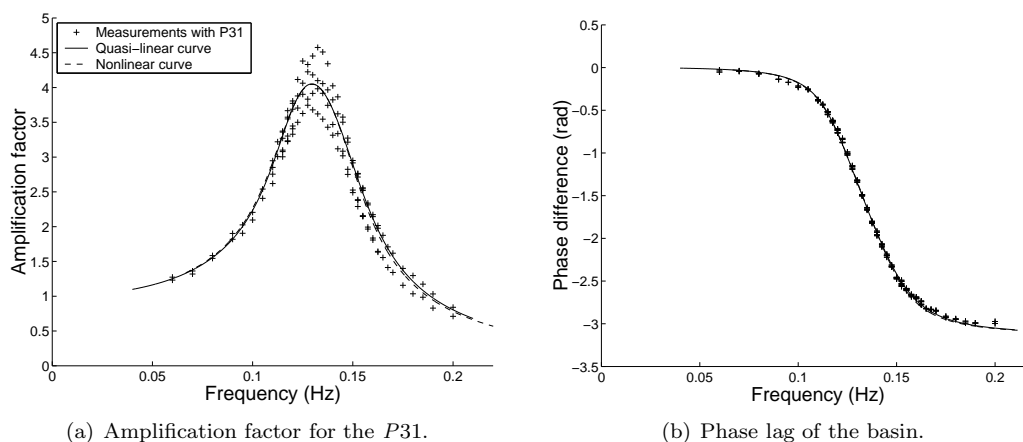


Figure 4.7: Measurements and fits for the *P31* pipes. The basin area is 0.232 m^2 and the tidal forcing amplitude is 1 mm . For *P31* the quasi-linear and (generic) nonlinear fit coincide, in comparison to the *C34* responses, for which the nonlinear theory yield a closer fit.

Due to the bending of the response curve, the frequency range in which the response decreases from strong amplification to weak amplification, becomes smaller. Differently formulated, the amplification curve becomes steeper. Figure 4.6 shows the same response curves as figure 4.4(a), but the forcing frequency is scaled with the eigenfrequency in this figure. This is done in order to compare the response curves with respect to bending. The dashed line is drawn through the maximum responses. This dashed line shows the displacement of the maximum response. In case of a quasi-linear response curve, all maximum responses are reached for frequencies lower than the eigenfrequency.

Although Γ decreases for decreasing basin area, the displacement of the maximum response is nearly constant for all basin areas. The displacement does not only depend on Γ , but on the amplification factor as well (see equation (2.43)). For decreasing basin area, the amplification factor increases. The increase of tidal amplification appears to be of equal importance as the decrease of Γ .

4.2.2 Comparison with results for a straight pipe

The previous results suggest that the strength of the nonlinear behaviour is related to the shape of the pipe end. A smooth pipe end may induce more nonlinearity than a straight pipe. In order to test this conjecture, the results are compared with measurements with a straight pipe.

The basin area was 0.232 m^2 during this experiment, i.e. the smallest basin area of the *C34* series. The *P31*-pipe has been used, because the *P31*-pipe has an equal external radius of the tube and an equal internal cross sectional area in comparison with the *C34*-pipe, and its effective length is comparable.

The parameters obtained by fitting on the generic nonlinear curve are listed in table 4.3. The response curves are drawn in figure 4.7. The response of the straight pipe differs of the response of the *C34* pipe for equal basin and forcing conditions as a result of the lower eigenfrequency — a result of a different effective pipe length — and the stronger damping. The value of Γ , derived for the measurements with the '*P*'-pipe, is significantly unequal to zero (table 4.3), but it is much smaller than the value for the *C34* pipe. In spite of the still large value of Γ , the bending of the response curve is hardly visible, due to the fact that

the response is twice as low as the response for the *C34* pipe. The bending of the curve decreases roughly quadratically for decreasing response amplitude (equation (2.43)), that is why the quasi-linear and nonlinear fit almost coincide.

It can be concluded that the straight pipe has a nonlinear response for a small basin area. The nonlinearity is much weaker than the nonlinearity, which has been measured for a trumpet-shaped pipe end. Therefore, it can be concluded that for a small basin the trumpet-shape of the pipe is the main source of nonlinearity in the experiment series with reduced basin area. Hence, the shape of the pipe of channel of a tidal Helmholtz resonator is an origin of nonlinear behaviour. The physical mechanism however is not satisfactorily established yet, the Helmholtz theory predicts a quasi-linear response. Therefore, the strength of the nonlinear behaviour due to the shape of the channel for tidal Helmholtz basins in nature is unclear.

4.2.3 Summary

The eigenfrequency and friction coefficient decrease with decreasing basin area. The eigenfrequency obeys the theoretical relation $\sigma_H = \sqrt{gO/AL_e}$. The friction coefficient increases more strongly than linearly with increasing basin area, contradicting the theoretical linear behaviour. Estimating the bottom friction coefficient from the first-order linear fit on the measurements, the friction coefficient was $1.6 \cdot 10^{-1}$. Finally, the deviation of the quasi-linear response curve, which is the theoretical predicted response, remains for experiments with smaller basin areas. The results match well the generic nonlinear response curve. The nonlinear bending parameter Γ in this curve decreases with decreasing basin area. At the same time, the response amplitude increases with decreasing basin area, which enlarges a bending of the amplification curve. The net bending stays rather equal, so these two transformations balance each other.

4.3 Multiple equilibria for uniform hypsonometry

In the previous section, the results for reduced basin area were discussed. The influence of basin area has been scanned systematically in these experiments. The measurements with the *C34*-pipe and a reference experiment with a *P31*-pipe were considered. Before these experiments were performed, experiments with pipes with smooth ends (*T*'-pipes) with different lengths and reduced basin area have been done. The smooth ends that have been used for these experiments, differ slightly from those that were used for the experiments discussed in the previous section¹. Pipes with smooth ends have been used, because they cause less friction. In this section, the interesting results from the latter experiments will be discussed.

The basin area was reduced in these earlier experiments with the same procedure as was used for the results in the previous section. For a description of this procedure see subsection 3.2.4. The main difference is the range of basin areas that could be made. In the previous section the basin was varied from 0.58 m^2 to 0.23 m^2 . In the experiments in this section, the basin was varied from 0.24 m^2 to 0.15 m^2 . This smaller range of basin areas is due to the position of the fixed partitions. The basin area that was bounded by these fixed partitions was much smaller during the experiments discussed in this section in comparison to the experiments of the previous section. During the experiments this bounded basin area could only be decreased.

The results with a *C34* pipe show nonlinear bending towards higher frequencies for all basin areas. In those experiments, multiple equilibria were not observed. In the experiments with a *T32* pipe, multiple equilibria, i.e. different stable responses (*branches*) in the basin

¹See section 3.2.5 for a description of these pipes.

for the same forcing frequency and amplitude, were observed. These results will be discussed below.

4.3.1 Results

Multiple equilibria were detected under a few set-up conditions. First the results with the largest frequency domain in which multiple equilibria exist, are shown in figure 4.8. The set-up conditions for these measurements were a basin area of 0.239 m^2 , forcing tide of 1 mm at sea (with a maximum deviation of 8%) and the *T32* pipe. The experiments were performed three times, to ensure that the phenomenon was not incidental. For the sake of clarity, the measurements of only one experiment and one response sensor (the sensor above the pipe) are shown in figure 4.8. Figure C.2 (appendix) contains all results.

The frequency range for which multiple equilibria exist has been determined. The procedure was that two series of measurements were performed, one for slowly increasing forcing frequency (up) and one for decreasing frequency (down). The response for the up series and the down series is equal for most forcing frequencies, one response equilibrium only is measured. In the frequency range where multiple equilibria exist the two responses differ, because the response of the system tends to remain in the branche it already was, until the forcing frequency is changed beyond the domain in which this branche exist. At that point, the system adjusts towards the other, remaining branche with a quite different tidal amplification and phase lag. The frequency domain with multiple equilibria with a width of about $5 \cdot 10^{-4} \text{ Hz}$ was found in this way.

Before such an experiment can be started, the interesting frequency domain has to be determined. This was done by measuring the response curve, likewise performed in the previous section. The rather deviating measurement for 0.1600 Hz in figures 4.8(c) and 4.8(d) (in both figures the upper square) belongs to this class of global experiments. So, it is not convincingly demonstrated that the higher branche exists up to 0.1600 Hz, where this branche was measured up to 0.1591 Hz in the experiment with slowly decreasing frequency. It indicates only that perhaps the mode exist beyond a forcing frequency of 0.1591 Hz.

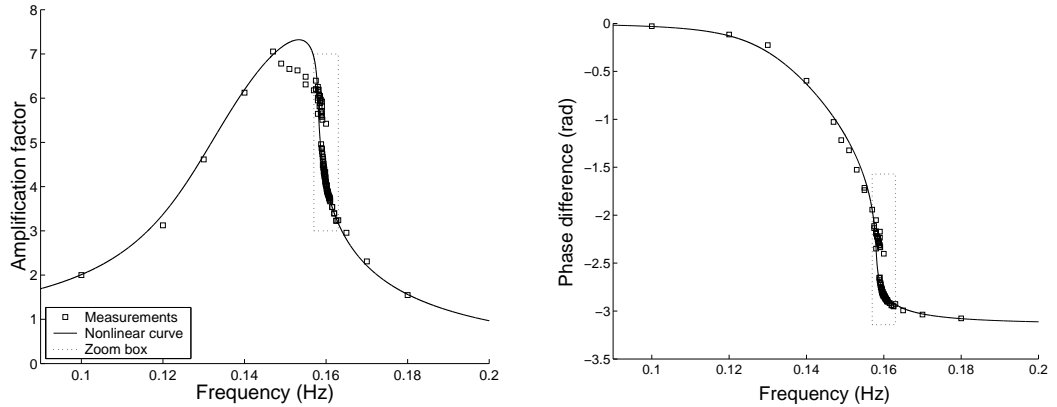
Although the nonlinear theoretical curve matches the measurements quite well on an overall level, a detailed look reveals clear differences: the best fitting generic nonlinear amplification curve, does not yield multiple equilibria yet. Even if the fit is based only on the measurements in the frequency range with multiple equilibria, the best fitting curve does not have multiple equilibria in that range. Apparently, the nonlinear behaviour that is observed with the multiple equilibria cannot be described with the general curve for weakly nonlinear Helmholtz basins. The obvious conclusion is that higher order nonlinear terms are responsible for this bending. This conclusion can be made, although the theoretical explanation and the mathematical description of the responsible phenomenon are unknown yet.

4.3.2 Persistence under changes in set-up conditions

In section 4.2, the effect of resizing the basin area on the response curve were discussed only. All set-up conditions has been changed one by one in order to study their influence on the multiple equilibria. The effect of an alteration of the mean water level has been investigated, but not any effect on the response has been observed. Therefore, the mean water level is not discussed further in this section.

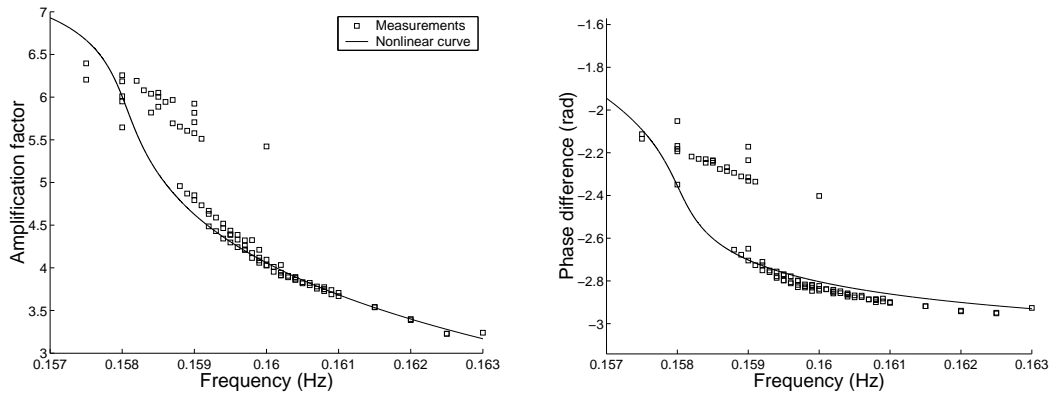
Increasing the tidal forcing amplitude

The results that were shown in the previous subsection were obtained with a forcing amplitude of 1 mm. Experiments were also performed with a tidal forcing of 2 mm. Lower



(a) The dotted box marks the domain which is enlarged in subfigure (c).

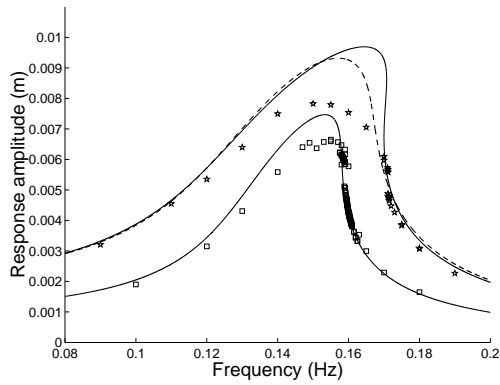
(b)



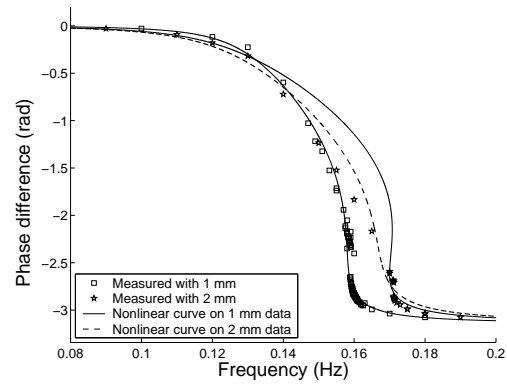
(c) Enlargement of figure (a), near the region of multiple equilibria.

(d) Enlargement of figure (b).

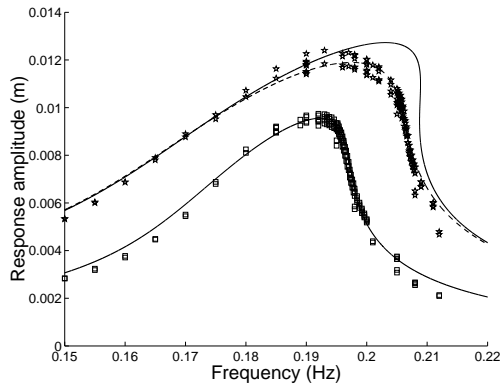
Figure 4.8: Response curves with multiple equilibria. A response curve with multiple equilibria, has always a gap. The responses with amplification factors and phase lags within the gap were unstable. Therefore, they cannot be reached. The measurements were observed with the *T32* pipe, a basin area of 0.239 m^2 and tidal forcing of 1 mm . Displayed are measurements of one experimental session only, the experiment were repeated 3 times, always yielding multiple equilibria in a small range of the forcing frequencies. The curve is based on all results.



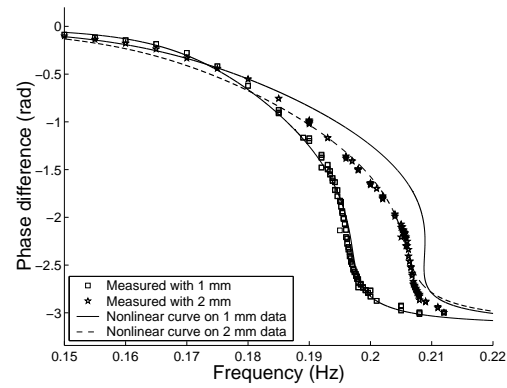
(a) Results for a basin area of 0.239 m^2 and pipe (T_{32}), but with stronger forcing.



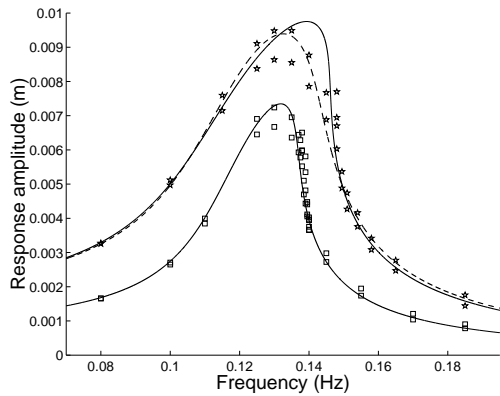
(b) Equal conditions as for (a).



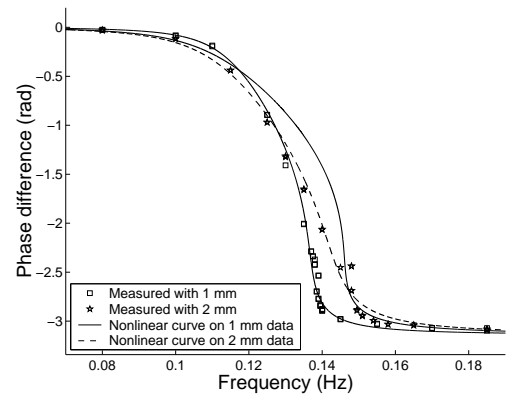
(c) Results for reduced basin area (0.15 m^2), but with equal pipe (T_{32}) and forcing.



(d) Equal conditions as for (c).



(e) As a, but with longer pipe (T_{42}).



(f) Equal conditions as for (e).

Figure 4.9: Tidal response curves in the basin with changed set-up conditions with respect to that resulted in figure 4.8. The applied forcing amplitudes are shown in figure C.3

forcing amplitudes were not applied, because the measurement accuracy is insufficient for those amplitudes (see sections 3.3.1 and 3.4.2).

Figures 4.9(a) and 4.9(b) show the response curves for a tidal forcing amplitude of 1 and 2 mm. The pipe length and shape and the basin area were unchanged. The lower solid curve is the generic nonlinear curve fitted on the measurements with 1 mm forcing amplitude. The upper solid generic curve was drawn for a forcing amplitude of 2 mm, using the same fitting parameters (i.e. σ_H , ν_0 and Γ) as the lower curve. So, this upper curve shows the responses for a forcing of 2 mm which may be expected for a forcing of 2 mm if the measured responses follow the generic nonlinear curve. The dashed curve is the generic nonlinear curve fitted on the 2 mm forcing amplitude measurements.

The upper solid line and the dashed line do not match. Consequently, the response does not follow the generic nonlinear curve for increasing forcing amplitude. Considering the multiple equilibria, interpolation of the results for 1 mm forcing to a forcing of 2 mm predicts an increase of the frequency range for which multiple equilibria are found. A decrease of this range has been measured instead. Therefore, the bending parameter Γ is not a constant, but a function of the forcing amplitude. Too less data is available to give a quantitative relation.

Moreover, the amplification in the frequency domain 0.13-0.15 Hz is weaker than expected. The increase of the response caused by increased tidal forcing is smaller than predicted in this domain as well. Furthermore, the phase lag of the 2 mm series increases quicker than expected. So, the friction increases more than quadratically to the channel current velocity for this situation.

Resizing the basin area

Secondly, the effect of area resizing on the nonlinear behaviour was investigated by reducing length or width of the basin area that was applied in the previous paragraph (0.239 m²). Experiments with larger basin area and a ‘*T*’-pipe were not carried out because of technical limitations. In section 4.2, experiments with different basin areas — from 0.92 to 0.23 m² — and the *C*34 pipe were discussed as well, but multiple equilibria were not detected in these experiments. The differences between a ‘*C*’ and a ‘*T*’-pipe are rather small, nevertheless multiple equilibria were not detected during experiments with ‘*C*’-pipes. The absence of multiple equilibria in these experiments makes a comparison with the results shown here difficult.

Figures 4.9(c) and 4.9(d) show the results for a basin area of 0.15 m². An increase of eigenfrequency and response amplitude with respect to the response that is shown in figures 4.9(a) and 4.9(b), can be seen again. The double lines of measured response amplitudes are related to the slight increase of the tidal amplitude towards the end of the basin. The solid and dashed lines are the fits on the generic nonlinear curve. They are determined equally as done for figures 4.9(a) and 4.9(b). The bending is decreased in comparison with the previous plots. An increase of the forcing amplitude leads to less bending as well. For these set-up conditions no multiple equilibria were found. The results shown here were obtained by reducing the basin length. Experiments performed with a reduced basin width gave similar results.

In the previous paragraph a weaker amplification was found in the frequency domain from 0.15 to 0.13 Hz, around the eigenfrequency. Although this is not visible in figures 4.9(c) and 4.9(d), a weaker amplification was measured for reduced basin area as well. The lack of visibility is due to the applied tidal forcing amplitude, see figure C.3(b). The generic nonlinear curve is derived for a forcing amplitude of 2 mm, but the applied forcing amplitude is 2.2 mm. When the generic nonlinear curve is adjusted to this forcing amplitude, the response amplitude of this curve is larger than the measured response, but the difference is smaller than the difference observed in figures 4.9(a) and 4.9(b).

Increasing the pipe length

Thirdly the pipe length has been increased from 32 cm to 42 and 52 cm.

In figures 4.9(e) and 4.9(f) the measurements using the *T42* pipe are shown. The two measured response amplitude curves for one forcing amplitude are caused by tidal amplitude differences within the basin. The fitted generic nonlinear curves were fitted similarly as done for figures 4.9(a) and 4.9(b). A decrease of the eigenfrequency and a slight increase of the tide amplification can be seen, similarly to the result behaviour for full basin area, discussed in section 4.1. The bending of the curve has been decreased in comparison with the *T32* pipe. The decrease of amplification with increasing forcing amplitude obeys better those prescribed by the generic nonlinear curve than found with in experiments using the *T32*-pipe. So, increasing of the pipe length leads to less nonlinear behaviour. Experiments using the *T52* pipe for identical set-up conditions show similar changes.

4.3.3 Summary

Multiple equilibria, as a consequence of bending, were found with the *T32* pipe and a basin area of 0.24 m^2 and a forcing tidal amplitude of 1 mm. Increasing pipe length or forcing amplitude decreases the bending; decreasing the basin area decreases the bending as well. The effect of an increase of the basin area on the tidal response in the basin has not investigated.

Before conclusions are drawn, it should be remarked that the Helmholtz theory does not give a nonlinear bending. The origin of the bending observed in these experiments is not well understood yet. The experiments indicate that the shape of the pipe does influence the nonlinear behaviour of the system. The largest effect of nonlinearity was measured with the pipe with full trumpet ends on both sides. A very weak bending of the response curve has been observed with straight pipes as well.

Moreover, the fact that the experiments in case of a full basin area and of a strongly decreased basin area show less bending of the response curve, suggest that there must be an optimum for basin area. This conclusion, combined with the insufficient theoretical understanding of the nonlinear response of the system, makes it difficult to generalize the results for all existing tidal Helmholtz basins, like the Wadden Sea. Nevertheless, it demonstrates that the shape of the connecting pipe or channel can generate nonlinear effects.

4.4 Experiments with non-uniform hypsometry

In the preceding two sections, all experiments were performed using a uniform hypsometry, i.e. with vertical walls. The experiments with different hypsometry will be discussed in this section, roughly in chronological order. The goal of these experiments is to investigate the effect of hypsometry on the tidal response in the basin. According to the theoretical model of Maas (1997), non-uniform hypsometry would induce non-linear phenomena such as a bending of the response curves and multiple equilibria. The theoretical model is described in section 2.4. A precise description of all inlays discussed here is given in subsection 3.2.4.

When designing experiments with inlays one must deal with two problems. On one hand, a hypsometry with large lateral slopes generates less intertidal area, which leads to a weak nonlinear effect. On the other side, an almost flat slope endures small-scale effects, such as cohesion, adhesion and phase differences on the inlay due to tidal delay. If phase differences appear on the inlay, the tide is no longer uniform and thus the Helmholtz theory is no longer valid. This section describes the different attempts to realize an inlay that generates sufficient nonlinearity without exciting small-scale effects.

4.4.1 Fixed inlay

The first inlay that was used is a fixed, convex inlay. A convex surface has been chosen, because the amount of generated nonlinearity is independent of the mean water level for constant Γ (equation (2.42)), and the results could be compared more easily with those obtained from nonlinear theory. *Pipe two* has been used during the experiments, because *Pipe two* causes less friction than *Pipe one* and the pipes with smooth ends were not yet available during these experiments.

The results are shown in figure 4.10. They were obtained from two different water levels. The left column contains the results for high water level, the right for low. The water level difference between high water level and low is 6 mm. For comparison, the height difference between the minimum and maximum basin area is 3.3 cm. The mean water level difference leads to an approximately 30% larger basin area for the experiments with high water than the experiments with low water level. Because the forcing amplitudes (figures 4.10(a) and 4.10(b)) differ considerably, they are shown as well. At this stage, corrections for the frequency dependence of the forcing characteristics (see section 3.2.3) were not made yet. The mean basin area is smaller in case of a lower water level, so the eigenfrequency and the amplification is higher for the corresponding measurements. The response curve based on quasi-linear theory is plotted in this figure as well. This curve turns out to yield an accurate fit of the data; hence, the nonlinear effect is small. One might think that the response amplitude for the high water (figure 4.10(c)) bends to the left, but this transition of the maximum response frequency is caused by the nonlinear effect of friction². If the nonlinear effect of friction would not cause this shift of the maximum response, the quasi-linear curves would not fit any more.

A fit with nonlinear theory is performed as well. The fitting curve has small positive Γ , that is a bending to the right, in the same order of magnitude as the value of Γ measured with the *P31* pipe in section 4.2. The nonlinear effect that is generated by this inlay is far too weak to be visible in a bending of the response curve.

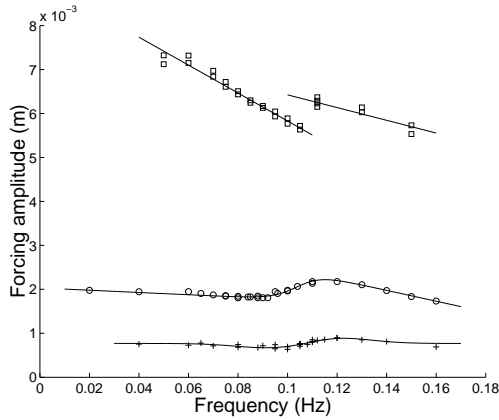
Although the inlay did not generate a visible bending of the response curve, it has an influence on the response of the basin. Figure 4.11 shows a tidal curve measured in case of a high mean water level near the eigenfrequency. The upper curve is the tidal forcing; the lower curve is the response in the basin. The dashed lines are reconstructed from the results of a harmonic analysis of the measured water levels in the basin (see section 3.4). The solid lines are based on a re-analysis of the measurements; the curve is made by transposing all measurements within one tidal period, subsequently smoothing the curve to erase outliers. Due to the inlay, the tidal response curve has not a sinusoidal shape. This tidal response has a shorter low-tide period than its high-tide period, which is caused by the area differences between high and low tide. This phenomenon is theoretically expected for an inlay (see section 2.4).

In summary, this inlay generated a clear difference between the period of high and low water in the tidal curve, but no significant influence on the response curve was found. The friction needs to be reduced or the slope increased for a successful demonstration of the conjecture that hypsometrical effects can cause bent resonance and other nonlinear phenomena.

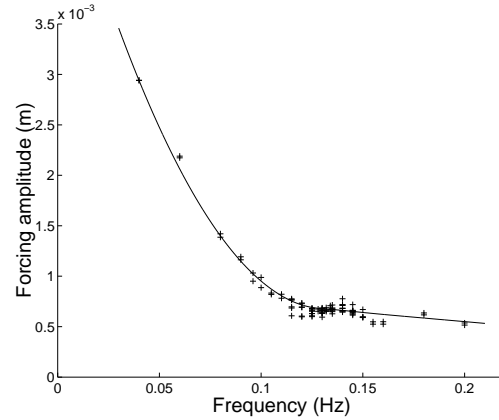
4.4.2 Planar inlays

In different ways linearly sloping bottom, causing an increase (or decrease) of the basin area with the water level, were constructed. First flat adjustable inlays will be discussed.

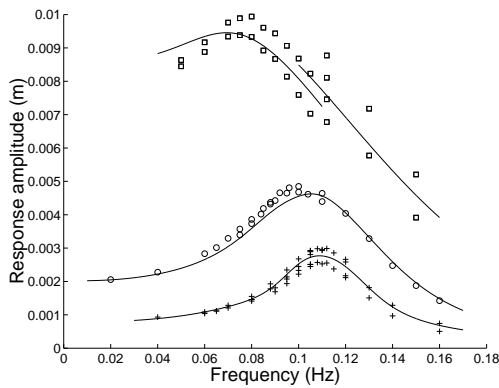
²See for a comparison the theoretical curves in figure 2.11



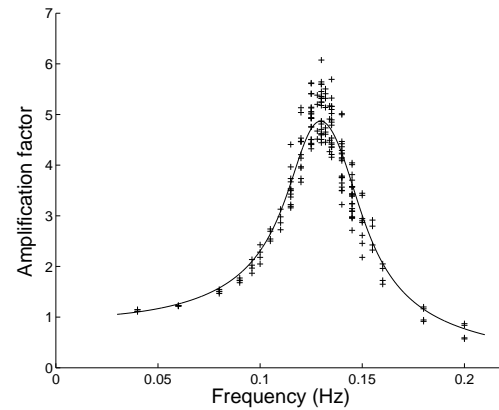
(a) Applied tidal forcing amplitude for high mean water level.



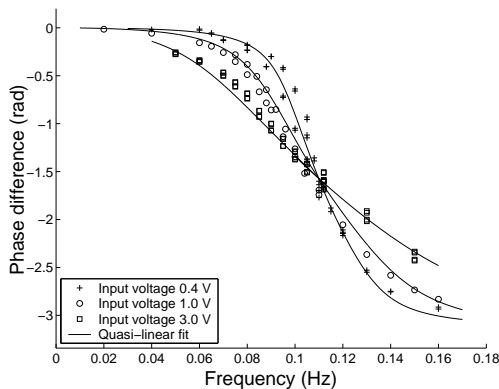
(b) Applied tidal forcing amplitude for low mean water level.



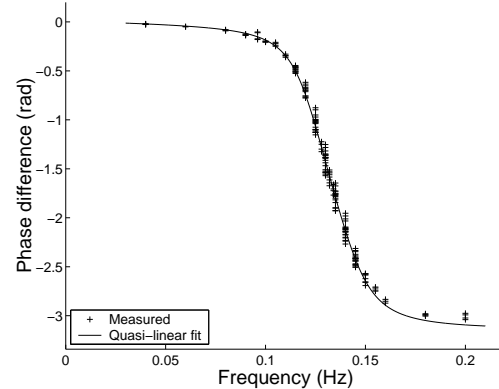
(c) Measured response amplitude for high mean water level.



(d) Measured amplification factor for low high mean water level.



(e) Measured phase lag for high mean water level.



(f) Measured phase lag for low mean water level.

Figure 4.10: Results obtained with the fixed inlay for high and lower mean water level. The mean water level difference between both was 0.6 mm. As a result the basin area at the mean water level is 30% increased in case of high mean water with respect to the lower mean water. All experimental results shown here, were performed with *Pipe two*.

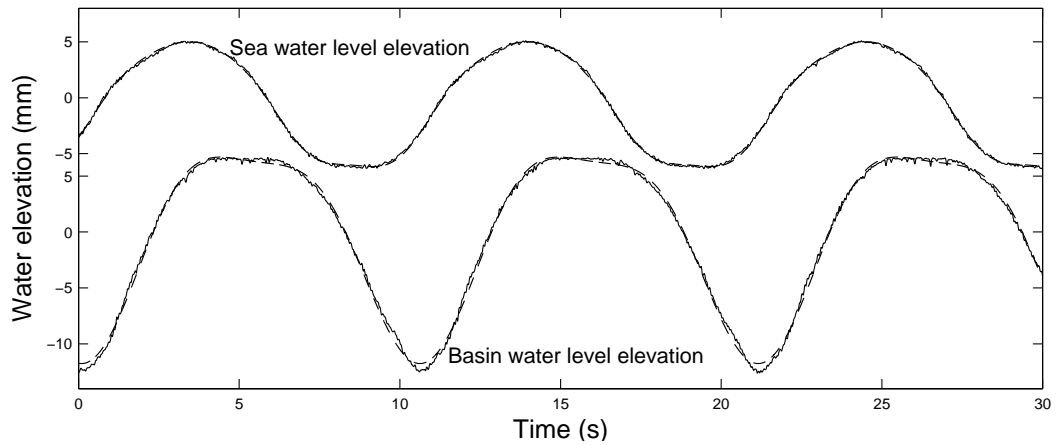


Figure 4.11: Tidal curve measured using the ‘fixed inlay’. The vibrating lines are smoothed curves through the measurements, the straight lines display the results obtained from a harmonic analysis of observed water level variations in the basin.

Almost flat adjustable inlay

An almost flat adjustable inlay was used in two experiments, for a full basin and for a reduced basin. The horizontal angle of the surface of these inlays can be varied. The inlay for a reduced basin can be set on a larger angle, which creates a small intertidal area, than the inlay for a full basin area.

Figure 4.12 shows typical tidal curves for these experiments. The phase lag between the tide at sea and the in basin is expected. However, a phase lag and different amplitude between the deeper and shallower parts of the basin were found as well. This phenomenon obstructs an experimental demonstration of presumed nonlinear behaviour in Helmholtz basins, because it breaks down the assumption that the tide is uniform in the basin, which is the basis of the Helmholtz theory.

The phase lag is caused by the shallow water layer on the inlay, in which the tide is delayed. This delay has a strong damping effect on the response. Furthermore, the waterline is deformed by cohesion and adhesion, as is sketched in figure 4.13. Cohesion and adhesion effects appear for inlay angles of ten degrees and lower. The effect of cohesion and adhesion on the tidal curve is visible at the intertidal sensor, number (4) in figure 4.12. When the water front passes sensor 4 at rising tide, the signal rises quickly. At falling tide, the water layer is ‘glued’ to the inlay by adhesion, causing the decay of the signal to be much slower. This asymmetry is caused by cohesive and adhesive effects and it could possibly increase the phase lag of the tide on the inlay. Teflon, a water repelling material, was tried out as top layer of the inlay, in order to reduce cohesion and adhesion, but it did not work. Therefore, only increasing the inlay angle decreases the capillary effects.

Capillary effects are hampering the experiments; the phase lag and corresponding damping however, make it impossible to investigate the nonlinear effect of the hypsonometry on the Helmholtz resonator in this way.

Sill

A sill can be considered as a horizontal inlay. The difference is that a horizontal inlay has a shallow water level over the entire inlay at high tide, in contrast with a sill, which

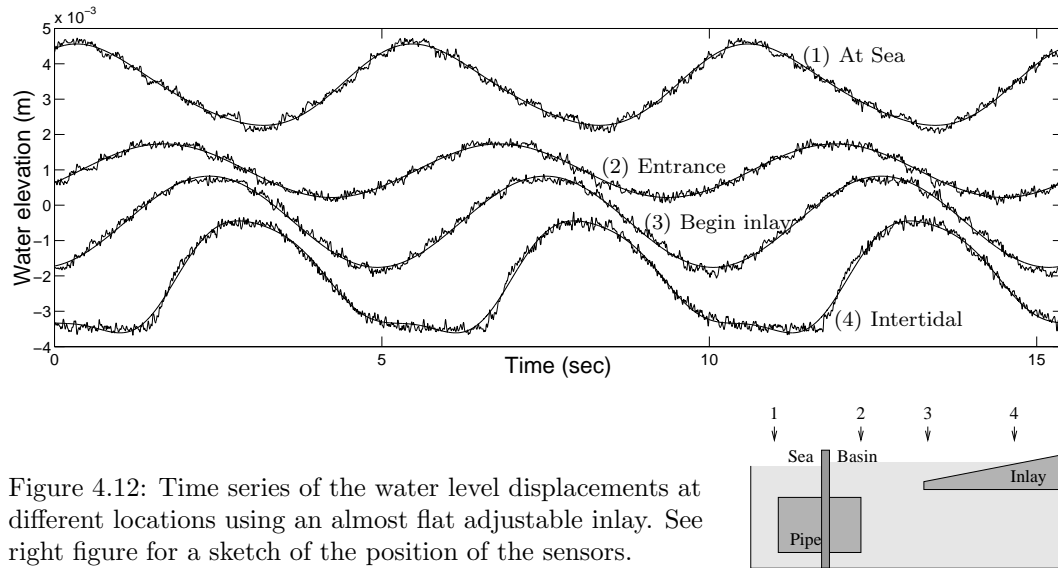


Figure 4.12: Time series of the water level displacements at different locations using an almost flat adjustable inlay. See right figure for a sketch of the position of the sensors.

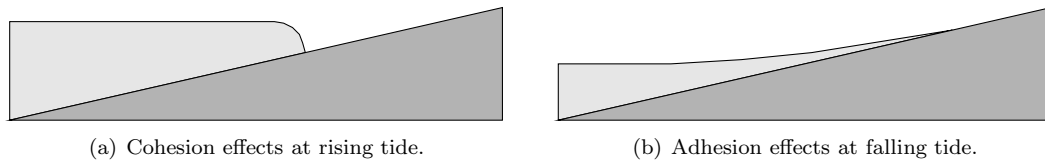


Figure 4.13: Small-scale effects at the waterline on the inlay

has a shallow water layer above the sill only. Therefore, a sill might endure less tidal lag effects than a horizontal inlay. Some experiments were performed with a sill, but the shallow water effects over the sill — the flow becomes supercritical — are strong, thereby almost completely choking the response behind the sill.

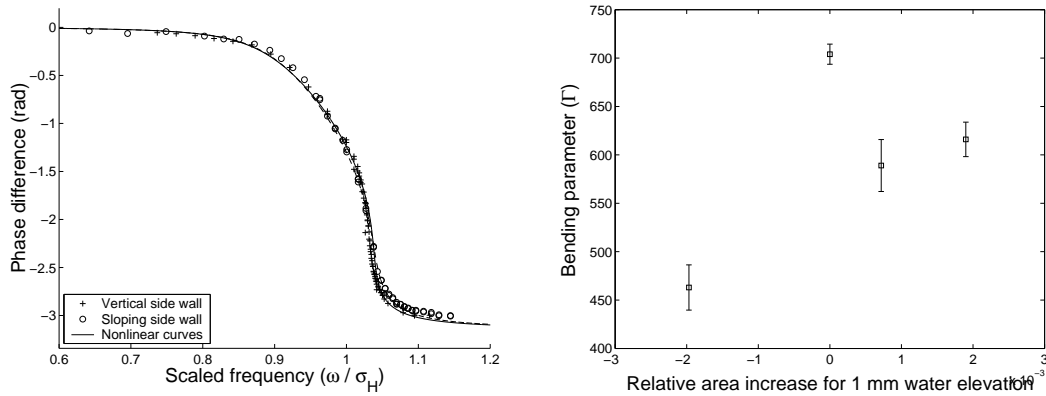
Steep inlay

An adjustable inlay was with a tilted sidewall as well. The slope realized with these tilted side walls could be much steeper — $> 30^\circ$ towards horizontal — than the previously discussed planar inlays which had to be almost horizontal. In this way, problems with tidal lag and capillary effects could be prevented. On the other hand, only a small change in the wet area between high and low tide is accomplished in this way. Measurements were done with a tilted side wall in the full basin, but all imaginable nonlinear effects are hidden by the fact that amplification is low for this basin area. Therefore, experiments were performed with a sloping sidewall and the smallest achievable basin area as well. The results are plotted in figure 4.14. Figure 4.14(a) shows the phase lag, in which only a slight difference is visible between the results for vertical and sloping side wall. The amplification factor is not shown, because the differences in the amplification factors are even smaller.

Theoretically, the slope would generate a negative bending. The reference measurement for the basin with vertical sidewalls however shows positive bending. In figure 4.14(a) the slope seems to have decreased the bending slightly, which could be considered to be consistent with the theory. Figure 4.14(b) shows the values of the bending parameter Γ for all measurements with steep inlays and small basin area. They are shown as a function of the relative increase of the basin area for a rise of the water level of 1 mm. All values of Γ that have been measured with a slope are lower than the Γ that was measured using vertical side-walls (relative area increase for 1 mm water elevation in figure 4.14(b) is 0). However, the expected parabolic pattern (see section 2.4) has not been found.

Summary

Summarizing all results with a planar slope, this method would never lead to multiple equilibria. An almost flat inlay generates a phase lag and capillary effects, which inhibit any experimental study on nonlinear tidal responses in Helmholtz basins. As a consequence the slope of the inlay must be rather steep. A steep inlay however, does not generate sufficient nonlinearity. In the most ideal situation, the smallest achievable basin area and 1 mm forcing, the bending generated by a steep inlay is small or even insignificant. The inlay must be almost flat before a significant bending might be generated. We conclude that the set-up must satisfy two conflicting demands. Therefore, within the settings of this experiment, single inlays ranging the entire basin would not lead to multiple equilibria.



(a) Phase lag curve for vertical and sloping side wall. In this figure the curves are shown for 0 (vertical side wall) and $2 \cdot 10^{-3}$ relative area increase for 1 mm water elevation.

(b) Dependence of the bending parameter Γ on the slope of the side wall. The tidal amplitude in the basin is ± 15 mm for maximum amplification.

Figure 4.14: Bending effects of sloping side walls. The experiments have been performed with a basin area of ± 0.15 m², the T32 pipe and a forcing amplitude of 1 mm.

Chapter 5

Discussion and conclusions

In this chapter, an overview of the results that were shown in chapter 4, is given. The results are compared with the goals formulated in chapter 1. In particular the correspondence with theoretical predictions and the need to adapt the theory are discussed. The reliability of the laboratory results is considered as well. Finally, recommendations for future research will be given.

The goals formulated in chapter 1:

- Verification of the existence of a Helmholtz resonator in a laboratory environment,
- Verification of the Lorentz-linearization principle for the formulation of the bottom friction,
- Investigation of the effect of a non-uniform hypsometry on the tidal response of the resonator,

will be used as guidelines in this section.

A Helmholtz resonator

Amplification of the tidal signal due to resonance of the Helmholtz mode was found in our laboratory set-up. Experiments with different basin areas, pipes and tidal amplitudes display amplification of the tide in the basin with respect to the tide in the sea. The observed amplification reached levels up to a factor of 3 for the largest basin up to a factor of 10 for the smallest basin area. The Helmholtz mode has a spatially uniform tide within the basin. Within the basin, a spatially uniform water surface elevation was measured for the largest basin area. Slight variations of the tidal amplitude within the basin were found for a smaller basin area. Nevertheless, the response can be modeled by a Helmholtz response, because the tidal phase remains constant in the entire basin.

Lorentz-linearized bottom friction

The tidal response of a Helmholtz basin that is damped by quadratic bottom friction (bottom shear stress), shows theoretically some characteristic phenomena. These phenomena were observed in the experimental results. The phenomena were: (i) A maximum amplification of the tide for a frequency just below the eigenfrequency, (ii) When forcing the system at the eigenfrequency, a phase lag of $\frac{1}{2}\pi$ (90°) was found, irrespective of the forcing amplitude. Moreover, the theoretically nonlinear behaviour of bottom friction for changing forcing amplitude was observed as well. The nonlinear behaviour for increasing forcing amplitude was characterized by: (i) A decrease of the maximum amplification, (ii) A decrease of the frequency for which the maximum amplification is reached, (iii) An increase of the phase lag if

the Helmholtz resonator is forced with a frequency lower than the eigenfrequency. Similarly, a decrease of the phase lag in case of a forcing frequency higher than the eigenfrequency.

The measurement results were also fitted on the theoretical response curves for qualitative insight in the accuracy of the theory. Fitting the theoretical response curves to the experimental results yields good results as well. Lorentz-linearization is thus a valuable linearization of bottom friction.

A deviation however has been observed. For increasing basin area (A), the friction coefficient ν_0 does not increase linearly with A , which is predicted by theoretical analysis. The experiments show that ν_0 depends on A with $\nu_0 \sim c_1 A + c_2 A^2$. This relation is not clarified yet.

Interlude: Unpredicted nonlinearity

The Helmholtz theory for a basin with vertical sidewalls area does not predict nonlinear behaviour. Nevertheless, nonlinear behaviour was measured in experiments with vertical sidewalls. The nonlinear behaviour was revealed by bending the response curves towards higher frequencies. In some experiments, a frequency domain in which multiple equilibria exist, has been observed.

The nonlinear behaviour was investigated to gain knowledge about its origin. The bend resonance curve compares rather well with a general weakly nonlinear response curve, which is derived in case of non-uniform hypsometry. The correspondence indicates that the source of nonlinearity is mathematically equivalent to that of the nonlinearity introduced by non-uniform hypsometry. Furthermore, experiments indicate that the shape of the connecting channel or pipe is important. Experiments with smooth pipe ends show much more nonlinear behaviour than comparable experiments with straight pipes. A theory quantitatively predicting this behaviour has not been found yet. Consequently, the relevance of this phenomenon for Helmholtz basins in nature is undetermined yet.

Non-uniform hypsometry

The investigation of the nonlinear behaviour caused by non-uniform hypsometry, has been hampered by several experimental difficulties. Theoretical predictions by Maas (1997) of bending, multiple equilibria or chaos caused by non-uniform hypsometry could neither be verified nor falsified yet.

The experimental bottleneck appears to be the realization of non-uniform hypsometry by introducing intertidal area. A rather steep inlay leads to little intertidal area; the nonlinear effect appears to be negligible compared to friction. Increasing the intertidal area by decreasing the inlay angle leads to unwanted small-scale effects, like tidal phase differences over the inlay¹. The small scale effects exhibit verification of the nonlinear theory. The experiments indicate that for laboratory-size basin a single inlay ranging the entire basin area cannot be used for this purpose.

In order to find useful experimental conditions, a numerical model was used. The results of the model were not discussed and compared with experimental results in this paper. Nevertheless, numerical modelling was an useful tool during the experiments.

Recommendations for future research

Further research is recommended in order to explore the origin and relevance of the nonlinear behaviour that was measured with vertical sidewalls and smooth pipe ends. Moreover, the possible effects of non-uniform hypsometry need attention still. A number of suggestions for carrying out relevant experiments can be given.

¹Green (1992) already noticed that phase lag could disturb the response of Helmholtz resonator with non-uniform hypsometry.

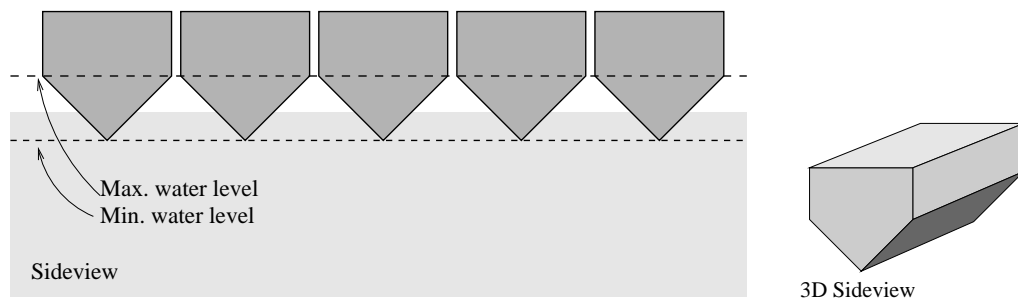


Figure 5.1: Sideview of suggested inlay. A dozen of these small ‘uplays’ generate a large intertidal area, whereas small-scale effects were reduced due to the large angle of the slope.

- In order to investigate the nonlinear behaviour that was measured with vertical side-walls and smooth pipe ends, the pipe could be replaced by a channel. Channels with straight and smoother ends could be used. The radius of the pipe could also be altered.
- Experiments have been done only with single inlays ranging the entire basin area. The nonlinear theory for non-uniform hypsometry is also valid if a set of small inlays are used. If the surface of the small inlay has a steep angle to the horizontal, unwanted small-scale effects and the tidal lag are decreased. An example is the ‘uplay’ shown in figure 5.1. Tidal lags will not occur on an ‘uplay’, because the water column below the ‘uplay’ is still nearly as deep as without ‘uplay’. Furthermore, an intertidal area that consist of several ‘uplay’s can be made easier than a similar intertidal area that consist of several inlays.
- Nonlinear behaviour has been measured during the experiments. The occurrence of chaos has not been investigated for these experimental conditions. Chaotic behaviour may occur according to theoretical models when the Helmholtz resonator is forced with more complex forcings in stead of a single harmonic forcing. An example of a complex forcing is the spring-neap cycle.
- All the results are gained from altimetry measurements. Although the velocity in the channel is directly related to the basin water level, measurements of the currents speeds is useful to check the validity of the Helmholtz equations.

Acknowledgements: I would kindly thank Guido Terra, Leo Maas and Huib de Swart for their help during my work for this mastersthesis. Without your help, it would not be this good. I would specially thank Guido for the inspiring cooperation and your effort to get this report written in *correct* English.

Appendix A

The Newton minimization procedure

Describing the harmonic analysis, in section 3.4, the Newton minimization procedure was mentioned. In this appendix, additional information on this procedure is provided.

With harmonic analysis, a reconstruction of the measured time series is made, writing it as a number of harmonic components, each with its own frequency f_k , amplitude a_k and phase φ_k . In most time series, less than 5 harmonic components are significant, although up to ten significant harmonic components have been observed in a few experiments. All together these harmonic components form a harmonic reconstruction that is defined by the formula

$$\zeta(t) = a_0 + \sum_k a_k \cos(2\pi f_k t + \varphi_k), \quad (\text{A.1})$$

in which a_0 is the mean water level. The best harmonic reconstruction is found by minimization of the differences between the reconstruction from formula (A.1) ζ and the measured heights h . For this purpose, the error function err is defined with

$$err = \sum_t (\zeta_t - h_t)^2. \quad (\text{A.2})$$

The error function is minimized with respect to the three *parameters* a_k , φ_k and f_k for each harmonic component and the mean water level a_0 . So, the dimension of the error function err increases quickly with increasing number of harmonic components.

The error function err is minimized in two different ways during the analysis procedure described in section 3.4.1. In step 6 of the procedure, f_k is fixed. In step 9 of the procedure, the minimization is with respect to all parameters, including the frequencies f_k .

Step 6, in which f_k is fixed, was done with linear algebra. Step 9 was done initially with the standard minimization routine of MATLAB[®]. The method is based on the simplex search method of Langarias *et al.* (1998), a direct search method which does not use numerical or analytic gradients. The method is very robust but time consuming. The necessary time grows exponentially with increasing harmonic components. For sessions with more than 5 significant harmonic components, it exceeds 30 minutes. Therefore a less time consuming method was implemented.

Description of a procedure based on Newton iteration

A much faster method is based on Newton iteration. The main idea behind this method is that near the minimum of the error function, the error function err is approximately quadratic. This idea is used to move quickly to the minimum of err .

The error function err is a scalar function, which depends on a number of parameters, subsequently to be denoted by Ψ . Thus, err is a function of Ψ , which contains the frequency, amplitude and phase, f_k, a_k, φ_k of the significant harmonic components, and the mean water level a_0 . At the minimum of err , the derivative with respect to all these parameters is zero, i.e. the gradient vector ∇err is zero. The derivative of ∇err is given by the second derivative \mathcal{H} of err , which is a matrix. The second derivative \mathcal{H} is used to find the value of Ψ , for which ∇err is zero, i.e. for which the error function err reaches its minimum.

The first guess for the value of the parameters (Ψ_0) is determined by harmonic analysis with fixed frequencies (step 6 in section 3.4.1). At Ψ_0 , the local gradient $\nabla err|_{\Psi_0}$ and the local Hessian matrix $\mathcal{H}|_{\Psi_0}$ can be calculated analytically. With $\mathcal{H}|_{\Psi_0}$ the new ‘point’ Ψ_1 where ∇err would be zero can be estimated by

$$\Psi_1 = \Psi_0 - (\mathcal{H}|_{\Psi_0})^{-1} \cdot \nabla err|_{\Psi_0}. \quad (\text{A.3})$$

If err would be a quadratic function, Ψ_1 would be the minimum of err exactly. If Ψ_0 is close enough to the minimum, the deviation from quadratic behaviour of err are that small that Ψ_1 is much closer to the minimum. This procedure can be repeated until Ψ_n is close enough to the minimum of err . The accuracy of the procedure strongly increases if the steps get smaller, since the parabolic assumption underlying equation (A.3) becomes more accurate the closer one gets to the minimum. Starting from a good first guess, the method converges to the minimum of err , in three to six steps, independent of the number of variables.

Problems caused by deficient robustness

Problems occur when the first guess is not close enough to the minimum. Away from the minimum, the parabolic approximation of err is not satisfied yet. This means that higher order derivatives determine the behaviour of err . In that situation, an iteration step according to (A.3), may not be directed towards the minimum. The checks and corrections, which have been implemented to increase the robustness of the procedure, are:

- The first guess can be improved. That is why in step 5 of the data analysis procedure (see section 3.4.1) the peaks obtained by Fourier analysis are replaced by the forcing frequency and its overtones. The simplex method of MATLAB[®] could deal with the frequencies obtained by Fourier transformation directly, but the correction is needed when using the Newton method.
- A restriction on the step, i.e. on $\Delta\Psi = \Psi_{n+1} - \Psi_n = (\mathcal{H}|_{\Psi})^{-1} \cdot \nabla err|_{\Psi}$, is implemented in the procedure. In this restriction, the vector p is used, which denotes the amplitude, frequency and phase of one harmonic component, i.e. $p = \{a_n, f_k, \varphi_n\} \forall k$. For each harmonic component, the relation $\Delta\Psi_p \cdot \nabla_p err > 0$ has to be satisfied, i.e. the direction of the step should be in the direction of an increasing gradient. If the latter relation is not satisfied, the sign of the step for these three variables, i.e. $\Delta\Psi_p$, is reversed, because the extremum that one is heading for, is a maximum instead of a minimum.

Other corrections for an errative direction have been tried as well, but the correction method above gives the best results. Reversing the sign of the entire step $\Delta\Psi$ if one is heading a maximum, or replacing the step by a step along the local gradient, both did not perform as well as the correction method above.

- A limit is set on the amount of change for each component of $\Delta\Psi$. The maximum change is set at $2 \cdot 10^{-4}$ Hz, $2 \cdot 10^{-4}$ m or 0.2 radians for the frequency, amplitude and phase, respectively. With this method, beter results are obtained than with a restriction on the absolute value of $\Delta\Psi$.

- Harmonic components whose amplitude become below 10^{-6} m are removed. If a harmonic component has a smaller amplitude, the phase becomes badly determined, which hamper the determination of the derivatives. Harmonic components with such small amplitudes may be neglected, because these components have an insignificant contribution to the harmonic reconstruction.

With these restrictions nearly all sessions could be handled, within a few seconds of processing time for each session. The few remaining sessions could be solved by improving the first guess manually.

Appendix B

The forcing of the sea

Before measurements can be carried out, the specific properties of the laboratory set-up must be known. Otherwise, unwanted effects could appear spontaneously disturbing the experiments. The experiments that are discussed in this appendix, test the tide in the sea part of the experimental set-up that is driven by the forcing tank. The importance of the experiments described in this appendix is to determine the range of forcing conditions (frequency and amplitude) that can be made with the laboratory set-up. A stable, single-component sinusoid at sea is required for the measurements. So, conditions under which higher harmonics or other disturbances become pronounced, cannot be used for experiments.

A sketch of the set-up is given in figure 3.1. In section 3.2.2, the construction of the driving mechanism is considered. The possible disturbances of the tide in the sea are discussed in section 3.2.3.

B.1 Results

The forcing frequency, amplitude and main sea level were varied during these experiments. At four locations, the water level was measured for measuring the properties of the tide simulator. One sensor measured the position of the forcing tank. Two sensors measure the tidal amplitude at the basin side and one measures at the far end of the sea. These positions are displayed in figure B.1.

The results are shown in figure B.2. For frequencies below 0.10 Hz, the response of the sea is uniform. The tidal amplitudes are similar at both sides of the basin. The sealevel is exactly in opposite phase as well.

Between 0.10 and about 0.22 Hz, the indications of a quarter-wavelength standing wave appear. A sketch of this wave was given in section 3.2.3, figure 3.3(a). The wave have a strong

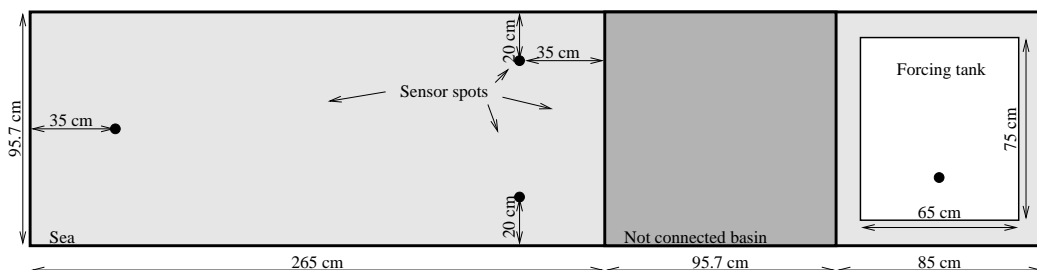


Figure B.1: Topview of the laboratory set-up, showing the positions of the sensors. The dots mark the locations.

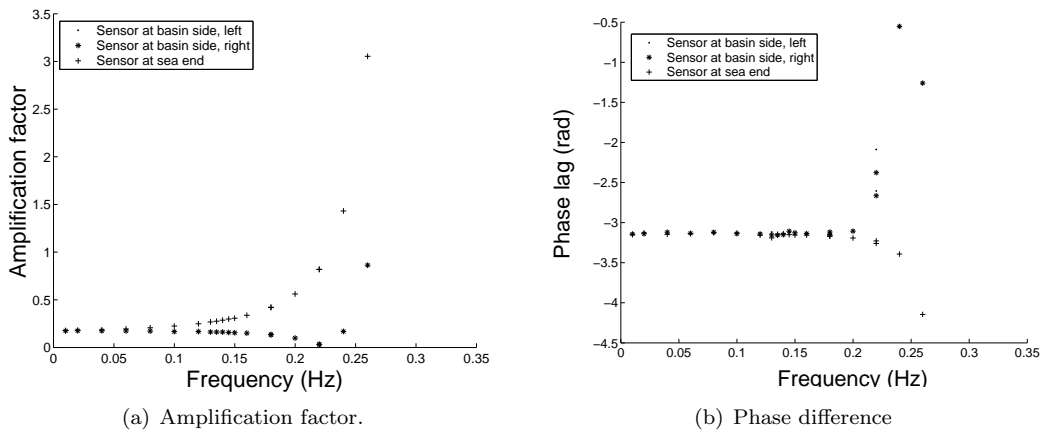


Figure B.2: The response of the sea. The tidal amplitude and phase at the sea are compared with the amplitude and phase of the forcing tank.

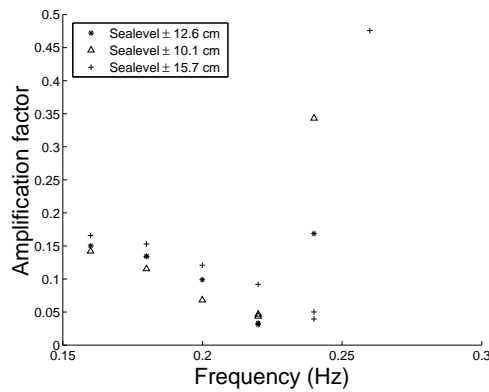


Figure B.3: The tidal amplitude at the basin side of the sea near the eigenfrequency of the quarter-wavelength standing wave. These experiments were done with different mean water levels.

tidal amplitude at the far end of the sea. The tidal amplitude at the basin side of the sea decreases. The decrease of the tidal amplitude at the basin side of the sea can be corrected by increasing the amplitude of the forcing tank. Near 0.22 Hz, the first overtide (≈ 0.45 Hz) becomes the dominant tidal component at this part of the sea, because the amplitude of the forced frequency vanished. The response becomes very irregular for frequencies higher than the quarter-wavelength eigenfrequency.

Mean water level

The effect of the mean water level on the tide in the sea is shown in figure B.3. The region around the first eigenmode, the quarter-wavelength standing wave, is enlarged in this figure. Only the measurements with the sensors at the basin side of the sea are shown.

The frequency for which the quarter-wavelength standing wave appears, increases with increasing mean water level. This is in accordance with long wave theory, which predicts increasing wave velocities with increasing water depth. In these testing experiments, water

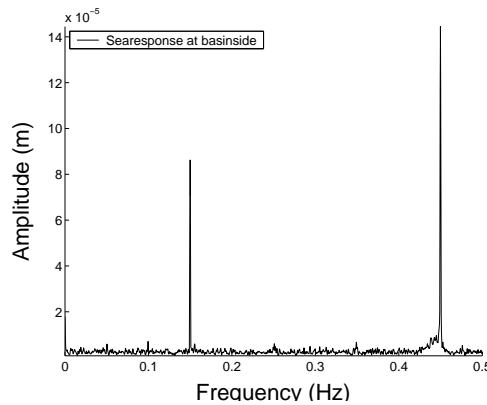


Figure B.4: Fourier spectrum of the tidal signal at the basin side of the sea. The forcing frequency is 15 Hz. The amplitude of the strong overtide at 0.45 Hz is larger than the amplitude of the forcing frequency.

levels up to 15.7 cm were used. During latter experiments, water levels up to 21 cm were used. In that situation, 0.21 Hz appears to be the highest frequency that could be used.

Overtides

Overtides have been measured not only near the eigenfrequency (0.22 Hz), but also near 0.15 Hz. If the sea is forced with frequencies around 0.15 Hz, the half-wavelength response with a frequency around 0.45 Hz is excited as well. The amplitude of this overtide can become even larger than that of forced frequency, as shown in figure B.4. If normal experiments were performed with such forcing, the tide in the basin is basically forced by two frequencies. During the experiments however, this extra forcing frequency appears not to be very important. The frequency of the half-wavelength response is much larger than the eigenfrequency of the Helmholtz basin, so that no significant response was measured. Moreover, the effect disappears when detuning the forcing frequency slightly from 0.15 Hz.

B.2 Conclusions

The response of the sea to the motion of the forcing tank is uniform for frequencies below 0.10 Hz. Spatial differences start to develop in the frequency domain between 0.10 and 0.22 Hz. The differences cause a decrease of the tidal amplitude at the basin side of the sea, but this decrease can be corrected by an adjustment of the forcing amplitude. Close to the eigenfrequency of the quarter-wavelength standing wave, experiments becomes impossible, because at that frequency the tidal amplitude of the forcing frequency at the basin side of the sea becomes negligible. Therefore, experiments can be performed with frequencies below 0.22 Hz only.

Appendix C

Additional figures

C.1 The reponse of *Pipe two*

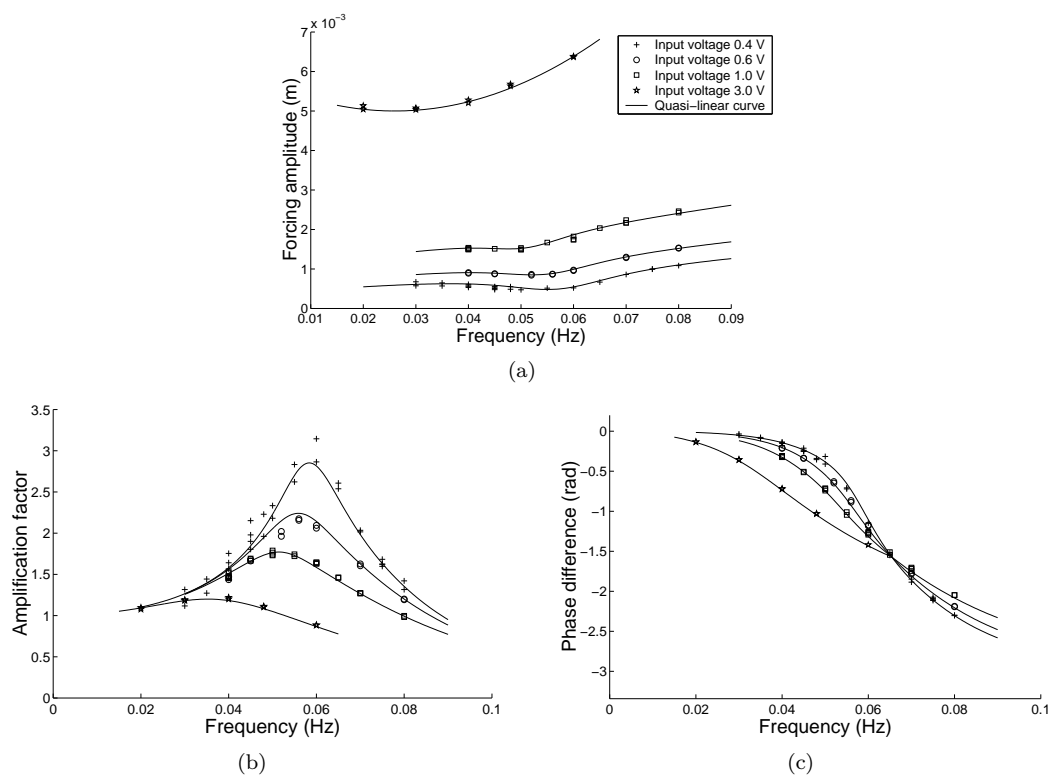
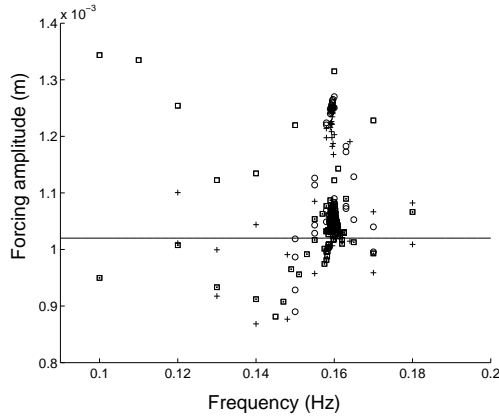
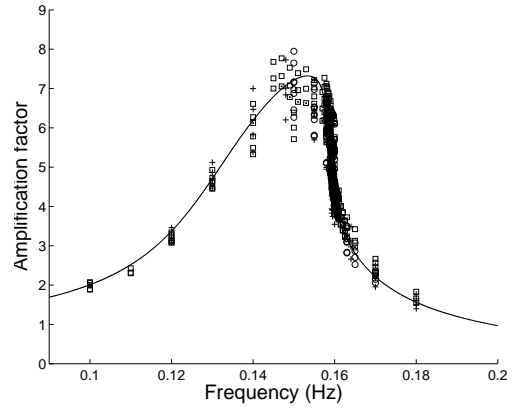


Figure C.1: Response curves for *Pipe two* and full basin area (0.91 m²). In subfigure (a), the applied tidal forcing amplitudes at sea is shown. The measured responses and the quasi-linear theoretical curve match well in subfigure (b) and (c).

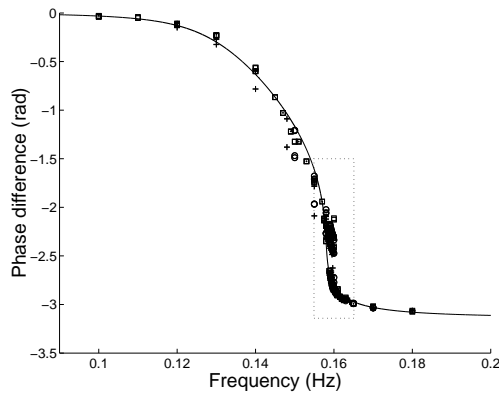
C.2 Multiple equilibria



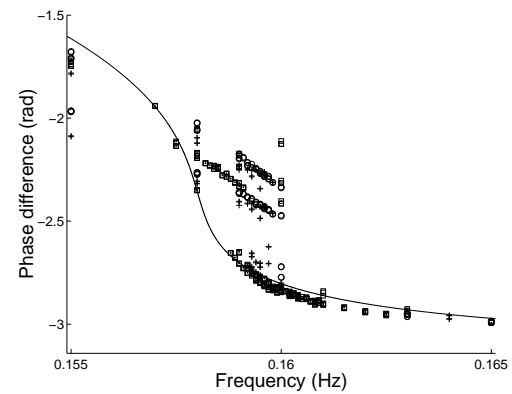
(a) All forcing amplitudes around 1 mm that have been applied. The measurements with 2 mm forcing amplitude were discussed in subsection 4.3.2.



(b) The measured amplification factors. The amplification factor of the tide is a bit smaller at the entrance of the basin than at the end. A sensor has been placed at both sides during these measurements. The difference in amplification factor is larger than the amplification difference between the two regimes in the region of multiple equilibria.

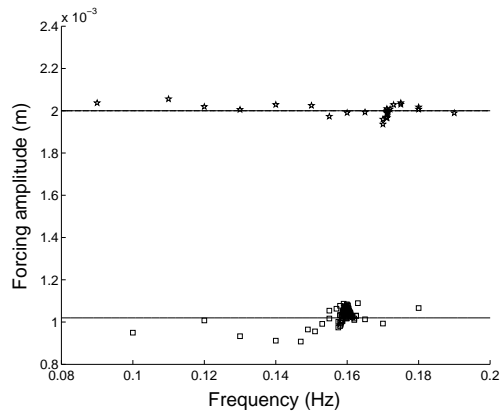


(c) The phase lag. Although the tidal amplification within the basin is not strictly uniform, the phase of the tide is constant over the entire basin. Therefore the phase jump between the regimes is clearly visible in this figure. The dotted box is enlarged in subfigure (d)

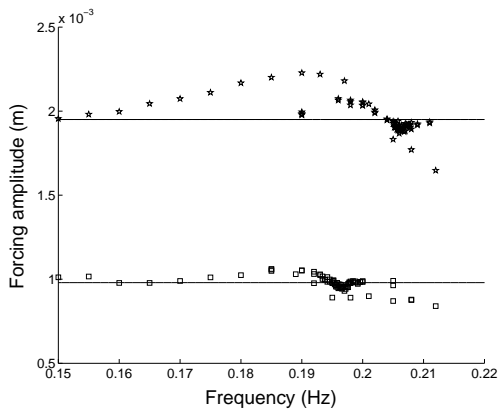


(d) Enlarged picture of the phase lag near the region where multiple equilibria were found. Two different lines are visible for the measured phase lag of the upper mode. The reason for this is the fact that the forcing amplitude is slightly higher for the upper line, hence increasing frictional effects.

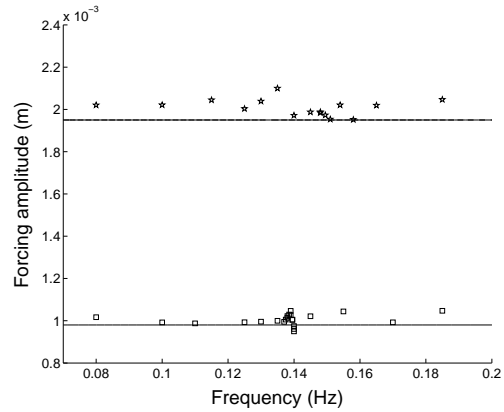
Figure C.2: All measurements for a basin area of 0.239 m^2 , forcing amplitude of $\pm 1 \text{ mm}$ and the $T32$ pipe. Circles, squares and crosses correspond with to the 3 different times the experiment was done. The solid line shows the best nonlinear fit, for which all measurements were used. The measurements that are shown in figure 4.8 are indicated by squares with a dot in their centre.



(a) Applied tidal forcing amplitudes for 0.239 m^2 basin area and $T32$ pipe. The results of the experiments that were done with these forcing amplitudes, are shown in figures 4.9(a) and 4.9(b).



(b) Applied tidal forcing for 0.15 m^2 basin area and $T32$ pipe. The corresponding results are shown in figures 4.9(c) and 4.9(d).



(c) Applied tidal forcing for 0.24 m^2 basin area and $T42$ pipe. The corresponding results are shown in figures 4.9(e) and 4.9(f).

Figure C.3: Applied forcings of experiments discussed in subsection 4.3.2

Bibliography

- CARTWRIGHT, D. E. 1999 *Tides: a scientific history*. Cambridge: Cambridge University Press.
- DEFANT, A. 1961 *Physical oceanography*. Oxford: Pergamon Press.
- DOELMAN, A., KOENDERINK, A. F. & MAAS, L. R. M. 2002 Quasi-periodically forced nonlinear Helmholtz oscillators. *Physica D* **164**, 1–27.
- GARRETT, C. J. R. 1975 Tides in gulfs. *Deep-Sea Res.* **22**, 23–35.
- GILL, A. E. 1982 *Atmosphere-ocean dynamics*. New York: Academic Press.
- GREEN, T. 1992 Liquid oscillations in a basin with varying surface area. *Phys. Fluids A* **4** (3), 360–362.
- LANGARIAS, J. C., REEDS, J. A., WRIGHT, M. H. & WRIGHT, P. E. 1998 Convergence properties of the Nelder-Mead simplex method in low dimensions. *SIAM Journal of Optimization* **9**, 112–147.
- LEBLOND, P. H. & MYSAK, L. 1978 *Waves in the ocean. Elsevier oceanography series* 20. Amsterdam: Elsevier.
- LEE, J.-J. 1971 Wave-induced oscillations in harbours of arbitrary geometry. *J. Fluid Mech.* **45**, 375–394.
- LORENTZ, H. A. 1922 Het in rekening brengen van den weerstand bij schommelende vloeistofbewegingen. *De Ingenieur* p. 695.
- MAAS, L. R. M. 1997 On the nonlinear Helmholtz response of almost-enclosed tidal basins with sloping bottoms. *J. Fluid Mech.* **349**, 361–380.
- MAAS, L. R. M. 1998 On an oscillator equation for tides in almost enclosed basins of non-uniform depth. In *Physics of Estuaries and Coastal Seas* (ed. Dronkers & Scheffers). Rotterdam: Balkema.
- MEI, C. C. 1989 *The applied dynamics of ocean surface waves*. Singapore: World Scientific.
- MORSE, P. M. 1948 *Vibration and Sound*. New York: McGraw-Hill.
- PROUDMAN, J. & DOODSON, A. T. 1924 The principal constituent of the tides of the North Sea. *Phil. Trans. R. Soc. London A*, **224**, 185–219.
- TERRA, G. M., MAAS, L. R. M. & DOELMAN, A. 2003 A weakly nonlinear approach to coastal resonance. Submitted to *Journal of Fluid Mechanics*.
- WACK, P. E. 1985 A variable-volume Helmholtz resonator. *The physics teacher* **23**, 49–51.
- ZIMMERMAN, J. T. F. 1992 On the Lorentz linearization of a nonlinearly damped tidal Helmholtz oscillator. *Proc. Kon. Ned. Akad. v. Wetensch.* **95**, 127–145.